UNIVERSITAT POLITÈCNICA DE CATALUNYA
BARCELONATECH
Departament d'Enginyeria Electrònica

"FAULT TOLERANT VECTOR CONTROL OF FIVE-PHASE PERMANENT MAGNET MOTORS"

Thesis submitted in partial fulfillment of the requirement for the PhD degree issued by the Universitat Politècnica de Catalunya, in its Electronic Engineering Program

Ramin Salehi Arashloo

Director: Jose Luis Romeral Martinez

July 2014

To my beloved parents,

ACKNOWLEDGMENTS

My first and sincere appreciation goes to Prof. Romeral, whose vast knowledge and experience, patience and encouragement has made this work possible. I am also most grateful for his faith in this study.

A special word of thanks to my family who tirelessly supported me, and offered me encouragement when it was most needed. To my parents Mahmood Salehi and Masoomeh Zaman for their unfading support during my entire life, and to my brother and sister, Peyman and Yasaman for their love and liveliness.

Abstract

Equipped with appropriate control strategies, permanent magnet (PM) machines are becoming one of the most flexible types of actuators for many industrial applications. Among different types of PM machines, five-phase BLDC machines are very interesting in fault tolerant applications of PM drives.

Torque improvement in five-phase BLDC machines can be accomplished by optimizing their mechanical structure or by enhancing their controlling methods. New current controllers are proposed in this thesis to improve the quality of generated torque under normal operations of five-phase BLDC machines. Proposed current controllers are based on combination of predictive deadbeat controlling strategy and Extended Kalman Filter estimation. These controllers will be the basis for accurate faulty operation of the motor.

Operation of five-phase BLDC machines under faulty conditions has also been considered in this study. To improve the generated torque under faulty conditions, both amplitude and phase angle of fundamental and third current harmonics are globally optimized for the remaining healthy phases.

Under faulty conditions, appropriate reference currents of a five-phase BLDC machine have oscillating dynamics both in phase and rotating reference frames. As a result, the implemented current controllers under these conditions should be robust and fast. Predictive deadbeat controllers are also proposed for faulty conditions of five-phase BLDC machines.

Fault tolerant five-phase BLDC machines are very interesting in automotive applications such as electrical vehicles and more electric aircraft. In addition, these devices are gaining more importance in other fields such as power generation in wind turbines. In all of these applications, the efficiency of PM machine is of most importance. The efficiency of a typical five-phase BLDC machine is evaluated in this thesis for normal and different faulty conditions.

Experimental evaluations are always conducted to verify the theoretical developments. These developments include proposed controlling methods, optimized reference currents, and simulated efficiency of five-phase BLDC machine under different operational conditions.

Contents

Acronyms

FOC:	Field Oriented Control
DTC:	Direct Torque Control
MPC	Model Predictive Control
PDC	Predictive Deadbeat Control
IPM:	Interior Permanent Magnet
PMSM:	Permanent Magnet Synchronous Machine
BLDC	Brushless Direct Current
AC:	Alternating Current
DC	Direct Current
PI:	Proportional Integral
PR:	Proportional Resonant
PWM:	Pulse-Width Modulation
SV:	Space Vector
SV-PWM:	Space-Vector Pulse-Width Modulation
EV	Electrical Vehicle
MMF	Magnetic Motive Force
EMF	Electro Motive Force
AFPM	Axial Flux Permanent Magnet
EOC:	Efficiency Optimizing Control
SR:	Switch Reluctance
FEM:	Finite Element Method
AIC:	Artificial Intelligence Control

List of Tables

List of Figures

1.

Chapter 1 Introduction

This chapter outlines the main lines of inquiry on which this thesis research is engaged. It takes the reader from an introduction of the research field to the thesis's contents, through the hypothesis statements and the exposition of the specific objectives.

CONTENTS:

1.1. Research Topic

Equipped with appropriate control strategies, permanent magnet (PM) machines are becoming one of the most flexible types of actuators for many industrial applications. The appearance of high performance magnets such as Neodymium-Boron-Iron, and Samarium Cobalt, allows these machines to have higher reliability, efficiency, and power density [1].

In addition, due to their increasing industrial applications, the quality of generated torque in multi-phase PM machines is gaining more importance.

Torque improvement can be achieved by either optimizing the motor design [2] [3] or by improving the controlling strategy [4] [5] [6]. In [7] it is shown that by increasing the number of phases, and applying appropriate winding distribution, generated torque ripple can be effectively reduced.

In parallel with new multiphase designs, controlling strategies have also been under investigation to improve the quality of generated torque. By controlling fundamental component of stator currents and their third harmonics in five-phase PM machines, it is possible to have high torque density of brushless direct current (BLDC) machines and controllability of permanent magnet synchronous machines (PMSM). In [8], this method has been applied to a new design of five phase BLDC machine with quasi-rectangular back EMF. In addition and similar to three phase drives, advanced controlling methods can also be applied to five phase PM machines [9] [10].

Reliability has always been one of the important aspects of PM drives [11] [12]. That is to continue the operation after the fault, or to shut the system down in a safe manner. Aiming to continue the operation under faulty conditions, various safety concepts have been proposed in literatures like fault-tolerant or redundant configurations [5] [13] [14] [15].

Several studies have been conducted to control multi-phase PM machines under faulty conditions. High safety applications like aerospace and electrical vehicles are the main motivation for the developed strategies [3] [5] [8] [15] [16]. Torque ripple reduction and output power improvement are the main objectives of fault tolerant strategies. To avoid high torque ripples, it is important to compensate important current harmonics. An analytical study has been conducted in [5] to generate a smooth electrical torque in five phase PM machines under faulty conditions. Both one and two faulty phases are considered, and the second-order and fourth-order of torque harmonics are cancelled by proper selection of reference currents in the remaining healthy phases. The same objective has been followed in [8] in the case of poly phase PM motors where each phase has been wound around one stator tooth to reduce the mutual inductance of faulty phase and the remaining phases.

1.2. Research problem

- The first considered problem of this thesis is related to current controller limitations in five-phase BLDC drives under healthy conditions. Many controlling methods are proposed in literature to

improve the dynamic behaviour of stator currents in PM machines [4] [5] [6]. There are several challenges in the design procedure of current controllers for five-phase BLDC drives. The controlling algorithm is preferred to be easy to understand. In addition, nonlinear behaviour of PM machines should be considered while designing the controllers. Moreover, designed current controllers should be able to cope with practical constraints of real drive systems such as limited dc-link voltage and switching frequency. These challenges in the design procedure of current controllers will be the main concern of chapter 2 for normal (healthy) operation of five-phase BLDC drives.

- Five-phase BLDC machines are very interesting for fault tolerant applications. Under faulty conditions, the average of generated torque is less and more torque ripples will be produced. To improve the generated torque of five-phase BLDC drives under faulty conditions, both amplitude and phase angle of fundamental and third current harmonics should be optimized in the remaining healthy phases. That is 16 unknown variables while missing one faulty phase, and 12 unknown variables in the case of missing two phases. Many studies have tried to optimize the reference values of stator currents, but due to high number of unknown variables in optimization procedure, almost all of previous studies have considered many simplifications to reduce the number of unknown variables and propose an analytical optimization method. Global optimization of stator current reference values under different faulty conditions is the second problem which will be considered in chapter 3 of this dissertation.

- It is interesting to mention that under faulty conditions, appropriate reference currents of a five-phase BLDC machine have oscillating dynamics both in phase and rotating-reference frames [17]. As a result, under faulty conditions, the implemented current controllers should be robust and fast. These two requirements for stator current controllers are the main challenges of current controller design procedure which will be considered in proposed deadbeat controllers of chapter 4.

- As it was mentioned at the beginning of this chapter, one of the main advantages of five-phase BLDC drives is related to their efficiency. However, the efficiency of these devices under faulty conditions is not considered in previous studies. Unknown values of efficiency in five-phase BLDC drives are the next concern of this thesis which will be considered in chapter 5.

1.3. Hypotheses

In order to address the presented research problems, the following hypotheses have been posed as a starting point for this research work:

- Development of electrical model for a five-phase BLDC machine under healthy and faulty conditions will be necessary for simulation of various controlling algorithms. It should be possible to use this model for different operational conditions (healthy and faulty). In addition, different harmonic orders of back-EMF waveform should be adjustable in this model.

- Implementation of fast and robust controlling methods can improve the behavior of current controllers in the structure of five-phase BLDC drives.

- Definition of some analytical indexes for generated electrical torque in five-phase BLDC machines, and considering these indexes in global optimization methods can lead to improve the reference values of stator phase currents under various faulty conditions.

- Implementation of fast and robust controlling methods to control the stator currents under faulty conditions can lead to better dynamic behaviour of five-phase BLDC machine while missing one and two stator phases.

- The efficiency of five-phase BLDC machine in different faulty conditions can be evaluated by simulations in MATLAB and other FEM simulating environments.

These exposed assumptions represent the basis of the resulting thesis research. The hypotheses are investigated by means of the research work reflected in this thesis document.

1.4. Aims and objectives

Covering the mentioned problems of section 1.2 are the main objectives of this dissertation. In general terms, **the final goal of this thesis is to develop controlling method for healthy and faulty conditions of five phases PM machines and to evaluate their dynamic behaviour and efficiency under different conditions**. In the following these objectives will be explained in more details:

Objective I:

To propose a fast and robust current controller for normal (healthy) operation of five-phase BLDC drive. Proposed controllers should be designed to cover two requirements of current controllers in five-phase BLDC drives. These two requirements are controlling method sensitivity respect system variations, and its ability in following reference currents during transient states. This objective will be faced in **chapter 3** of the dissertation.

Objective II:

To globally optimize the stator reference currents of a five-phase BLDC drive under different faulty condition. To have a global optimization, no simplification will be considered. First and third harmonic component of stator currents will be considered in the case of having both one and two faulty phases. Amplitude and phase angle of stator current harmonics are separately optimized in the remaining healthy phases. To consider all conditions, the limiting constraint of having zero sum of stator currents is removed by connecting machine´s neutral point to the inverter through an extra half-bridge leg. Rated RMS value of stator phase currents will also be considered as the main limiting factor of generated electrical torque. This objective will be the focus of **chapter 4** in this study.

Objective III:

Optimized current values of five-phase BLDC machines under faulty conditions have oscillating nature both in phase and rotating reference frames, and as a result fast and robust controllers are required to control the stator currents of five-phase BDLC machines under faulty conditions. The third objective of this thesis will be **to propose, implement and evaluate a fault tolerant current controller for five-phase BLDC motor drives under faulty conditions**. Open circuit fault is considered for one, two adjacent and two nonadjacent stator phases. Proposed controllers are aimed to improve two aspects of current controllers. These two aspects are firstly, the sensitivity of proposed controllers, and secondly, their ability in rapidly following the reference current values. This objective is considered in **chapter 5** of this thesis.

Objective VI:

Finally, the last (fourth) objective of this study will be **to provide an evaluation on the efficiency of a fault-tolerant five-phase BLDC drive under healthy and different faulty conditions**. Open-circuit fault will be considered for one, two-adjacent and two-nonadjacent stator phases, and in each case, optimized reference current values will be used to drive the faulty machine. This evaluation includes iron losses, copper losses and inverter losses of a five-phase BLDC drive. This objective will be discussed in **chapter 6** of the dissertation.

1.5. Control Methodology Approach of the Thesis

Aiming to have a prefect control on machine stator currents, Field-Oriented Control (FOC) and Direct-Torque Control (DTC) were introduced to the world respectively in the 70´s and 80´s, and now, these two methods are forming the base of other controlling strategies which are used to control the stator currents in PM drives. Today, new proposed controlling methods are usually a combination of basic principles of FOC (or DTC) with more advanced controlling algorithms such as “Sensorless methods”, “expert and artificial intelligent controlling systems (AIC)”, and “model predictive control (MPC) methods”. In this subsection, implemented control methodologies of this study and their correspondent motivations will be briefly reviewed.

Among different advanced controlling algorithms, predictive deadbeat control (PDC) has recently become a suitable option for electrical drives. Its concept is easy to understand, and various constraints and nonlinearities can be directly included in its structure. Moreover, the resulting controller is easy to implement [18], [19]. PDC method can be effectively implemented in five-phase BLDC drives because linear models of these machines are quite well known and developed through analytical methods. Deadbeat predictive control can be considered as an extension of traditional FOC. In this category, inner-loop PI controllers are removed and replaced by predictive controllers and the reverse motor model is used to calculate appropriate reference voltages. Moreover a modulator is usually used to generate the computed reference voltages [20] [21]. Figure 1-5-1 shows the basic structure of predictive deadbeat control for a five-phase BLDC machine.

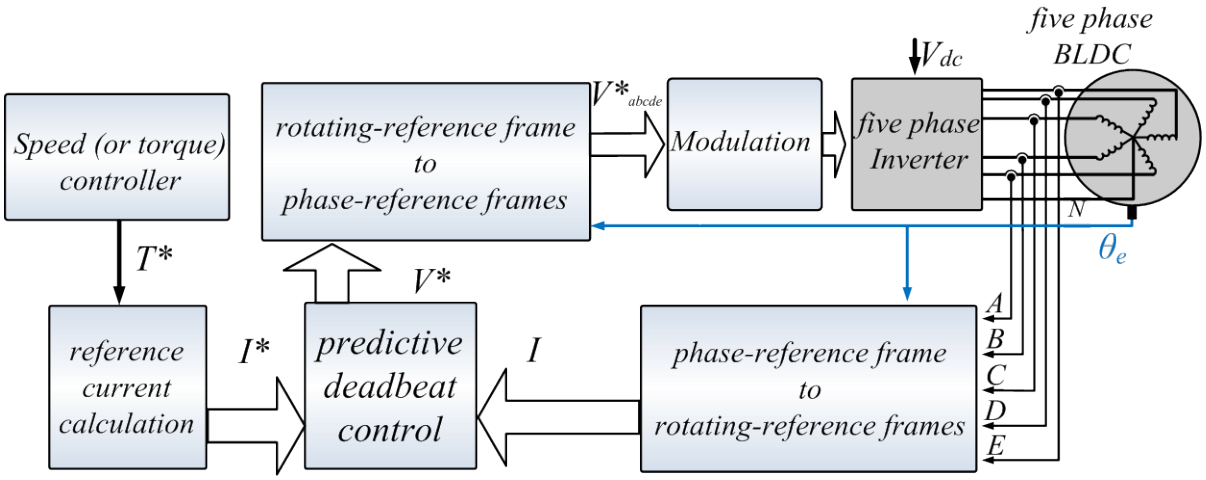

Fig. 1-5-1 General block diagram of current control in rotating reference frames

While controlling the stator currents of a PM machine by PDC algorithm, the motor model is directly used to estimate the future values of system outputs (currents). Consequently, the precision of model parameters play an important role in final accuracy of the estimated values. Moreover, stator currents are

measured at the beginning of MPC algorithm, and as a result, measurement noise can also affect the precision of controlling algorithm [22].

Extended Kalman filter (EKF) is a powerful recursive estimation algorithm which can be used to reduce the effect of parameter variation and measurement noise. All available measurements are processed by EKF regardless of their accuracy to provide a fast and precise estimation of all system states [23].

Although the computational load of EKF algorithm is quite high, but as the model of healthy machine is simple in rotating reference frame, it is possible to use this method for reducing the effect of introduced disturbances of electrical drive. On the other hand, under faulty conditions, additional equations should be added to machine´s model to consider the impact of winding faults in five-phase BLDC machines. These new equations will increase the computational load of predictive deadbeat controllers. Moreover, under faulty conditions, appropriate reference current values have oscillating dynamics which require higher sampling frequency and less computational time in controlling unit. As a result, EKF is not combined with predictive deadbeat controllers under faulty conditions. Figure 1-5-2 illustrates the general steps of applied control methodologies along this thesis.

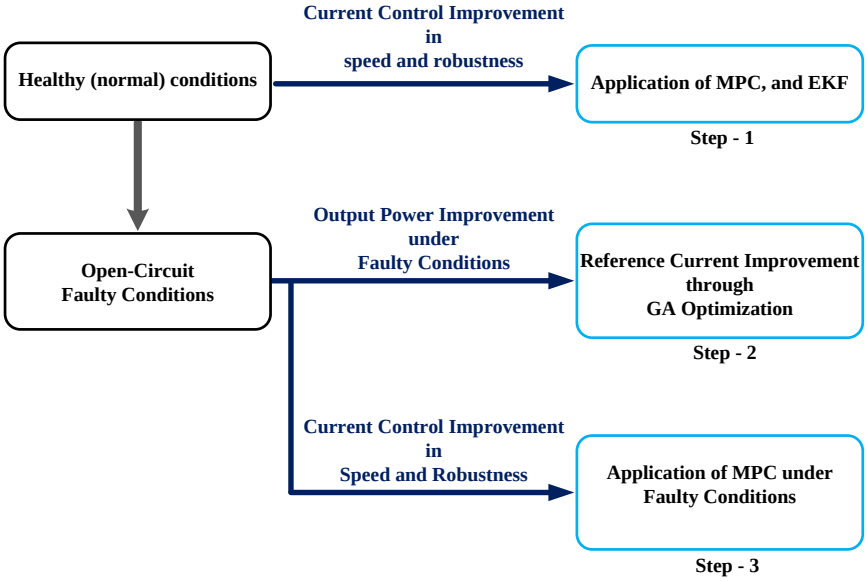

Fig. 1-5-2 General steps of applied controlling methods for different operational conditions of five-phase BLDC machine

1.6. Chapter descriptions

A general review on different controlling algorithms is conducted in **chapter 2**. The basics of FOC and DTC are explained, and a brief review on different fault categories in electrical machines is presented. In addition, two fault tolerant inverter structures are briefly reviewed namely double-switch redundant topology, and phase redundant topology.

Predictive deadbeat control is one of the important categories of model predictive control methods in which the reverse system model is used to calculate the appropriate inputs for the next iteration of

controlling process. The main focus of **chapter 3** is to propose a new improved deadbeat algorithm to control the stator currents of a five-phase BLDC machine. Extended Kalman filter is used in the estimation step of the proposed method, and system model equations are used to calculate the appropriate voltages for the next modulation period. Two aspects of proposed controlling method are evaluated including its sensitivity to system variations and its speed in following the reference currents during transient states. Proposed controlling method is evaluated both by simulations and experimental evaluations.

Chapter 4 is dedicated to improve the output power of five-phase BLDC motors under different faulty conditions. Different machine connections are considered while having open circuit fault in one and two stator phases, and both fundamental and third harmonic component of stator currents are controlled to improve the amplitude and quality of generated torque under faulty conditions. Rated RMS value of stator phase currents is considered as the main limiting factor of generated electrical torque. Genetic algorithm (GA) is used in the optimization procedure of stator reference currents to avoid additional simplifying constraints and gain more output power under the fault. To verify the theoretical developments, experimental tests are conducted on a five-phase BLDC motor with in-wheel outer-rotor configuration.

In **chapter 5**, model predictive deadbeat controllers are proposed to control the stator currents of five-phase BLDC machines under normal and faulty conditions. Open circuit fault is considered for both one and two stator phases, and the behaviour of proposed controlling method is evaluated. This evaluation is generally focused on first, sensitivity of proposed controlling method and second, its ability in following reference current values with fast speed. Proposed method is simulated and is verified experimentally on a five-phase BLDC drive

In **chapter 6**, the efficiency of an outer-rotor five phase BLDC drive is evaluated under normal and different faulty conditions. Open-circuit fault is considered for one, two adjacent and two non-adjacent faulty phases. Iron core losses are calculated via FEM simulations in Flux-Cedrat® software, and moreover, inverter losses and winding copper losses are simulated in MATLAB® environment. Experimental evaluations are conducted to evaluate the efficiency of the entire BLDC drive which verifies the theoretical developments.

In **Chapter 7** the thesis work is analyzed from a general point of view, and the conclusions and contributions are clearly exposed.

Finally, the publications and collaborations resulting from the research work development are presented in **Chapter 8.**

1.7. References

[1] H. Zhu, X. Xiao, Y. Li, ”Torque Ripple Reduction of the Torque Predictive Control Scheme for Permanent-Magnet Synchronous Motors”, IEEE Transactions on Ind. Elec., Vol. 59, No. 2, February 2012

[2] K. Atallah, J. Wang, D. Howe, “Torque-Ripple Minimization in Modular Permanent-Magnet Brushless Machines”, IEEE Trans. on Ind. App., vol. 39, no. 6, Nov/Dec 2003

[3] L. Parsa, H. A. Toliyat, “Fault-Tolerant Interior-Permanent-Magnet Machines for Hybrid Electric Vehicle Applications”, IEEE Trans. on Vehicular Technology, vol. 56, no. 4, July 2007

[4] J. D. Ede, K. Atallah, J. Wang, D. Howe, “Effect of Optimal Torque Control on Rotor Loss of Fault-Tolerant Permanent-Magnet Brushless Machines”, IEEE Trans. on Magnetic, vol. 38, no. 5, Sep. 2002

[5] N. Bianchi, S. Bolognani, M. Dai Pré, “Strategies for the Fault-Tolerant Current Control of a Five-Phase Permanent-Magnet Motor”, IEEE Trans. on Ind. App., vol. 43, no. 4, July/August 2007

[6] J. Wang, K. Atallah, D. Howe, "Optimal Torque Control of Fault-Tolerant Permanent Magnet Brushless Machines", IEEE Trans. on Magnetics, vol. 39, no. 5, Sep. 2003

[7] L. Parsa, H. A. Toliyat, A. Goodarzi, “Five-Phase Interior Permanent-Magnet Motors With Low Torque Pulsation”, IEEE Trans. On Ind. App., vol. 43, no. 1, Janurary/February 2007

[8] F. Baudart, B. Dehez, E. Matagne, D. Telteu-Nedelcu, P. Alexandre, Fr. Labrique, “Torque Control Strategy of Polyphase Permanent-Magnet Synchronous Machines with Minimal Controller Reconfiguration under Open-Circuit Fault of One Phase”, IEEE Trans. On Ind. Elec., vol. 59, no. 6, June 2012

[9] L. Parsa, H. A. Toliyat, “Sensorless Direct Torque Control of Five-Phase Interior Permanent-Magnet Motor Drives”, IEEE Trans. on Ind. App., vol. 43, no. 4, July/August 2007

[10] L. Guo, L. Parsa, “Model Reference Adaptive Control of Five-Phase IPM Motors Based on Neural Network”, IEEE Trans. on Ind. Elec., vol. 59, no. 3, March 2012

[11] D. Diallo, M. E. H. Benbouzid, and A. Makouf, “A Fault tolerant control architecture for induction motor drives in automotive applications” IEEE Trans. Veh. Technol., vol. 53, no. 6, pp. 1847–1855, Nov. 2004.

[12] A. Garcia, J. Cusido, J. Rosero, J. Ortega, and L. Romeral, “Reliable electro-mechanical actuators in aircraft,” IEEE Aerosp. Electron. Syst. Mag., vol. 23, no. 8, pp. 19–25, Aug. 2008.

[13] M. Villani, M. Tursini, G. Fabri, L. Castellini, “High Reliability Permanent Magnet Brushless Motor Drive for Aircraft Application”, IEEE Trans. on Ind. Elec., vol. 59, no. 5, May 2012

[14] Y.Jeong, S.Sul, S. E. Schulz, N. R. Patel, “Fault Detection and Fault-Tolerant Control of Interior Permanent-Magnet Motor Drive System for Electric Vehicle”, IEEE Trans. on Ind. App., vol. 41, no. 1, Jan./Feb. 2005

[15] S. Dwari, L. Parsa , “An Optimal Control Technique for Multiphase PM Machines Under Open-Circuit Faults”, IEEE Trans. on Ind. Elec., vol. 55, no. 5, May 2008

[16] J. D. Ede, K. Atallah, J. Wang, .D. Howe, “Effect of Optimal Torque Control on Rotor Loss of Fault-Tolerant Permanent-Magnet Brushless Machines”, IEEE Trans. on Magnetics, vol. 38, no. 5, Sep. 2002

[17] Dwari, S., Parsa, L. :'Fault-Tolerant Control of Five-Phase Permanent-Magnet Motors With Trapezoidal Back EMF', IEEE Trans. Ind. Electron., 2011 , 58 , (2), pp 476 – 485

[18] A. Linder and R. Kennel, “Model predictive control for electrical drives,” in Proc. IEEE Power Electron. Spec. Conf., Recife, Brazil, 2005, pp. 1793–1799.

[19] P. Cortés, M. P. Kazmierkowski, R. M. Kennel, D. E. Quevedo, and J. Rodríguez, “Predictive control in power electronics and drives,” IEEE Trans. Ind. Electron., vol. 55, no. 12, pp. 4312–4324, Dec. 2008.

[20] A. Linder and R. Kennel, “Model predictive control for electrical drives,” in Proc. IEEE Power Electron. Spec. Conf., Recife, Brazil, Jun. 2005, pp. 1793–1799.

[21] S. Mariethoz, A. Domahidi, and M. Morari, “Sensorless explicit model predictive control of permanent magnet synchronous motors,” in Proc. IEEE Int. Elect. Mach. Drives Conf.,Miami, FL,May 2009, pp. 1250–1257.

[22] Errouissi, Rachid ; Ouhrouche, M. ; Wen-Hua Chen ; Trzynadlowski, A.M.
Robust Cascaded Nonlinear Predictive Control of a Permanent Magnet Synchronous Motor With Antiwindup Compensator
IEEE Transactions on Industrial Electronics Volume: 59 , Issue: 8

[23] R. Dhaouadi, N. Mohan, and L. Norum, “Design and implementation of an extended Kalman filter for the state estimation of a permanent magnet synchronous motor,” IEEE Trans. Power Electron., vol. 6, pp. 491–497, July 1991.

2.

Chapter 2 Fault Tolerant Control of Permanent Magnet Machines – Literature Review

Fault tolerant concept is becoming more important in high safety applications where sudden interruptions are not acceptable. Electrical vehicles and more electric aircrafts are good examples of such systems where high safety and being able to operate after fault occurrence is crucial. A fault tolerant system should be able to operate under faulty conditions, or shut down the system in a safe manner.

Fault tolerant concept in PM electrical drives is dependent on the mechanical structure of the motor, inverter configuration and control algorithm. In this chapter, a literature review will be conducted on different aspects of fault tolerant PM drives. These aspects include three-phase and multi-phase motor structures, basic controlling methods of PM machines, different fault types of PM drives, fault tolerant control and fault tolerant inverter structures.

CONTENTS

2.1 Introduction – Multiphase Electrical Drives

Comparing to 3-phase machines, multiphase systems, namely 5-phase machine are distinguished with several advantages which make them proper candidates in applications where safety and reliability is important. They have more abilities to work after the occurrence of fault in one (or even two) of the phases.

In this chapter of the dissertation, a general review on different current controlling algorithms of PM machines is conducted. Field Oriented Control (FOC) and Direct Torque Control (DTC) are the main standards in the field of PM stator current control.

The basics of these two controlling methods are explained in the following. A brief review on different fault categories in electrical machines is presented including air-gap eccentricity, bearing damage, stator faults, actuator faults, and sensor faults. In addition, two fault tolerant inverter structures are briefly reviewed namely double-switch redundant topology, and phase redundant topology.

Multi-phase PMSM can continue its operation after loss of one, or even two of its phases. This capability is very important in applications where safety is the first priority. In other words, under the lack of opened phases, the remaining phases should provide an undisturbed rotating MMF.

The most important types of electric drives can be classified in four different groups namely DC, Induction, Switched Reluctance SR, and PM BL drives, which are summarized in Fig. 2-1-1 [1]. As it can be seen, there are two main categories, namely the brushed, and brushless, and each one of these categories, can be divided into variable subgroups.

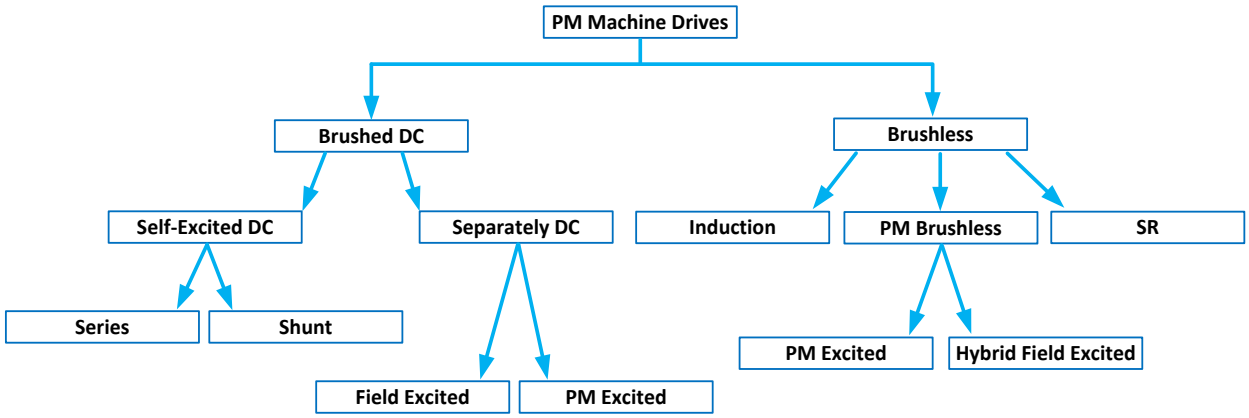

Figure 2-1-1: classification of more important PM drive types [1]

The simplest controlling algorithms are related to DC Drives. This is due to the orthogonal disposition of field and armature MMFs in these types of machines. However, regarding their commutators and brushes, the DC drives have never been a good option for maintenance free operation [1].

On the other hand, in the brushless category, the Induction Drives are the most accepted type which is due to their low price, high reliability, and low required maintenance. The main challenge in controlling

Induction Machines is related to their nonlinear behaviour. However, with the increasing power of microcomputers, the principle of Field Oriented Control is effectively used to overcome their nonlinearities. In addition, other more advanced controlling methods like efficiency-optimizing-control (EOC) are also developed which increase the efficiency.

SR Drives are very simple to construct. They are not expensive, and they have outstanding torque-speed characteristics. But from the control point of view, they usually exhibit high torque ripple and acoustic-noise problems and their design is very challenging.

The main focus of this study will be on AC Permanent Magnet Brushless Machines, namely BLAC Drives. There are several outstanding advantages in this category. Regarding low rotor losses, PM machines are very efficient, and due to their magnets, these machines usually have high power density, and they are reliable. The main weak point is their high cost which is because of their magnets.

BLAC machines are mainly divided in two categories, namely permanent magnet synchronous machines (PMSM), which have sinusoidal back-EMF, and brushless dc machines (BLDC) that have trapezoidal back-EMF [1].

2.1.1 Multi-Phase Electrical Motors

Electrical motors with more than three phases are usually called as Multi-Phase machines. Facing with faulty conditions, multiphase systems are distinguished with several advantages which make them proper candidates in applications where safety and reliability is important. Comparing to three-phase machines, multiphase systems, namely 5-phase machines have several advantages under faulty conditions. They have more abilities to work after fault occurrence in one (or even two) of the phases. To continue the operation under faulty conditions, it is only required to change the controlling algorithm, and there is no crucial need to additional hardware such as extra inverter leg, or neutral point connection [2].

Multiphase machines contain other benefits which can be summarized as:

- Lower amplitude of currents in each phase
- Lower torque ripples with higher ripple frequency
- Reduced operational noise
- Reduced copper loss in the stator.

In fact, five-phase PMSMs produce higher torque (around 15%) and less torque ripple (around 71% less) than initial three-phase PMSMs with the same copper loss [3].

2.2 Design of Multiphase Electrical Machines

To have better fault tolerant capabilities, there are several options which should be considered while designing multiphase machines and their controlling drives. The main parameters are simply explained in [4] as:

- The windings should be concentrated around each tooth to reduce the mutual thermal and magnetic effect between coils
- Low mutual inductance between phases to reduce the short circuit current effect
- Increasing the self-inductance of each phase to reduce the short circuit current. To reduce the amplitude of short circuit current below 1 PU, it is required to increase the self-inductance higher than 1 PU.

In addition, by using full-bridge PWM converter for each phase, the current of each phase can be controlled separately without affecting other phases. Complementing these approaches, there are several studies in literatures regarding the design and control of fault tolerant multi-phase PMSMs. Regarding the industrial applications of voltage source inverter (VSI) drives, the design methodology of multiphase PMSMs supplied by PWM VSI is considered in [3].

In [5] and [6] the design of five-phase interior permanent magnet machine (IPM) is considered to reduce the produced torque pulsations. The mathematical model of the machine is derived to consider the most efficient combination of slot number, winding distribution, and phase numbers. In addition the appropriate fault tolerant control strategy is proposed.

Fractional-slot concentrated windings configuration is also considered in [4] to reduce the effect of machine phases on each other. That is to reduce the electrical, magnetic and thermal effect of each phase on others. Other winding configurations like polygonal-winding have also been considered in literatures [7].

In addition, there are several attempts to design fault tolerant axial flux PMSMs in literatures. Seven-phase axial flux PMSMs are considered in [8] using finite element method (FEM) simulation, and in additions there are other studies to improve the torque and power of in-wheel axial flux permanent magnet machines (AFPM) in [9].

2.3 Basic Controlling Methods of PM Machines

Aiming to have a prefect control on the machine, Field-Oriented Control (FOC) and Direct-Torque Control (DTC) were introduced to the world respectively in the 70´s and 80´s, and now, they are recognized as two high-performance control strategies for PM drives. The main objectives are to perfectly control the machine´s torque and flux, namely to track the command trajectory under variable loads and disturbances [10].

There are other controlling methods which can be combined with the basic principles of FOC and DTC to improve the behavior of PM machines. Sensorless methods, expert and artificial intelligent controlling systems (AIC), and model predictive control (MPC) methods are some examples of these advanced controlling algorithms. In the following sections, the basic principles of FOC and DTC will be explained, and a brief review will be presented on advanced types of current control in these machines.

2.3.1 Direct Torque Control

Direct torque control (DTC) method was first introduced in 1985, and regarding its fast torque and flux control, it was widely used in the control of electrical motors. Its application in electrical drives is simple [11] [12] [13].

Its application to control PMSMs was first simulated in 1997 [14]. Implementing more advanced methods, hysteresis controllers were replaced by PI controllers in PMSM DTC, and their relationship with produced torque is analyzed [15].

Several reviews have been done on different DTC strategies and their associated problems including current measurement problems, rotor resistance variation, and position measurement [13] [16]. Figure 2.3.1 shows the basic principles of direct torque controlled PMSM drive system.

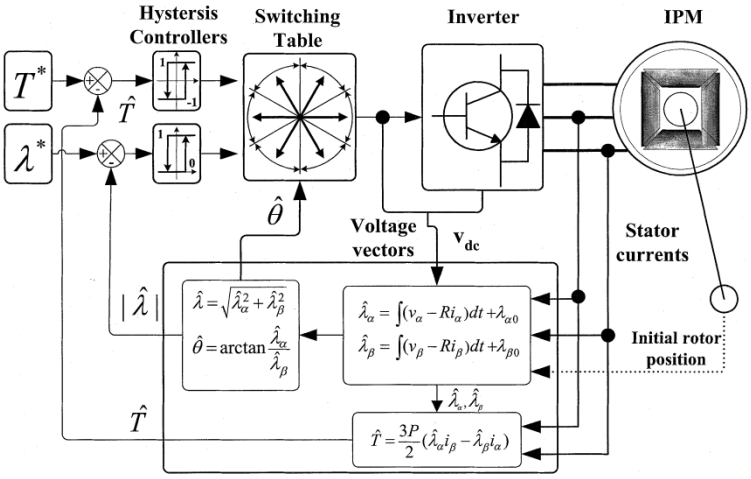

Fig. 2.3.1 Block diagram of direct torque control scheme

The basic principle in DTC is to control the position and amplitude of stator magnetic flux by selecting proper voltage vector using a pre-defined switching table. In simplest form, the stator flux linkage can be calculated as:

$$\phi_s(t) = \int_0^t (V_s - R_s I_s)dt + \phi_{s0}$$

Eq. 2-3-1

where ϕ_{s0} is the initial value of the stator flux linkage. The stator voltage is equal to the output voltage of the inverter.

$$V_s(S_A; S_B; S_C) = \frac{2}{3}U_0(S_A + S_B e^{j2\pi/3} + S_C e^{j4\pi/3})$$

Eq. 2-3-2

S_A, S_B and S_C represent the states of the inverter legs, 1 meaning that the phase is connected to the positive terminal of the DC voltage source and 0 meaning that the phase is connected to the negative. Measuring the three phase currents, the stator current space vector can be presented as:

$$i_s = \frac{2}{3}(i_A + i_B e^{j2\pi/3} + i_C e^{j4\pi/3})$$

Eq. 2-3-3

Figure 2-3-2 presents the obtained voltage vectors.

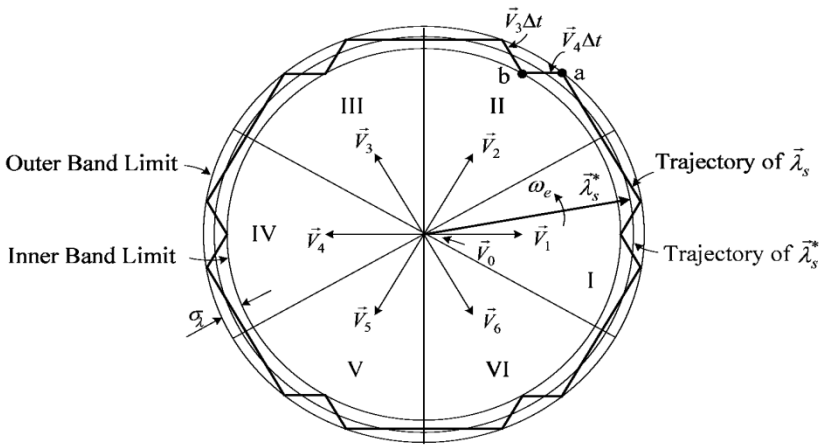

Figure 2-3-2 voltage vectors for DTC

The composite α and β components of vector ϕ_s can be calculated using the following equations:

$$\begin{cases} \phi_{sa} = \int_0^t (V_{sa} - R_s I_{sa})dt \\ \phi_{s\beta} = \int_0^t (V_{s\beta} - R_s I_{s\beta})dt \end{cases}$$

Eq. 2-3-4

and stator flux linkage and its electrical angle will be derived as:

$$\phi_s = \sqrt{(\phi_{sa})^2 + (\phi_{s\beta})^2}$$

$$\theta_s = arctg\frac{\phi_{s\beta}}{\phi_{sa}}$$

Eq. 2-3-5

The basics of DTC for five-phase PMSM are similar to its three-phase version, except in this case, there are more active vectors available, and as a result, the flexibility of five-phase DTC is more.

As it can be seen, DTC is only dependent on the stator resistance which is only important in low speed operations. The amplitude of inductances and the rotor magnetic flux constant (which are dependent on saturations and temperature) are not used in hysteresis controllers [14] [15] [17] [18]. As the current controllers are not used to control in DTC scheme, there is no need for coordinate transformation, and as a result, using a position sensor is not crucial either. But to have control on the speed, and in addition to make the whole scheme more robust, the soft estimation of position and speed is of interest. In [19], sensorless DTC is developed for a multiphase PMSM.

Normally, the bandwidth of flux controllers in DTC is set at 5% of stator flux rated value. The ripples of produced torque and flux are the main consideration of DTC. It is shown that while operating with low values of stator flux, the sampling interval must be very small (40 us for induction motors, and even 10 us for PMSM machines) [14]. This is because the inverter remains at the same switching state as long as the outputs of flux and torque hysteresis controllers remain unchanged. Another main consideration is the variable switching frequency, which changes with speed, load torque, and bandwidth of flux and torque hysteresis controllers. Recently, multilevel inverters which provide more voltage space vector are used in DTC scheme to reduce the flux and torque ripple. Another solution is to use multiphase machines. For example in a five phase system, there are inherently 32 space vectors which prepare more flexibility in switching [19].

2.3.2 Field Oriented Control

2.3.2.1 Motor Model Used in FOC of PM Machines

The basic voltage equations of PMSM in ABC reference frame can be written as:

$$u_s^s = R_s i_s^s + d\psi_s^s / dt$$

Eq. 2-3-6

FOC is mainly focused on the control of dq components of current. The following equations can be used to transfer the real ABC current values to dq coordination which is rotating with synchronous frequency in PMSM. Assuming that dq frame is rotating with $\omega = \omega_k = \omega_s$ it can be written[1][20]:

$$u_s^s = u_s^k e^{j\vartheta_k}$$

Eq. 2-3-7

$$i_s^s = i_s^k e^{j\vartheta_k}$$

[1] Subscript *s* refers to $\alpha\beta$ frame, and subscript *f* refers to dq frame variables.

Eq. 2-3-8

$$\psi_s^s = \psi_s^k e^{j\vartheta_k}$$

Eq. 2-3-9

$$\Rightarrow \frac{d}{dt}\psi_s^s = e^{j\vartheta_k}\frac{d}{dt}\psi_s^k + \psi_s^k (j\omega_k e^{j\vartheta_k})$$

Eq. 2-3-10

By substituting Eq. (2-3-7)-(2-3-9) in (2-3-10), it can be derived that:

$$u_s^f = R_s i_s^f + \frac{d}{dt}\psi_s^f + j\omega_s \psi_s^f$$

Eq. 2-3-11

$$\psi_s^f = L_s i_s^f + \psi_p^f$$

Eq. 2-3-12

while L_s is the stator inductance including leakage inductance and rotor mutual inductance ($L_s = L_{\sigma s} + L_m$). Moreover, ψ_p^f is the rotor magnet flux, and as d-axis is oriented with magnet flux, its projection on q axis would be zero[2]:

$$\psi_p^f = \psi_{pd} + j\psi_{pq} = \psi_{pd} + 0 = \psi_{pd}$$

Eq. 2-3-13

$$\psi_{sd} = L_{sd} i_{sd} + \psi_p$$

Eq. 2-3-14

$$\psi_{sq} = L_{sq} i_{sq}$$

Eq. 2.3.15

Substituting (2-3-14) and (2-3-15) in (2-3-9) will result in:

$$u_{sd} + ju_{sq} = R_s(i_{sd} + ji_{sq}) + \frac{d}{dt}\left[(L_{sd} i_{sd} + \psi_p) + j(L_{sq} i_{sq})\right] + j\omega_s\left[(L_{sd} i_{sd} + \psi_p) + j(L_{sq} i_{sq})\right]$$

$$\Rightarrow u_{sd} = R_s i_{sd} + L_{sd}\frac{d}{dt} i_{sd} - \omega_s L_{sq} i_{sq}$$

[2] These equations are written for a simple model of PMSM (PMSM without DC windings). In the case of using stator DC windings (which is inevitable in high speed applications), it is important to consider the magnetic flux of DC windings in the calculation of dq voltages and produced torque. The calculations would not be very different, and if the sampling frequency is high enough, the equivalent term for DC winding will be similar to ψ_p as a constant coefficient in (12).

Eq. 2.3.16

$$\Rightarrow u_{sq} = R_s i_{sq} + L_{sq}\frac{d}{dt} i_{sq} + \omega_s L_{sd} i_{sd} + \omega_s \psi_p$$

Eq. 2.3.17

As a result by adjusting the applied voltage in d and q directions, the exact values of dq currents can be achieved. Figure 2-3-3 presents the basic block diagram of FOC.

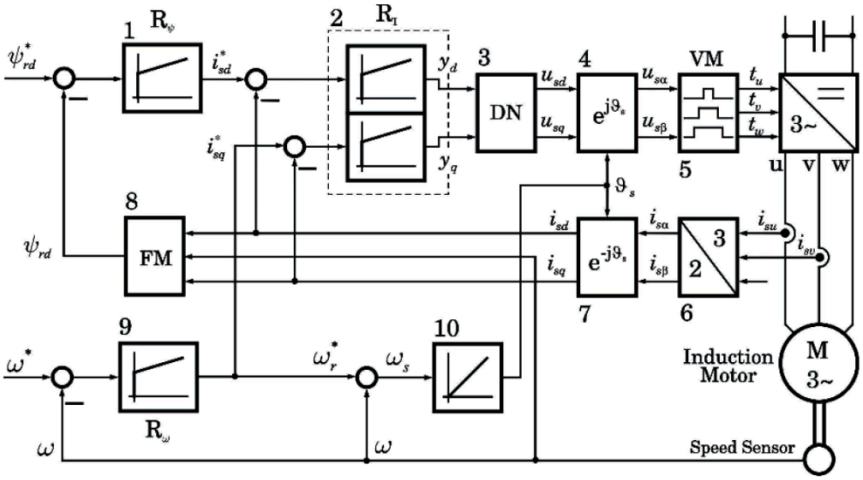

Figure 2-3-3 Block diagram for the field oriented control strategy for a PMSM

Regardless from three-phase systems, the general vector control can be extended for an n-phase PMSM [20]. The following transformation can be used to transform five-phase parameters to alpha-beta plane.

$$\begin{bmatrix} x_0 \\ x_1 \\ x_2 \\ x_3 \\ x_4 \end{bmatrix} = \begin{pmatrix} 1 & 1 & 1 & 1 & 1 \\ 1 & a^1 & a^2 & a^3 & a^4 \\ 1 & a^2 & a^4 & a^6 & a^8 \\ 1 & a^3 & a^6 & a^9 & a^{12} \\ 1 & a^4 & a^8 & a^{12} & a^{16} \end{pmatrix} \begin{bmatrix} V_0 \\ V_1 \\ V_2 \\ V_3 \\ V_4 \end{bmatrix}$$

Eq. 2-3-18

while $a = e^{(j2\pi/5)}$

The first row of transformation matrix is to compute the zero component, while the second (or fifth) row, and fourth (or third) row can be used to transform the first and third harmonics respectively into alpha-beta plane.

Selecting the first, second and fourth rows of (2-3-18), five-phase Clarke transformation can be written as:

$$\begin{bmatrix} x_1 \\ x_3 \\ x_0 \end{bmatrix} = \begin{bmatrix} 1 & a^1 & a^2 & a^3 & a^4 \\ 1 & a^3 & a^6 & a^9 & a^{12} \\ 1 & 1 & 1 & 1 & 1 \end{bmatrix} \begin{bmatrix} V_0 \\ V_1 \\ V_2 \\ V_3 \\ V_4 \end{bmatrix}$$

Eq. 2-3-19

which can be illustrated in Fig. 2-3-4

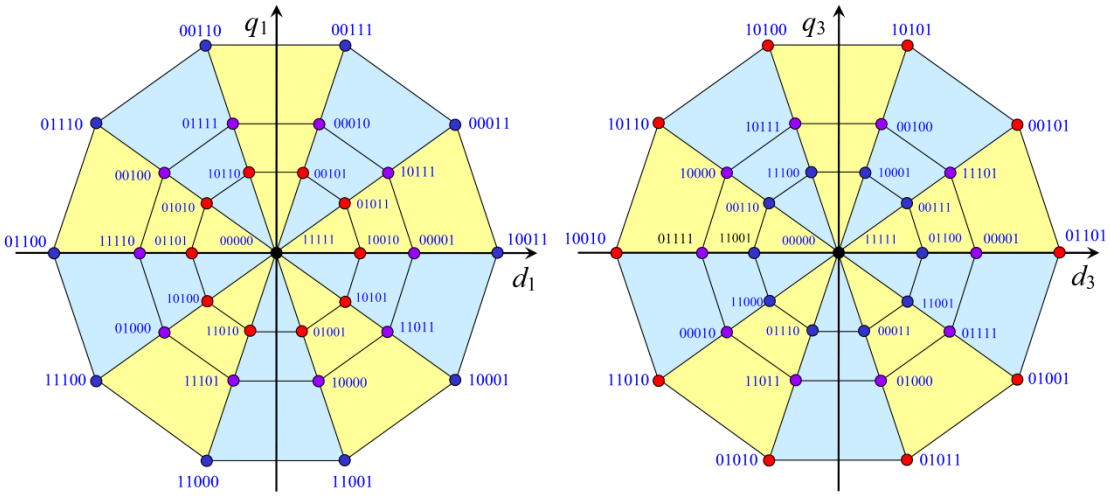

Figure 2-3-4 Multiple space vectors of a five-phase inverters, represented in planes d_1-q_1 and d_3-q_3

By using the rotational coordination, Park transformation can be derived for five-phase systems as:

$$\begin{bmatrix} x_1 \\ x_3 \\ x_0 \end{bmatrix} = \begin{bmatrix} 1e^{-j\omega t} & a^1e^{-j\omega t} & a^2e^{-j\omega t} & a^3e^{-j\omega t} & a^4e^{-j\omega t} \\ 1e^{-j3\omega t} & a^3e^{-j3\omega t} & a^6e^{-j3\omega t} & a^9e^{-j3\omega t} & a^{12}e^{-j3\omega t} \\ 1 & 1 & 1 & 1 & 1 \end{bmatrix} \begin{bmatrix} V_0 \\ V_1 \\ V_2 \\ V_3 \\ V_4 \end{bmatrix}$$

Eq. 2-3-20

Which can again be rewritten as:

$$\begin{bmatrix} x_{d1} \\ x_{q1} \\ x_{d3} \\ x_{q3} \\ x_0 \end{bmatrix} = \frac{2}{5}\begin{bmatrix} \cos(\omega t) & \cos(\omega t-2\pi/5) & \cos(\omega t-4\pi/5) & \cos(\omega t-6\pi/5) & \cos(\omega t-8\pi/5) \\ -\sin(\omega t) & -\sin(\omega t-2\pi/5) & -\sin(\omega t-2\pi/5) & -\sin(\omega t-2\pi/5) & -\sin(\omega t-2\pi/5) \\ \cos 3(\omega t) & \cos 3(\omega t-2\pi/5) & \cos 3(\omega t-4\pi/5) & \cos 3(\omega t-6\pi/5) & \cos 3(\omega t-8\pi/5) \\ -\sin 3(\omega t) & -\sin 3(\omega t-2\pi/5) & -\sin 3(\omega t-2\pi/5) & -\sin 3(\omega t-2\pi/5) & -\sin 3(\omega t-2\pi/5) \\ 1 & 1 & 1 & 1 & 1 \end{bmatrix}\begin{bmatrix} V_0 \\ V_1 \\ V_2 \\ V_3 \\ V_4 \end{bmatrix}$$

Eq. 2-3-21

Similar to three-phase case, five-phase PMSM FOC is dependent on the basic equations of the machine. The basic algorithms of control modeling and vectorial decomposition is particularly considered for a five-phase machine in [21] and [22], and it is shown that from the torque point of view, a five-phase machine can be considered as two magnetically decoupled PMSMs [21] [23]. These equations will be developed in the next chapter.

Different space vector modulation techniques are used to improve the vector control of PMSMs in [22]. In addition to PMSM type of machines, 3rd harmonic injection is used to increase the torque amplitude in five-phase reluctance motor up to 110% its value in normal operation [24].

Moreover, reference [25] takes the advantage of quasi-rectangular winding, and as mentioned before, by deriving the machine´s equations in rotating reference frame, vector control can be used for a semi-BLDC type of five-phase PM machine.

2.3.2.2 Field Weakening Strategies under Faulty and Healthy Conditions of Multi-Phase Machines

By weakening the machine´s flux above the base speed, torque control can be improved. This adjustment is done in [26] to analyze the behavior of flux weakening control of a five-phase PMSM under healthy and faulty conditions.

This method is investigated in [27] in the case of using carrier-based PWM and multidimensional-orthogonal-decomposition vector control of five-phase PMSM.

2.3.3 Advanced Controlling Methods

There are several advanced controlling strategies which can be added to DTC and FOC to improve the machine´s behavior. All artificial-intelligence-based control strategies (AIC) can be considered in this group. Among these, fuzzy logic control, neural networks, genetic control, Nero-fuzzy control, and model predictive control (MPC) are the most important groups which can be used to cope with the nonlinearities and parameter variations of PMSMs [1] [28]. The combination of fuzzy logic and traditional PID controllers is simulated in [29] to result in a better field oriented control on five-phase PMSM.

In addition, model predictive control is simulated [30], and also implemented to control multi-phase PMSMs (namely 5 and 6 phase PMSMs) [31].

In the field of electric drives, MPC algorithms can be generally divided into two main categories. The first group is an extension of traditional direct-torque control (DTC) in which the lookup table is removed and optimized switching state of the inverter is computed directly in MPC algorithm to minimize a predefined cost function [32][33][34][35]. This cost function should be computed for all possible switching states, and as a result the computational burden of controlling algorithm is relatively high. By appearance of powerful digital processors, it is now possible to use this algorithm for fast dynamic systems such as PM drives [36], [37]. Considering the finite amount of possible switching states in the converter unit, this type of control algorithm is also famous as “finite set model predictive control” (FS-MPC). However, higher number of inverter legs and possible switching states, results in higher computational burden of MPC algorithm in multiphase motor drives [38].

On the other hand, the second group can be considered as an extension of traditional field-oriented control. In this group, the inner PI controllers are removed and replaced by predictive controllers and the reverse motor model is used to calculate appropriate reference voltages. Moreover a modulator is usually used to generate the computed reference voltages [39] [40].

Position information is almost crucial in high performance PM drives, but using position sensors is costly, and reduces the reliability of the system. Consequently, position sensorless control (PSC) is becoming attractive [1]. The main strategies of PSC of PMSMs can be classified as [19]:

- Inductance changes due to saturation
- Flux estimation
- High frequency signal injection
- Back-EMF evaluation
- State observers

It should be reminded that all of PSC methods can be potentially combined with other control strategies like DTC, FOC and MPC.

2.3.4 Comparison of Control Strategies

Table 2-3-1 summarizes the main advantages and weak points of aforementioned control strategies, and the corresponding control block diagrams are illustrated in Fig. 2-3-5 [1].

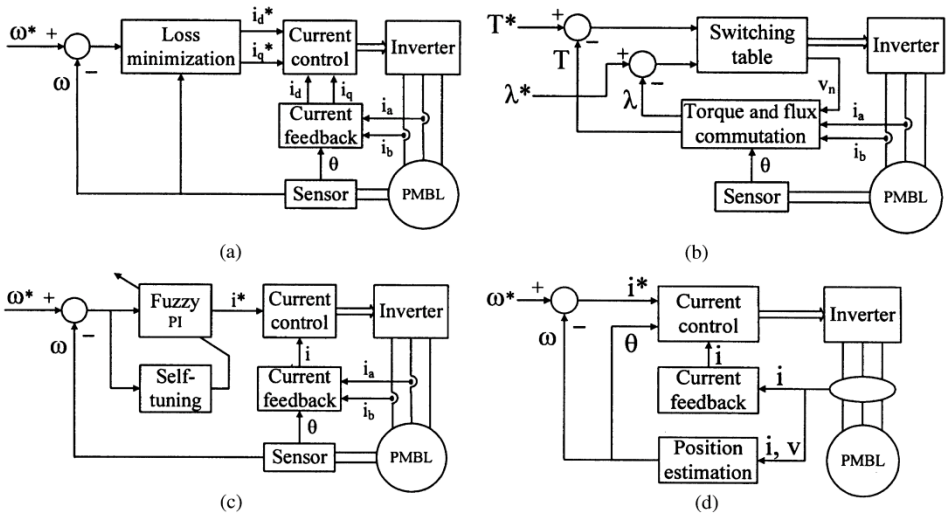

Figure 2-3-5 simplified controlling block diagrams (a) FOC. (b) DTC. (c) AIC. (d) PSC [1]

Table 2-3-1 Comparison of Control Strategies

	Advantages	Disadvantages	Techniques
FOC	Low losses, wide speed range, powerful capabilities under faulty conditions.	Higher computational load. Position information requirement. Dependency on PMSM parameters	Direct control of d and q axis currents.
DTC	Fast dynamics of torque. No need for direct current control. Low parameter dependency.	Variable switching frequency. Dependency to variation of stator.	Impose the voltage vectors depending on the amplitude of torque and flux.
AIC	High flexibility in control. Adaption to nonlinearities and parameter variation.	Require expert knowledge. High computational load.	Incorporate fuzzy logic, neural network, or other AI into traditional control
PSC	No need for physical sensor control. Can be combined to other controlling strategies.	High computational load.	Estimate position by using the variation of inductances, or back EMF, or other observers

2.4 Different Faults in PM Drives

The most important fault categories of PM machines are illustrated in Fig. 2-4-1 [41]. There are several reasons which can lead to mechanical and electrical faults in PM drives such as mechanical wearing, harsh working environment, aging and severe voltage stresses regarding the inverter output [42]. In Fig. 2-4-1 and Fig. 2-4-2, the main categories of different faults will be explained briefly, and they are discussed in next paragraphs.

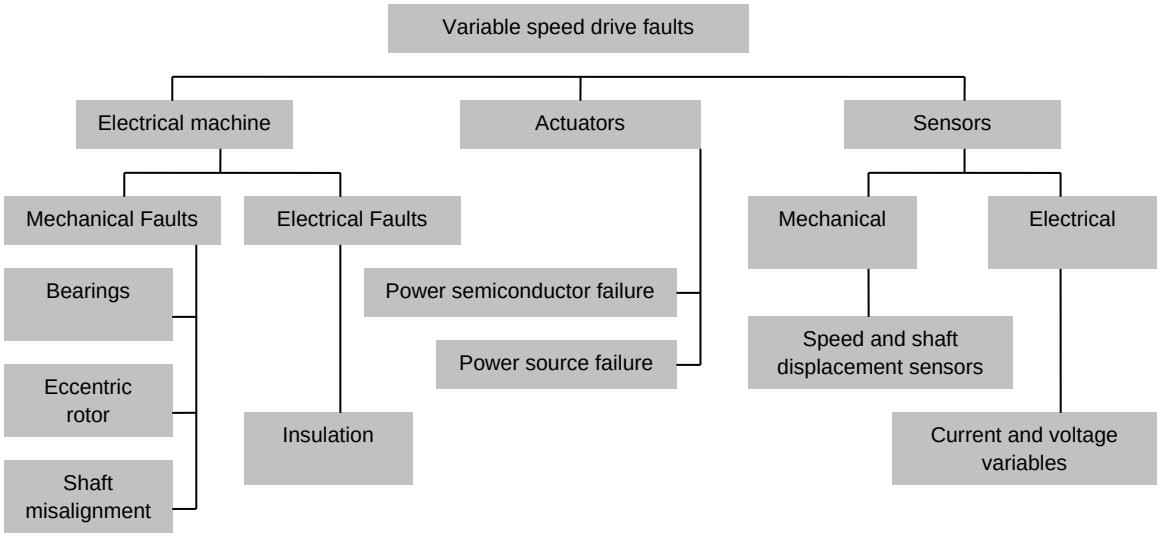

Figure 2-4-1 The most typical faults in variable speed drive systems

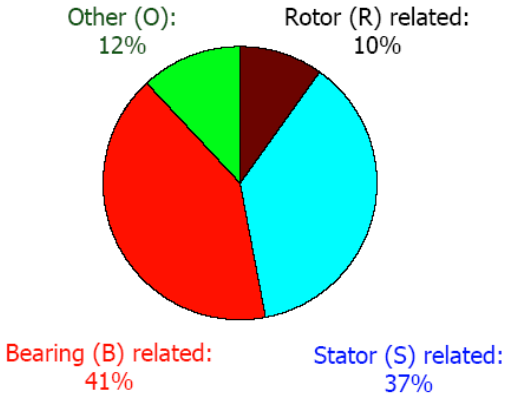

Figure 2-4-2 General distribution of fault categories in electrical motors

2.4.1 Air-Gap Eccentricity

This fault is due to an unequal air gap distributed between rotor and stator which results in unbalanced radial forces in the machine. There are mainly two types of eccentricity namely static eccentricity and dynamic eccentricity. Static eccentricity can have several reasons like false positioning of the rotor or stator while assembling. On the other hand, in dynamic eccentricity, the position of maximum air gap is a function of time and space and is dependent on the position of the rotor. The main reasons of dynamic eccentricity can be bearing wear, bearing misalignment and thermal bowing of the rotor [42].

2.4.2 Bearing Damage

Almost 40-50% of all motor faults are related to bearings which can be classified as: (a) outer race fault, (b) inner race fault, (c) ball fault and (d) train fault. The main reasons which can lead to these faults are

contamination and corrosion, improper maintenance like improper lubrication, and improper installation of the machine [42].

2.4.3 Stator or Armature Faults

Stator faults can be mainly categorized as: (i) inter turn short circuit in stator coils, (ii) phase to phase short circuit (iii) ground fault, and (iv) open circuit fault. The main reason of stator faults can be classified as: (i) high operational temperatures, (ii) lack of mechanical joints, and loos bracing, and (iii) electrical discharge [42].

2.4.4 Actuator Faults

This category is mainly involved with faults in power supply part or the converter. The most important faults in this category can be summarized as (i) open gate or base drive in power semiconductor, (ii) short circuit fault in power semiconductor, (iii) short circuit in DC-link capacitor [42].

2.4.5 Sensor Faults

Different types of electrical and mechanical sensors are normally used in controlling schemes. Mechanical sensors are less reliable than electrical sensors. Different faults in sensors can generally be classified as [41] [43]:

- DC-link voltage sensor fault
- Current sensor faults
- Input source voltage
- Sensor gain

The occurrence of sensor fault can lead to instability. Nevertheless, if sensor fault is detected, different fault tolerant controlling algorithms can be applied to avoid system fail. As an example, the use of virtual sensors, or observers, or Kalman filter can be implemented to prepare the required information [42]. In [43] a set of current sensors and associated observers are combined for rotor flux estimation. A comparison between observer outputs and sensor outputs is usually used to evaluate the system condition.

2.5 Fault Tolerant Drives

As a definition, fault tolerant motor drive should have the ability of isolating the fault, and continuing the operation with minimal derating in performance [44]. More precisely, the general steps for fault compensation in fault tolerant drives can be summarized as [45]:

- Fault detection: evaluation of the system for determination of its situation. If the system is healthy, normal controlling algorithm will be applied, if not, the following steps will be executed:
    a. Faulty switch (or phase winding) isolation: isolation of the related damaged parts from power source and motor terminals.

b. Reconfiguration: depending on the fault, and available fault tolerant facilities, the power supply part can reconfigure itself to a new after-fault mode.

c. Control adaption: changing the control algorithm, and calculation of duty cycles for post-fault topology

Different aspects of fault tolerant controlling strategies in variable speed drives are considered in [46], including fault detection, power supply reconfiguration, and control accommodation. The transition speed to post-fault condition should be as fast as possible. Regarding the required adaptability, PMSM Fault tolerant controlling strategies, are mainly based on field oriented and space vector control of machines in literatures.

Five-phase PMSMs can continue their operation after loss of one, or even two of their phases. This capability is very important in applications where safety is of first priority. In other words, under the lack of opened phases, the remaining phases should provide an undisturbed rotating MMF. For a five-phase PMSM, the fundamental current amplitude in the remaining phases should increase up to 1.38 times their initial value [19] [47].

2.6 Main Configurations of Fault Tolerant Inverters

There are many different fault tolerant inverter structures mentioned in literatures, and all of them are designed to be used with three-phase systems. In the following, four important fault tolerant inverter structures will be reviewed.

2.6.1 Switch Redundant Topology

This topology is shown in Fig. 2-6-1 and incorporates four TRIACs or back-to-back connected SCRs and three fast acting fuses. The fuses are connected in series with the load phases. This topology is a combination of topologies and control methods to accommodate an opened phase, and a shorted switch, they will be considered separately [48].

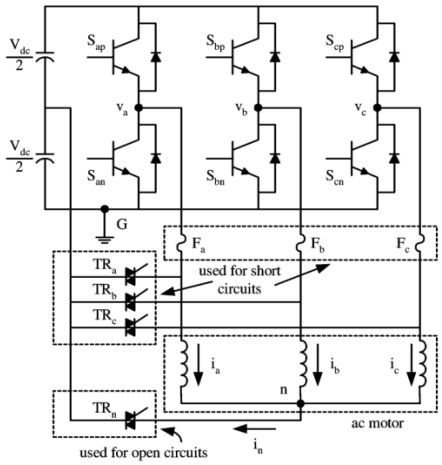

Figure 2-6-1: Switch redundant topology [49]

In the case of an opened phase fault only TRIAC needs to be present in the topology of Fig. 2-6-1, and the presence of the three series fuses is not required. When the system detects an opened phase fault, TRIAC is fired in order to connect the neutral of the motor to the midpoint of the dc bus.

In order to maintain a constant flux trajectory and insure disturbance free operation of the system, the phase currents of the unfaulted phases need to be increased in magnitude by a factor of $\sqrt{3}$ and A phase shift of 30° away from the axis of the faulted phase. The phasor diagram of this condition for an open-circuit fault on phase A is shown in Fig.2-6-2 [48].

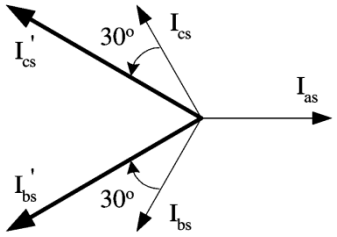

Figure 2-6-2 Current phasor relationships before and after an open phase fault on phase A

In the case of a short-circuit, the circuit of Fig. 2-6-1 operates as follows: It is assumed that some type of hardware based short-circuit protection in the inverter will automatically open the complementary transistor in order to avoid a shoot-through failure by short-circuiting the dc bus. Using this signal and additional control logic, the controller turns on TRIAC T_{RA}.

This causes a short circuit through the lower half of the dc bus, the failed-shorted switch, the TRIAC, and the fast blow fuse. As a result, the fuse will open and clear the shorted switch out of circuit. The TRIAC T_{RA}, is subsequently controlled to be continuously on during this post-fault condition.

2.6.2 Double Switch-Redundant Topology

This topology consists of a four-leg inverter with additional components for fault tolerance control of a four terminal motor.

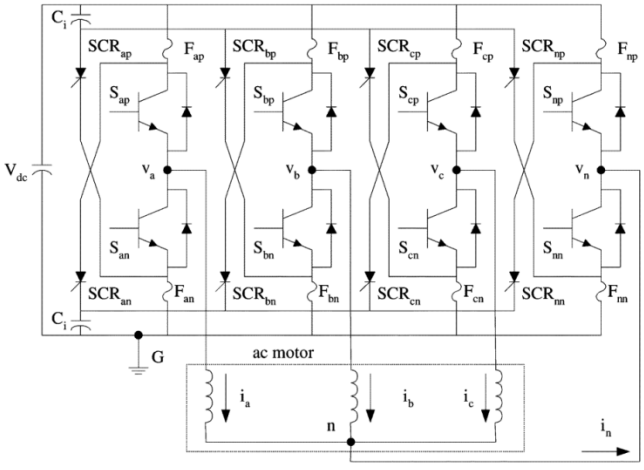

Figure 2-6-3 Double switch-redundant topology [49].

The double switch-redundant topology is shown in Fig. 2-6-3. The topology consists of a four-leg inverter with additional components for fault tolerance control of a four terminal motor. The additional components needed for fault tolerance include two fuses and two SCRs per phase leg. Also, one pair of capacitors C_i is needed in order to clear the fuses and isolate a short circuit path [48].

After detecting a fault, (phase a for example), the control sends signals to SCR_{ap} and SCR_{an} to turn on. For each IGBT in the phase leg, this causes a transient short-circuit through the main dc link, the auxiliary capacitor C_i , the SCR, and fuse.

By using the charge transferred to the auxiliary capacitor, the fuse will be cleared and the faulted phase-leg is removed from the circuit. The auxiliary capacitors need to be large enough to provide enough amplitude and duration of current for clearing the fuse [48]. The post-fault control strategy in terms of commanded currents of the double switch-redundant inverter is identical to that of the switch-redundant inverter to an opened phase fault.

2.6.3 Phase-Redundant Topology

The ability to isolate a faulty phase-leg opens the possibility of introducing a spare inverter leg for improved fault tolerance as shown in Fig. 2-6-4. The configuration will be referred to as the phase-redundant topology. This circuit topology incorporates the fault isolating SCRs and fuses in only three active legs of the inverter. A spare fourth leg of the inverter will be connected in place of faulty phase-leg after fault isolation. During normal operation, this spare leg is inactive and not switching. As a result, the three TRIACs shown in the topology act as static transfer switches only when needed. This topology, which was not tested in the paper, has the unique ability of maintaining the rated output power in post-fault operating mode [48].

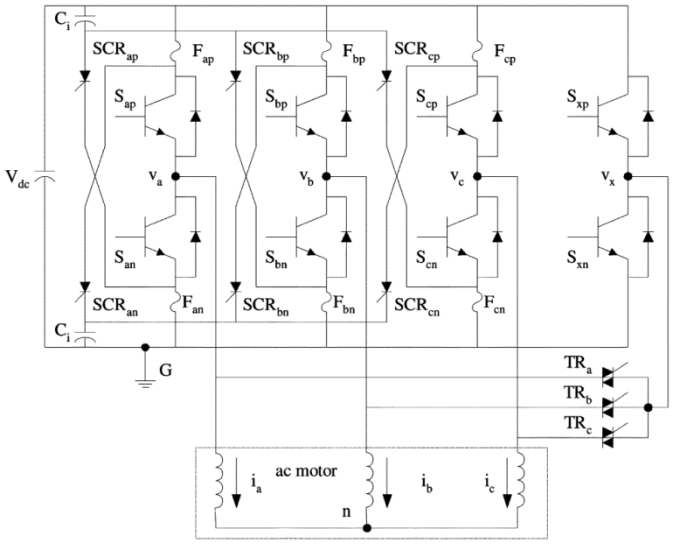

Figure 2-6-4 Phase-redundant topology [48]

2.6.4 Cascade Topology

The proposed cascaded inverter topology is simply a repartitioning of the phase legs found in a standard single-phase or three-phase inverter, and is shown in Fig. 2-6-5. The cascaded inverter allows for the full bus voltage to be applied to each of the motor phases.

Fault tolerant capabilities of cascaded topology shown in Fig.2-6-5 are somehow limited. The inverter provides fault tolerance for an opened phase fault. In this case, the two-phase control method can be used. However, protection for a short-circuited fault cannot be provided by turning off the remaining switches in the phase because a current circulating path remains consisting of the winding, the shorted switch, and a diode in the unfaulted inverter [48].

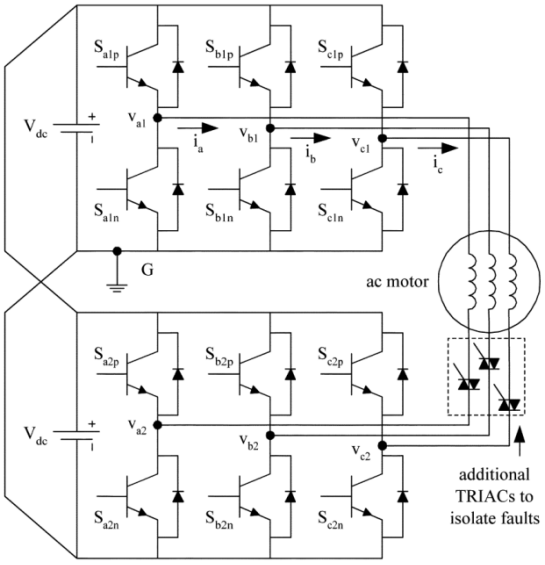

Figure 2-6-5 Cascaded inverter topology

2.7 References

[1] K. T. Chau, C. C. Chan, C. Liu, "Overview of Permanent-Magnet Brushless Drives for Electric and Hybrid Electric Vehicles", IEEE Transactions on Industrial Electronics, Vol. 55, No. 6, June 2008

[2] S. Dwari, L. Parsa, “An Optimal Control Technique for Multiphase PM Machines Under Open-Circuit Faults”, IEEE Transactions on Industrial Electronics, Vol. 55, No. 5, May 2008

[3] F. Scuiller, E. Semail, J.F. Charpentier, P. Letellier, “Multi-criteria-based design approach of multi-phase permanent magnet low-speed synchronous machines”, IET Electric Power Applications, 2008

[4] O. Poncelas, J.A. Rosero, J. Cusido, J.A. Ortega, L. Romeral, “Motor Fault Detection Using a Rogowski Sensor Without an Integrator”, IEEE Transactions on Industrial Electronics, Vol 56 , No 10, 2009

[5] L. Parsa, H. A. Toliyat, “Fault-Tolerant Interior-Permanent-Magnet Machines for Hybrid Electric Vehicle Applications”, IEEE Transactions on Vehicular Technology, Vol. 56, No. 4, July 2007

[6] L. Parsa, H. A. Toliyat, A. Goodarzi, "Five-Phase Interior Permanent Magnet Motor with Low Torque Pulsation", IEEE Transactions on Industry Applications, Vol. 43, No1, January/February 2007

[7] Y. Wang, K. T. Chau, J. Gan, C. C. Chan, J. Z. Jiang, "Design and Analysis of a New Multiphase Polygonal-Winding Permanent-Magnet Brushless DC Machine", IEEE Transactions On Magnetics, Vol. 38, No. 5, September 2002

[8] P. Cortes, M. P. Kazmierkowski, R. M. Kennel, D. E. Quevedo, and J. Rodriguez, "Predictive control in power electronics and drives," IEEE Trans. Ind. Electron., vol. 55, no. 12, pp. 4312–4324, Dec. 2008.

[9] J.W.K.K. Jayasundara, D.A.I. Munindradasa, "Design of Multi Phase In-Wheel Axial Flux Permanent Magnet Motor for Electric Vehicles", International Conference on Industrial and Information Systems, ICIIS 2006

[10] J. R. Ruiz; J.A. Rosero, A.G. Espinosa, L. Romeral, "Detection of Demagnetization Faults in Permanent-Magnet Synchronous Motors Under Nonstationary Conditions", IEEE Transactions on Magnetics, Vol 45 , No 7 , 2009

[11] A. Chikhi, M. Djarallah, K. Chikhi, "A Comparative Study of Field-Oriented Control and Direct-Torque Control of Induction Motors Using An Adaptive Flux Observer", Serbian Journal of Electrical Engineering, Vol. 7, No. 1, May 2010

[12] D. Casadei, F. Profumo, G. Serra, A. Tani, "FOC and DTC: Two Viable Schemes for Induction Motors Torque Control", IEEE Transactions on Power Electronics, Vol. 17, No. 5, September 2002

[13] M. F. Rahman, M. E. Haque, L. Tang, L. Zhong," Problems Associated With the Direct Torque Control of an Interior Permanent-Magnet Synchronous Motor Drive and Their Remedies", IEEE Transactions on Industrial Electronics, Vol. 51, No. 4, August 2004

[14] L. Zhong, M. F. Rahman, W. Y. Hu, K. W. Lim, "Analysis of Direct Torque Control in Permanent Magnet Synchronous Motor Drives", IEEE Transactions on Power Electronics, Vol. 12, No. 3, May 1997

[15] Y. Inoue, S. Morimoto, M. Sanada, "Examination and Linearization of Torque Control System for Direct Torque Controlled IPMSM", IEEE Transactions on Industry Applications, Vol. 46, No. 1, January/February 2010

[16] G. S. Buja, M. P. Kazmierkowski, "Direct Torque Control of PWM Inverter-Fed AC Motors—A Survey", IEEE Transactions on Industrial Electronics, Vol. 51, No. 4, August 2004GUST 2004

[17] T. G. Habetler, F. Profumo, M. Pastorelli, L. M. Tolbert," Direct Torque Control of Induction Machines Using Space Vector Modulation", IEEE Transactions on Industry Applications, Vol. 28, No. 5, September/October 1992

[18] H. F. A. Wahab, H. Sanusi, "Simulink Model of Direct Torque Control of Induction Machine", American Journal of Applied Sciences 5 (8): 1083-1090, 2008 ISSN 1546-9239 Publications

[19] L. Parsa, H. A. Toliyat, "Sensorless Direct Torque Control of Five-phase Interior Permanent Magnet Motor Drives", IEEE Transactions On Industry Applications, Vol. 43, No. 4, July/August 2007

[20] Quang NP, Dittrich JA. "Vector Control of Three-Phase AC Machines, System Development in the Practice", Springer: Berlin, 2008; 1–190.

[21] E. Semail, X. Kestelyn, A. Bouscayrol, “Right Harmonic Spectrum for the Back-Electromotive Force of a n-phase Synchronous Motor”, Industry Applications Conference, 2004 IEEE

[22] S. Xue, X. Wen, Z. Feng, “Multiphase Permanent Magnet Motor Drive System Based on A Novel Multiphase SVPWM”, Power Electronics and Motion Control Conference, IEEE 2006

[23] E. Semail, X. Kestelyn, A. Bouscayrol, “Right Harmonic Spectrum for the Back-Electromotive Force of a n-phase Synchronous Motor”, Industry Applications Conference, 2004

[24] R. Shi, H. A. Toliyat, A. El-Antably, “Field Oriented Control of Five-phase Synchronous Reluctance Motor Drive with Flexible 3rd Harmonic Current Injection for High Specific Torque”, Industry Applications Conference, IEEE 2009

[25] L. Parsa, H. A. Toliyat, “Five-Phase Permanent-Magnet Motor Drives”, IEEE Transactions On Industry Applications, Vol. 41, No. 1, January/February 2005

[26] Z. Sun, J. Wang, G. W. Jewell, D. Howe, "Enhanced Optimal Torque Control of Fault-Tolerant PM Machine Under Flux-Weakening Operation", IEEE Transactions On Industrial Electronics, Vol. 57, No. 1, January 2010

[27] S. Xuelei, W. Xuhui, C. Wei, “Research on Field-weakening Control of Multiphase Permanent Magnet Synchronous Motor”, International Conference on Electrical Machines and Systems, 2011 IEEE

[28] L. Guo, L. Parsa, “Model Reference Adaptive Control of Five-phase IPM Motors Based on Neural Network”, IEEE Transactions On Industrial Electronics, Vol. 59, No. 3, March 2012

[29] B. Heber, L. Xu, Y. Tang, “Fuzzy Logic Enhanced Speed Control of an Indirect Field-Oriented Induction Machine Drive”, IEEE Transactions on Power Electronics, Vol. 12, No. 5, September 1997

[30] J.A. Riveros, J. Prieto1, F. Barrero1, S. Toral, M. Jones, “Predictive Torque Control for Five–Phase Induction Motor Drives”, Annual Conference on IEEE Industrial Electronics Society, 2010

[31] M. J. Durán, F. Barrero, S. Toral, M. Arahal, J. Prieto, “Improved Techniques of Restrained Search Predictive Control for Multiphase Drives”, Electric Machines and Drives Conference, IEEE 2009

[32] T. Geyer, “Low complexity model predictive control in power electronics and power systems,” Ph.D. dissertation, Automatic Control Laboratory, ETH Zurich, Zurich, Switzerland, 2005.

[33] T. Geyer, “Generalized model predictive direct torque control: Long prediction horizons and minimization of switching losses,” IEEE Conf. Decis. Control, Shanghai, China, Dec. 2009, pp. 6799–6804.

[34] T. Geyer, G. Papafotiou, and M. Morari, “Model predictive direct torque control—Part I: Concept, algorithm and analysis,” IEEE Trans. Ind. Electron., vol. 56, no. 6, pp. 1894–1905, Jun. 2009.

[35] Yilmaz Sozer1, David A. Torrey2, Erkan Mese3, “Adaptive predictive current control technique

for permanent magnet synchronous motors", Published in IET Power Electronics 2012 doi: 10.1049/iet-pel.2012.0155

[36] S. Bolognani, L. Peretti, and M. Zigliotto, "Design and implementation of model predictive control for electrical motor drives," IEEE Trans. Ind. Electron., vol. 56, no. 6, pp. 1925–1936, Jun. 2009.

[37] F. Morel, J. M. Rétif, X. Lin-Shi, and C. Valentin, "Permanent magnet synchronous machine hybrid torque control," IEEE Trans. Ind. Electron., vol. 55, no. 2, pp. 501–511, Feb. 2008.

[38] F. Barrero,M. R. Arahal, R. Gregor, S. Toral, andM. J. Durán, "A proof of concept study of predictive current control for VSI-driven asymmetrical dual three-phase ac machines," IEEE Trans. Ind. Electron., vol. 56, no. 6, pp. 1937–1954, Jun. 2009.

[39] A. Linder and R. Kennel, "Model predictive control for electrical drives," in Proc. IEEE Power Electron. Spec. Conf., Recife, Brazil, Jun. 2005, pp. 1793–1799.

[40] S. Mariethoz, A. Domahidi, and M. Morari, "Sensorless explicit model predictive control of permanent magnet synchronous motors," in Proc. IEEE Int. Elect. Mach. Drives Conf.,Miami, FL,May 2009, pp. 1250–1257.

[41] S. Bolognani, M. Zordan, M. Zigliotto, "Experimental Fault-Tolerant Control of a PMSM Drive", IEEE Transactions on Industrial Electronics, Vol. 47, No. 5, October 2000

[42] D. U. C. Delgado, D. R. E. Trejo, E. Palacios, "Fault-tolerant control in variable speed drives: a survey", IET Electric Power Applications Journal, Vol. 2, No. 2, pp. 121-134, August 2007

[43] M.E. Romero, M.M. Seron, J.A. De Dona, "Sensor Fault-Tolerant Vector Control of Induction Motors", IET Journal of Control Theory and Applications, April 2010

[44] O. Poncelas, J.A. Rosero, J. Cusido, J.A. Ortega, L. Romeral, "Motor Fault Detection Using a Rogowski Sensor Without an Integrator", IEEE Transactions on Industrial Electronics, Vol 56 , No 10, 2009

[45] R. L. A. Ribeiro, C. B. Jacobina, E. R. C. Silva, A. M. N. Lima, "Fault-Tolerant Voltage-Fed PWM Inverter AC Motor Drive Systems", IEEE Transactions on Industrial Electronics, Vol. 51, No. 2, April 2004

[46] D.U. Campos-Delgado, D.R. Espinoza-Trejo, E. Palacios, "Fault-Tolerant Control in Variable Speed Drives: a Survey", IET journal of Electric Power Applications, August 2007

[47] A.G. Espinosa, J.A Rosero, J. Cusido, L. Romeral, J.A. Ortega, "Fault Detection by Means of Hilbert–Huang Transform of the Stator Current in a PMSM With Demagnetization", IEEE Transactions on Energy Conversion, Vol 25 , No 2, 2010

[48] B. A. Welchko, T. A. Lipo, T. M. Jahns, S. E. Schulz, "Fault Tolerant Three-Phase AC Motor Drive Topologies: A Comparison of Features, Cost, and Limitations", IEEE Transactions on Power Electronics, Vol. 19, No. 4, July 2004

[49] O. Wallmark, L. Harnefors, O. Carlson, "Control Algorithms for a Fault-Tolerant PMSM Drive", IEEE Transactions on Industrial Electronics, Vol. 54, No 4, August 2007

3.

Chapter 3 Predictive Current Control of Five-Phase BLDC Machine - Healthy Conditions

Model predictive control algorithms have recently gained more importance in the field of power electronics and motor drives. One of the important categories of model predictive control methods is improved deadbeat control in which the reverse system model is used to calculate the appropriate inputs for the next iteration of controlling process. In this chapter a new improved deadbeat algorithm is proposed to control the stator currents of a five-phase BLDC machine. Extended Kalman filter is used in the estimation step of the proposed method, and system model equations are used to calculate the appropriate voltages for the next modulation period. Comparing to faulty conditions, the computational load of EKF is less while the machine is under normal (healthy) conditions. As a result, it is possible to use EKF in estimation step of predictive current controllers. Two aspects of proposed controlling method are evaluated including its sensitivity to system variations and its speed in following the reference currents during transient states. Proposed controlling method is evaluated both by simulations and experimental evaluations.

CONTENTS

3.1 Introduction

Several methods are proposed in literature to have a better control on stator phase currents of BLDC machine drives. Among these algorithms, model predictive control (MPC) has become a suitable option recently. Its concept is easy to understand, and various constraints and nonlinearities can be included in its structure. Moreover, the resulting controller is easy to implement [1], [2]. These types of controllers can be effectively implemented in electrical drives because linear models of electrical motors are quite well known and developed through analytical methods.

MPC has been examined in the case of multiphase drives [3]–[11]. Comparing to standard three-phase systems, multi-phase structure of an electrical drive results in several advantages such as lower power per inverter leg, lower current per phase, and lower amplitude and higher frequency of torque ripple [12][13].

Deadbeat predictive control is one of the main MPC categories which can be considered as an extension of traditional field-oriented control. In this category, inner-loop PI controllers are removed and replaced by predictive controllers and the reverse motor model is used to calculate appropriate reference voltages. Moreover a modulator is usually used to generate the computed reference voltages [14] [15].

While controlling the stator currents of a multiphase machine by MPC algorithms, motor model is directly used to estimate the future values of system outputs (currents). Consequently, the precision of model parameters play an important role in final accuracy of the estimated values. Moreover, stator currents are measured at the beginning of MPC algorithm, and as a result, measurement noise can also affect the precision of controlling algorithm [16].

Extended Kalman filter (EKF) is a powerful recursive estimation algorithm which can be used to reduce the effect of parameter variation and measurement noise. All available measurements are processed by EKF regardless of their accuracy to provide a fast and precise estimation of all system states [17].

In [18] and [19] EKF is used to estimate the rotor position and rotor speed of a permanent magnet synchronous motor (PMSM). Moreover, by comparing final estimations of this algorithm with measured values of system states a fault detection and isolation algorithm is developed in [20]. As the mathematical model of BLDC machine is sufficiently well developed, EKF is ideally suited for the case of BLDC machine drive applications [21].

In the first step of this chapter, electrical model of five-phase BLDC machine under normal (healthy) conditions is developed, and after that an extended Kalman filter based predictive deadbeat control is proposed for five-phase drives. Proposed controlling algorithm includes two main steps namely “current estimation step” and “voltage application step”. EKF is developed for five-phase BLDC machine model, and is executed during “current estimation step” to reduce the effect of parameter variation and measurement noise. Two main aspects of proposed controlling algorithm are evaluated both by simulations and

experimental tests. These two aspects are controlling method sensitivity respect system variations, and its ability in following reference currents during transient states.

3.2 Mathematical Model of Five-Phase PM Machine

The general structure of an outer-rotor five-phase BLDC motor with a two-layer winding topology is briefly reviewed in this section. Figure 3-2-1 presents the general configuration of motor outer-rotor and its inner-stator.

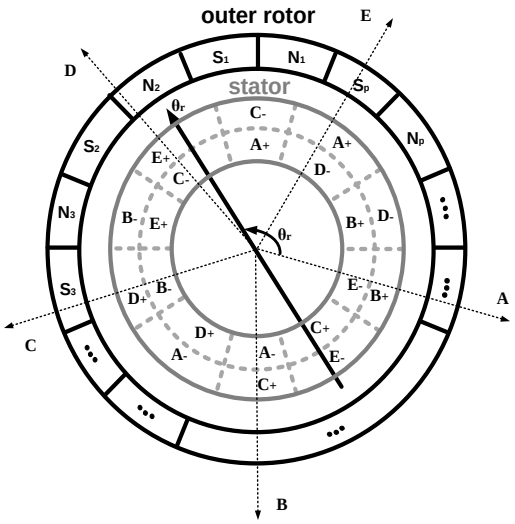

Figure 3-2-1 Outer-rotor five-phase BLDC structure with double-layer winding distribution and p pole pairs

To develop the electrical model, let us consider the idealized representation of five phase PM motor with *P* poles. The machine is considered symmetric, and saturation of iron is neglected. As the first step, the general equation of machine´s electrical dynamics can be written as:

$$[V_S]=[R_S][I_S]+\frac{d}{dt}[\Lambda_S]$$

Eq. 3-2-1

where *Rs*, *I*, and Λs are respectively representing resistance, current and magnetic flux of stator windings. Magnetic flux linkage Λs can be written in terms of stator windings flux and permanent magnets flux.

$$\Lambda_S = \lambda_s + \lambda_{PM}$$

Eq. 3-2-2

Having a uniform air gap in the machine, stator winding flux can itself be expressed as the multiplication of stator inductance and stator five phase currents.

$$\Lambda_s = L_{ss} I_s + \lambda_{PM}$$

Eq. 3-2-3

where L_{ss} is the inductance matrix of the stator windings.

Similar to Park transformation concept in three-phase systems, parameters of a five-phase BLDC motor can be projected into two decoupled reference frames and a homopolar axis. These reference frames are known as d_1-q_1 plane (rotating at synchronous speed) and d_3-q_3 plane (rotating at three times synchronous speed) [22] [23]. Considering θ as rotor electrical angle, the transformation equation can be written as (3.2.4).where *T* is the transformation matrix and *F* represents electrical current, electrical voltage or magnetic flux.

$$F_{d_1q_1d_3q_3o} = T\, F_{ABCDE}$$

$$T_{d_1q_1d_3q_3o}(\theta) = \frac{2}{5}\begin{bmatrix} \cos(\theta) & \cos(\theta-2\pi/5) & \cos(\theta-4\pi/5) & \cos(\theta-6\pi/5) & \cos(\theta-8\pi/5) \\ -\sin(\theta) & -\sin(\theta-2\pi/5) & -\sin(\theta-4\pi/5) & -\sin(\theta-6\pi/5) & -\sin(\theta-8\pi/5) \\ \cos 3(\theta) & \cos 3(\theta-2\pi/5) & \cos 3(\theta-4\pi/5) & \cos 3(\theta-6\pi/5) & \cos 3(\theta-8\pi/5) \\ -\sin 3(\theta) & -\sin 3(\theta-2\pi/5) & -\sin 3(\theta-4\pi/5) & -\sin 3(\theta-6\pi/5) & -\sin 3(\theta-8\pi/5) \\ 1/\sqrt{2} & 1/\sqrt{2} & 1/\sqrt{2} & 1/\sqrt{2} & 1/\sqrt{2} \end{bmatrix}$$

Eq. 3-2-4

Using this transformation, electrical equations of a healthy BLDC machine in d_1-q_1 and d_3-q_3 reference frames can be summarized as [24] [25]:

$$v_{d1} = r_s i_{d1} - \omega_e L_{q1} i_{q1} + L_{d1}\frac{di_{d1}}{dt}$$

Eq. 3-2-5

$$v_{q1} = r_s i_{q1} + \omega_e (L_{d1} i_{d1} + \lambda_{m1}) + L_{q1}\frac{di_{q1}}{dt}$$

Eq. 3-2-6

$$v_{d3} = r_s i_{d3} - 3\omega_e L_{q3} i_{q3} + L_{d3}\frac{di_{d3}}{dt}$$

Eq. 3-2-7

$$v_{q3} = r_s i_{q3} + 3\omega_e (L_{d3} i_{d3} + \lambda_{m3}) + L_{q3}\frac{di_{q3}}{dt}$$

Eq. 3-2-8

$$v_o = r_s i_o + L_o\frac{di_o}{dt}$$

Eq. 3-2-9

where λ_{m1} and λ_{m3} are the first and third harmonic components of rotor magnet flux; i_{d1}, i_{q1}, i_{d3}, i_{q3} and i_o are transformed values of stator currents in each rotating frame; r_s is the stator resistance; L_{d1}, L_{q1}, L_{d3}, L_{q3} and L_o are transformed values of stator inductances, and ω_e is electrical rotational velocity. Generated electrical torque can be computed as:

$$T_e = T_{e1} + T_{e3}$$

Eq. 3-2-10

$$T_{e1} = \frac{5}{2}\frac{P}{2}[i_{d1}i_{q1}(L_{d1} - L_{q1}) + \lambda_{m1}i_{q1}]$$

Eq. 3-2-11

$$T_{e3} = \frac{5}{2}\frac{P}{2}[-3i_{d3}i_{q3}(L_{d3} - L_{q3}) + 3\lambda_{m3}i_{q3}]$$

Eq. 3-2-12

where the number of rotor poles is denoted by *P.* In the case of non-salient rotor structure, the inductances are both equal in *d*- and *q*-directions, and equations (3-2-11) and (3-2-12) can be reduced to [23]:

$$T_{e1} = \frac{5}{2}\frac{P}{2}[\lambda_{m1}I_{q1}]$$

Eq. 3-2-13

$$T_{e3} = \frac{5}{2}\frac{P}{2}[3\lambda_{m3}I_{q3}]$$

Eq. 3-2-14

3.3 Torque Control of Five-Phase BLDC Machine

Vector control can be applied to control the stator currents in both reference frames. In the case of normal operation with a healthy motor, i_{d1}* and i_{d3}* are set to zero to avoid rotor demagnetization or iron saturation. i_{q1}* can be simply proportional to torque demand. As shown in Fig. 3-3-1, the reference value of electrical torque can be determined directly (in the case of torque controlled applications) or it may be adjusted by speed loop controller (in the case of speed controlled applications). i_{q3}* can be used to increase the power density or reduce the ripples, and i_o is usually forced to zero by disconnecting machine´s neutral point.

General structure of stator current control under normal operation is shown in Fig. 3-3-1 Motor stator currents are measured and then compared to their reference values. Computed current errors are used in controller blocks to compute V_{d1}*, V_{q1}*, V_{d3}*, V_{q3}* and V_o*. These voltages will then be imposed to the motor by inverter unit.

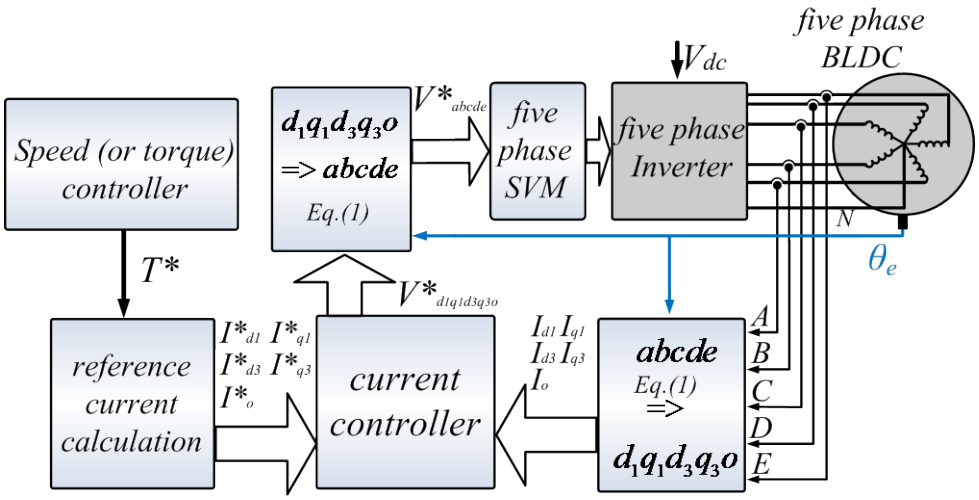

Fig. 3-3-1 General block diagram of current control in two rotating reference frames - normal operation

Reference voltage values are sent to the space vector modulation (SVM) block to generate the required controlling pulses of inverter. Depending on their voltage length, active space vectors can be divided into three categories in both rotating planes: large vectors, medium vectors and small vectors [26] [27]. A combination of two medium vectors and two large vectors is used in each modulation period to generate the required reference voltage [28] [29].

3.4 Predictive Control of Stator Phase Currents

One of the important categories of model predictive control methods is improved deadbeat control in which the reverse system model is used to calculate the appropriate inputs for the next iteration of controlling process. In this section, a new improved deadbeat algorithm is developed to control the stator currents of a five-phase BLDC machine. Extended Kalman filter is used in the estimation step of proposed method, and system model equations are used to calculate the appropriate voltages for the next modulation period.

In the case of BLDC drive applications, the main purpose of deadbeat control algorithm is to eliminate the stator current errors in the smallest possible number of switching periods. As it is shown in Fig. 3-4-1, stator phase currents are sampled at the beginning of k^{th} modulation period. In addition, the duty cycles of each voltage vector are getting updated by the beginning of each modulation period.

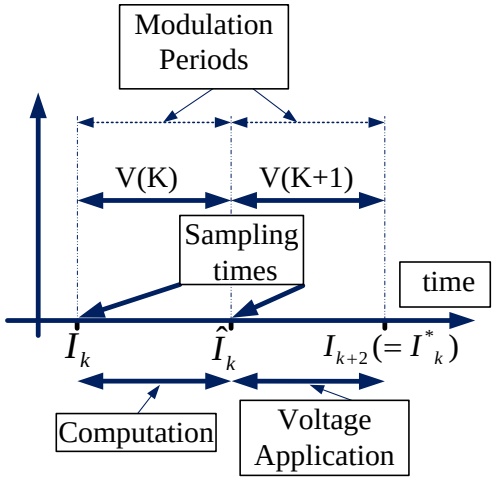

Figure 3-4-1 Deadbeat MPC sequences

By knowing the measured values of phase currents (I_k) and applied voltage values (V_k) during k^{th} modulation period, it is possible to calculate the estimated value of stator currents ($\hat{I}_k$) by the end of current modulation period.

The main objective of deadbeat control is to produce the reference values of stator currents (I^*) by the end of next modulation period. Considering machine model equations, and by knowing the estimated value of ($\hat{I}_k$), the desired voltage values for the next modulation period can be calculated as:

$$V_{d1}(k+1)=\frac{L_{d1}}{T_m}(i^*_{d1}-\hat{i}_{d1})+r_s\hat{i}_{d1}-\omega L_{q1}\hat{i}_{q1}$$

Eq. 3-4-1

$$V_{q1}(k+1)=\frac{L_{q1}}{T_m}(i^*_{q1}-\hat{i}_{q1})+r_s\hat{i}_{q1}+\omega(L_{d1}\hat{i}_{d1}+\psi_{pm1})$$

Eq. 3-4-2

$$V_{d3}(k+1)=\frac{L_{d3}}{T_m}(i^*_{d3}-\hat{i}_{d3})+r_s\hat{i}_{d3}-3\omega L_{q3}\hat{i}_{q3}$$

Eq. 3-4-3

$$V_{q3}(k+1)=\frac{L_{q3}}{T_m}(i^*_{q3}-\hat{i}_{q3})+r_s\hat{i}_{q3}+3\omega(L_{d3}\hat{i}_{d3}+\psi_{pm3})$$

Eq. 3-4-4

As it can be seen, to calculate the required voltages, it is important to estimate the stator phase currents at the end of current modulation period. In this chapter, EKF is used to estimate the stator phase currents of a healthy machine. In the next section this estimation method is explained in details.

3.5 EKF-Based Estimation of Stator Phase Currents

As it was mentioned in section 3.4, Extended Kalman Filter (EKF) is used to estimate the stator currents at the end of current modulation period. Due to its more practical aspects, stationary $\alpha\beta$ reference frame is selected in the development of EKF equations. The transformation matrix between phase- and stationary-reference frames can be simply derived by setting $\theta = 0$ in (3-2-4):

$$F_{\alpha 1\beta 1\alpha 3\beta 3o} = T\big|_{\theta=0} F_{abcde}$$

Eq. 3-5-1

Nonlinear state model presentation of five-phase BLDC machine can be written as:

$$\dot{x} = f(x) + Bu(t) + w(t)$$

$$y(t) = cx(t) + v(t)$$

Eq.3-5-2

where

$$x = \begin{bmatrix} i_{\alpha 1} & i_{\beta 1} & i_{\alpha 3} & i_{\beta 3} & i_o & \omega_e & \theta_e \end{bmatrix}^T$$

$$u = \begin{bmatrix} v_{\alpha 1} & v_{\beta 1} & v_{\alpha 3} & v_{\beta 3} & v_o \end{bmatrix}^T$$

$$y = \begin{bmatrix} i_{\alpha 1} & i_{\beta 1} & i_{\alpha 3} & i_{\beta 3} & i_o \end{bmatrix}^T$$

Eq. 3-5-3

$$f(x) = \begin{bmatrix} -\frac{R_s}{L_{d1}} i_{\alpha 1} + \frac{\psi_{pm1}}{L_{d1}} \omega_e \sin\theta_e \\ -\frac{R_s}{L_{q1}} i_{\beta 1} - \frac{\psi_{pm1}}{L_{q1}} \omega_e \cos\theta_e \\ -\frac{R_s}{L_{d3}} i_{\alpha 3} - \frac{\psi_{pm3}}{L_{d3}} 3\omega_e \sin 3\theta_e \\ -\frac{R_s}{L_{q3}} i_{\beta 3} + \frac{\psi_{pm3}}{L_{q3}} 3\omega_e \cos 3\theta_e \\ -\frac{R_s}{L_o} i_o \\ 0 \\ \omega_e \end{bmatrix}$$

Eq. 3-5-4

$$B=\begin{bmatrix} 1/L_{d1} & 0 & 0 & 0 & 0 \\ 0 & 1/L_{q1} & 0 & 0 & 0 \\ 0 & 0 & 1/L_{d3} & 0 & 0 \\ 0 & 0 & 0 & 1/L_{q3} & 0 \\ 0 & 0 & 0 & 0 & 1/L_{o} \\ 0 & 0 & 0 & 0 & 0 \\ 0 & 0 & 0 & 0 & 0 \end{bmatrix}$$

$$C=\begin{bmatrix} 1 & 0 & 0 & 0 & 0 & 0 & 0 \\ 0 & 1 & 0 & 0 & 0 & 0 & 0 \\ 0 & 0 & 1 & 0 & 0 & 0 & 0 \\ 0 & 0 & 0 & 1 & 0 & 0 & 0 \\ 0 & 0 & 0 & 0 & 1 & 0 & 0 \end{bmatrix}$$

Eq. 3-5-5

In addition, w(t) represents system noise vector, and v(t) is the measurement noise vector, and it is assumed that w(t) and v(t) are uncorrelated and have zero-mean stochastic values.

Implemented EKF consists of two main steps. In the first step, a prediction of digitalized system states ($\hat{x}_{k|k-1}$) and its covariance ($\hat{P}_{k|k-1}$) is performed by knowing the previous estimation of system states ($\hat{x}_{k-1|k-1}$) and system inputs (u_{k-1}) during one sampling period:

$$\hat{x}_{k|k-1}=\hat{x}_{k-1|k-1}+T_s f(\hat{x}_{k-1|k-1},u_{k-1})$$

$$\hat{P}_{k|k-1}=\hat{P}_{k-1|k-1}+F\hat{P}_{k-1|k-1}F^T+Q$$

Eq. 3-5-6

In the second step, the measured quantities will be used to correct the estimated states and covariance matrix:

$$\hat{x}_{k|k}=\hat{x}_{k-1|k-1}+K_k\left[y_k-h(\hat{x}_{k|k-1})\right]$$

$$\hat{P}_{k|k}=\hat{P}_{k|k-1}-K_k H\hat{P}_{k|k-1}$$

$$K_k=\hat{P}_{k|k-1}H^T(H\hat{P}_{k|k-1}H^T+R)^{-1}$$

Eq. 3-5-7

where *H* is the measurement matrix and *K* is famous as Kalman gain [28].

Estimated values of system states ($\hat{x}_{k|k}$) can now be used in model predictive algorithm to calculate the required reference voltages of the next modulation period. Figure 3-5-1 illustrates the general structure of proposed EKF-based deadbeat control while modulation frequency is 10 kHz, and controlling algorithm frequency is 4 kHz.

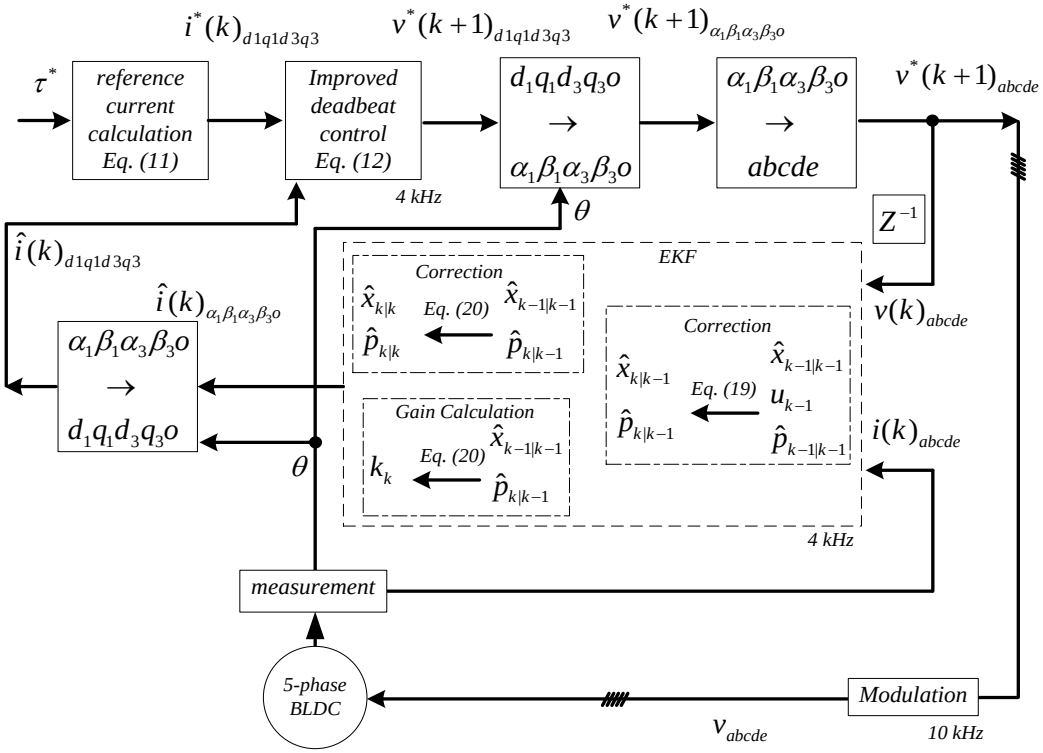

Figure 3-5-1 General structure of proposed EKF-based deadbeat control

3.6 Sensitivity Analysis of EKF-PDC

Simulations are conducted to evaluate the sensitivity of proposed EKF-based predictive deadbeat control (EKF-PDC) method. Five phase BLDC machine is simulated at 1-pu of its rated speed, and while delivering its nominal power. The parameters of simulated machine are brought in Table 3-6-1 which are also correspondent to their real values in laboratory test bench.

Table 3.6.1 Electrical (measured) parameters of five-phase BLDC machine (used both in simulations and experimental evaluations)

Number of Pole Pairs		26
Stator Resistance		0.1 Ω
Stator Inductance	L_{aa}	1500 *uH*
	L_{ab}	35 *uH*
	L_{ac}	42 *uH*
Nominal Torque		32 *Nm*
Nominal Phase Current		19 Amp (rms)
DC-bus Rated Voltage		48 V
Nominal current frequency		43.3 Hz
Permanent Magnet Flux		0.0178 *Wb*

3.6.1 Simulation Steps

Simulations consist of five different steps. In each step a different source of disturbance is introduced to the system. Simulation five steps are summarized in Table 3-6-2.

Table 3-6-2 Considered parameters during each simulation

Test number	Introduced disturbance
1	Ideal Condition
2	dc-link voltage drop
3	Nonlinear Inverter Characteristics
4	Inaccurate phase resistance
5	Inaccurate PM flux

The first case (test-1) is dedicated to ideal operation. Precise model of the machine is used in the estimation block, and ideal switches are used in inverter block.

The second case (test-2) is related to the impact of dc-bus voltage drop in the inverter block. During test-2, dc-link voltage is reduced to 0.8 its rated value.

The third case (test-3) is related to inverter nonlinear characteristics. Considered inverter characteristics include 3*us* of dead time, and respectively 0.016Ω and 0.014Ω of forward resistance for anti-parallel diodes and IGBTs in each leg, and moreover, 2.17 V and 1.85 V of voltage drop for anti-parallel diodes and IGBTs respectively.

Machine parameters are the main concern of the next simulations (tests 4 and test 5). Higher operational temperature and conductor skin effect can lead to higher values of operational stator resistance. During test-4 stator resistance is increased up to twice its rated value to study the sensitivity of proposed method to resistance changes.

High temperatures, aging and mechanical stresses can reduce the strength of rotor magnets in a BLDC machine. To evaluate the sensitivity of proposed method to magnet flux variations, during test-5 magnetic flux of machine rotor is reduced to 0.8 its rated value.

3.6.2 Simulation Results

In each simulation test, stator current errors are measured at the end of "current estimation step" and "voltage application step". That is the error between estimated ($\hat{I}_k$) and measured (I_{k+1}) current values at the end of current modulation period (e_1), and the error between real (I_{k+2}) and reference current values (I^*) by the end of next modulation period (e_2). In each case the energy of e_1 and e_2 are integrated on one period of fundamental frequency under steady states. As a result, during each test E_1 represents the error energy in "current estimation step", and E_2 is the energy of stator current errors after completely executing one round of control algorithm:

$$E_1 = \int_T \sum_{j=d1,q1,d3,q3,o} \left[\hat{I}_j(K) - I_j(K+1)\right]^2$$

$$E_2 = \int_T \sum_{j=d1,q1,d3,q3,o} \left[I_j^* - I_j(K+2)\right]^2$$

Eq. 3-6-1

Computed values of estimation error energy (E_1) and voltage application error energy (E_2) are summarized in Fig. 3-6-1. Moreover, simulated values of generated electrical torque under each condition are summarized in Fig. 3-6-2 In all conditions, rated value of torque is generated while the machine is rotating in its nominal speed and under steady state.

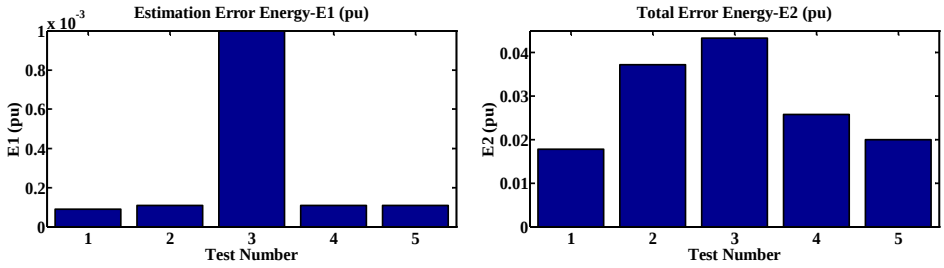

Figure 3-6-1 Simulated values of current errors in "current estimation step" (E_1) and "voltage application step" (E_2) of control algorithm

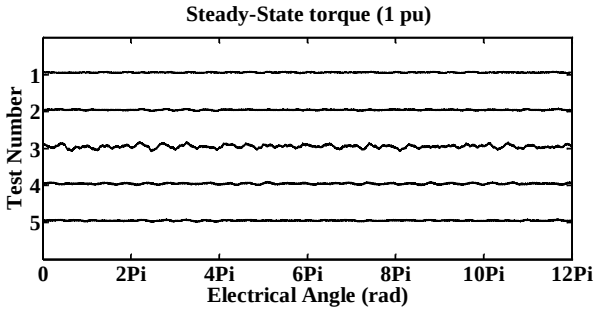

Figure 3-6-2 Generated electrical torque of five-phase BLDC machine during test-1 to test-5

3.6.3 Discussion on Simulation Results

In each case, the estimation step of control algorithm is realized by EKF, and after that, the required reference voltages are directly calculated by using machine equations. As it can be seen from Fig. 3-6-1, implementation of EKF in the estimation step leads to lower values of error energy (E_1) for all of the simulated cases. Standard deviations of E_1 and E_2 after completing all of these tests are S_1=4.007e-004 and S_2=0.0124, respectively. Lower amplitude of S_1 is due to automatic adaptation of EKF to system variations in each test. Error energy values of E_1 and E_2 while working with a healthy machine and under ideal conditions are respectively 8.92e-005 and 0.0178.

During test 2, the amplitude of dc-link voltage is reduced by 20% while its correspondent value in controlling algorithm is not changed. Comparing to healthy conditions, the increment of current error in estimation level (E_1) is 22%.

However, as machine´s equations are directly used during voltage application level, the increment of E_2 during this step is higher (108%). Again, the main reason of less error in the estimation step is adaptation of

EKF to system variations. Equation (3-4-1) is used during voltage application step. Considering this equation, in the case of dc-link voltage drop it is possible to write the following equation in d_1-direction:

$$i_{d1}(k+2) = \hat{i}_{d1}(k) + \frac{T_m}{L_{d1}}\left[V_{d1}(k+1) + \Delta V_{d1}(k+1) - r_s\hat{i}_{d1}(k) + \omega L_{q1}\hat{i}_{q1}(k)\right]$$

$$= \hat{i}_{d1}(k) + \frac{T_m}{L_{d1}}\left[V_{d1}(k+1) - r_s\hat{i}_{d1}(k) + \omega L_{q1}\hat{i}_{q1}(k)\right] + \frac{T_m}{L_{d1}}\Delta V_{d1}(k+1)$$

$$= i_{d1}(k+2)_{norm} + \Delta i_{d1}(k+2)$$

Eq. 3-6-2

where $\Delta V_{d1}(k+1)$ is the imposed voltage in d_1-direction due to existing error in dc-bus voltage, $i_{d1}(k+2)_{norm}$ is calculated current amplitude under normal operation, and $\Delta i_{d1}(k+2)$ is the additional current component which is generated due to existing error in dc-link voltage. As it can be seen, increasing the switching frequency (reduction of T_m) and increasing the machine inductances can directly reduce the error of stator current. However, final amount of current error is also dependent on the amplitude of applied voltage $V_{d1}(k+1)$ in $(k+1)^{th}$ modulation period. Following the same procedure, stator current error in other directions due to dc-link voltage drop can be calculated:

$$\Delta i_{q1}(k+2) = \frac{T_m}{L_{q1}}\Delta V_{q1}(k+1)$$

$$\Delta i_{q3}(k+2) = \frac{T_m}{L_{q3}}\Delta V_{q3}(k+1)$$

$$\Delta i_{d3}(k+2) = \frac{T_m}{L_{d3}}\Delta V_{d3}(k+1)$$

Eq. 3-6-3

Test 3 is dedicated to nonlinear characteristics of the inverter. As it can be seen from Fig.3-6-1, this test is correspondent to the highest amplitude of E_1 and highest torque ripples. In other words, implemented EKF during estimation step has more difficulties in adapting the system to reduce the impact of inverter nonlinear characteristics. The main reason of this fact is continuous variation of voltage drop along simulated semiconductors. Forward voltage drops in semiconductors can be considered as a periodic disturbance in dc-link voltage. The amplitude of this voltage disturbance changes each time the current flow path changes from an IGBT to its anti-parallel diode or vice versa. Simulated values of stator phase currents and applied voltage of phase A are shown in Fig. 3-6-3 while nonlinear characteristics of the inverter are included in simulations. As it can be seen, continuous periodic change of applied voltage (while stator current is crossing the zero) is the main reason of higher estimation error and higher torque ripple.

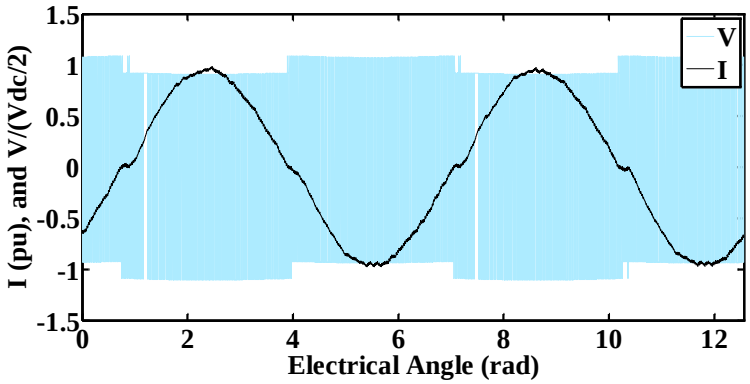

Figure 3-6-3 Simulated values of stator phase current including nonlinear characteristics of inverter

Nonlinear characteristics of the inverter have also led to higher values of E_2. This time, generated voltage drops along the conducting semiconductors change the effective value of applied voltages to machine stator phases, and this fact leads to higher values of current error. Similar to the case of dc-link voltage reduction, in this case higher values of stator inductance and modulation frequency can reduce the amplitude of E_2.

During test 4, stator resistance is changed from 0.1Ω to 0.2Ω in motor block while its value is remained fixed in controlling algorithm. This variation of stator resistance can happen due to load variation of PM machine. Comparing to test-1 (ideal operational conditions), E_1 increment is 22% which is much less than E_2 increment (44%). This fact is due to effective adaptation of EKF respect to machine´s resistance change. However, a fixed change in stator resistances will not lead to noticeable torque ripples. By the end of each modulation period, stator phase current in d_1-direction can be calculated as:

$$i_{d1}(k+2) = \hat{i}_{d1}(k) + \frac{T_m}{L_{d1}}\left[V_{d1}(k+1) - 2r_s\hat{i}_{d1}(k) + \omega L_{q1}\hat{i}_{q1}(k)\right]$$

$$= \hat{i}_{d1}(k) + \frac{T_m}{L_{d1}}\left[V_{d1}(k+1) - r_s\hat{i}_{d1}(k) + \omega L_{q1}\hat{i}_{q1}(k)\right] - \frac{T_m}{L_{d1}}\left[r_s\hat{i}_{d1}(k)\right]$$

$$= i_{d1}(k+2)_{norm} + \Delta i_{d1}(k+2)$$

Eq. 3-6-5

where $i_{d1}(k+2)_{norm}$ is stator current value in the case of operating under normal conditions, and $\Delta i_{d1}(k+2)$ is the error which is imposed to the system due to higher values of stator phase resistance. This error in other directions can be calculated as:

$$\Delta i_{q1}(k+2) = \frac{T_m}{L_{q1}}\left[r_s\hat{i}_{q1}(k)\right]$$

$$\Delta i_{d3}(k+2) = \frac{T_m}{L_{d3}}\left[r_s\hat{i}_{d3}(k)\right]$$

$$\Delta i_{q3}(k+2) = \frac{T_m}{L_{q3}}\left[r_s \hat{i}_{q3}(k)\right]$$

Eq. 3-6-6

As it can be seen, generated value of E_2 is directly proportional to stator resistance error and modulation period. Moreover, higher inductance values can lead to less error in stator phase currents. During test 5, generated flux of PM machine is decreased by 20%. This case can happen in the machine by aging, high operational temperatures, long-time mechanical vibration or high current amplitudes in d-directions. Although, generated torque ripples are negligible in this case, but comparing to the ideal case (normal operation), both E_1 and E_2 are increased by 22% and 46% respectively. Again the increment of E_1 is not as high as E_2 which is due to automatic adaptation of estimation step by its implemented EKF. The main effect of PM flux variations on proposed controlling algorithm will show its effect on q_1- and q_3-directions. Considering (3-4-1–3-4-4) it is possible to write:

$$i_{q1}(k+2) = \hat{i}_{q1}(k) + \frac{T_m}{L_{q1}}\left[V_{q1}(k+1) - 2r_s\hat{i}_{q1}(k) + \omega L_{d1}\hat{i}_{d1}(k) + \omega\psi_{pm1} + \omega\Delta\psi_{pm1}\right]$$

$$= \left[\hat{i}_{q1}(k) + \frac{T_m}{L_{q1}}\left(V_{q1}(k+1) - 2r_s\hat{i}_{q1}(k) + \omega L_{d1}\hat{i}_{d1}(k) + \omega\psi_{pm1}\right)\right] + \left[\frac{T_m}{L_{q1}}\left(\omega\Delta\psi_{pm1}\right)\right]$$

$$= i_{q1}(k+2)_{norm} + \Delta i_{q1}(k+2)$$

Eq. 3-6-7

$$i_{q3}(k+2) = \hat{i}_{q3}(k) + \frac{T_m}{L_{q3}}\left[V_{q3}(k+1) - 2r_s\hat{i}_{q3}(k) + 3\omega L_{d3}\hat{i}_{d3}(k) + \omega\psi_{pm1} + 3\omega\Delta\psi_{pm3}\right]$$

$$= \left[\hat{i}_{q3}(k) + \frac{T_m}{L_{q3}}\left(V_{q3}(k+1) - 2r_s\hat{i}_{q3}(k) + \omega L_{d3}\hat{i}_{d3}(k) + 3\omega\psi_{pm3}\right)\right] + \left[\frac{T_m}{L_{q3}}\left(\omega\Delta\psi_{pm3}\right)\right]$$

$$= i_{q3}(k+2)_{norm} + \Delta i_{q3}(k+2)$$

Eq. 3-6-8

where $i_{q1}(k+2)_{norm}$ and $i_{q3}(k+2)_{norm}$ are stator current in q_1- and q_3-directions by the end of $(k+1)^{th}$ modulation period and under normal conditions. In addition, $\Delta i_{q1}(k+2)$ and $\Delta i_{q3}(k+2)$ are the introduced error in this direction due to variation of rotor PM flux.

3.7 Experimental Evaluation of EKF-PDC

Experimental tests are conducted in laboratory to evaluate the behaviour of EKF-based controlling method. Figure 3-7-1 illustrates the experimental test bench. The existing test bench and experimental results will be explained in the following subsection.

3.7.1 Experimental Test Bench

Figure 3-7-1(a) presents the different parts of experimental test bench. The stator has a double-layer fractional-slot winding configuration. Due to its outer-rotor structure and high torque it is possible to directly mount the BLDC motor inside the vehicle wheel. In addition, because of its high number of poles, rotor magnets are simply installed on the inner surface of the rotor. Fast Fourier transform of the measured back-EMF waveform results in 11% of third harmonic and 5% of seventh harmonic.

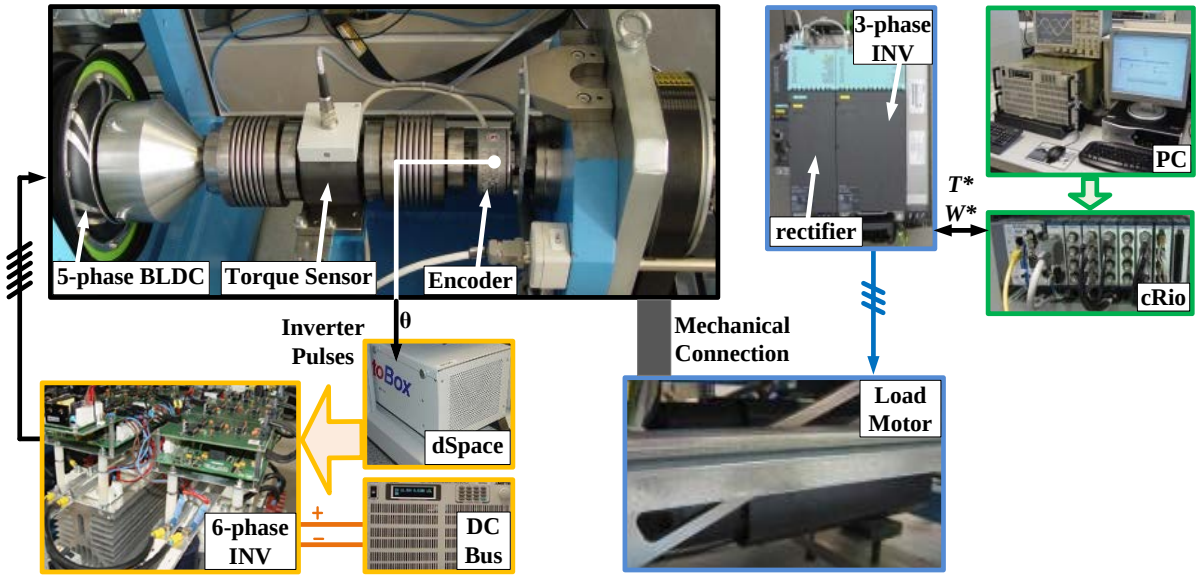

(a)

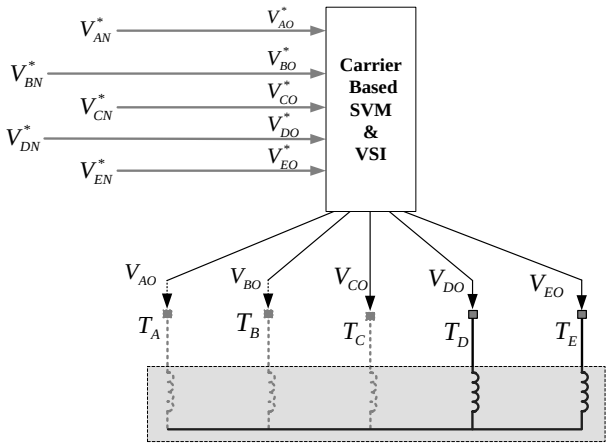

(b)

Figure 3-7-1 (a) Test bench configuration, (b) Motor voltage application configuration

An IGBT-based six-leg two-level voltage source inverter (VSC) is connected to motor five terminals and its neutral point. The speed is fixed. under each condition, real values of stator currents are compared to their reference values, and the resultant current errors are entered to proportional-resonant (PR) controllers to calculate the reference voltages of each stator phase [31].

Produced voltages at the controller outputs are applied to the pulse width modulation (PWM) block, and generated signals of PWM block are applied to voltage source inverter (VSI). Computed reference values of phase-to-neutral voltages can be written as { V^*_{AN}, V^*_{BN}, V^*_{CN}, V^*_{DN}, V^*_{EN}}.

During experimental tests, mechanical speed is fixed on 200 rpm by the load system. A DS1005 dSpace board is used to implement the control algorithms of five-phase stator currents. In addition, inverter controlling pulses are generated in dSpace block. Stator current feedbacks are realized by Hall Effect sensors, and a 9000-pulse/revolution incremental encoder is used to measure the mechanical position of the motor shaft. Motor speed is fixed by load system which is an independent AC SIEMENS drive (known as SINAMICS-S120) with a commercial three-phase PMSM motor. As a result, control schemes implemented are equivalent to torque control. A real-time National Instruments controller (known as cRio) prepares the required interference between the host PC and three-phase drive.

3.7.2 Experimental Result Evaluation

Experimental tests are conducted in laboratory to evaluate the behaviour of proposed controlling method. Measured values of stator phase currents are presented in Fig. 3-7-2 while changing the reference value of torque from 0.33 pu → 0.66 pu → 1.0 pu → 0.66 pu → 0.33 pu. Due to limited number of available oscilloscope channels, each part of this figure only contains 4 measurements. In addition, to have a better evaluation on dynamic behaviour of proposed controlling method, measured values of mechanical torque and stator currents are shown in Fig. 3-7-3 for two periods of fundamental current component.

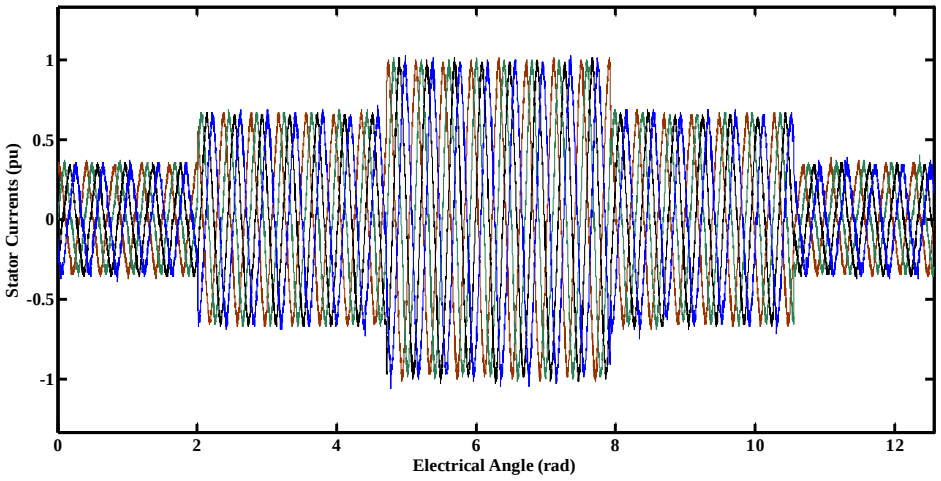

(a)

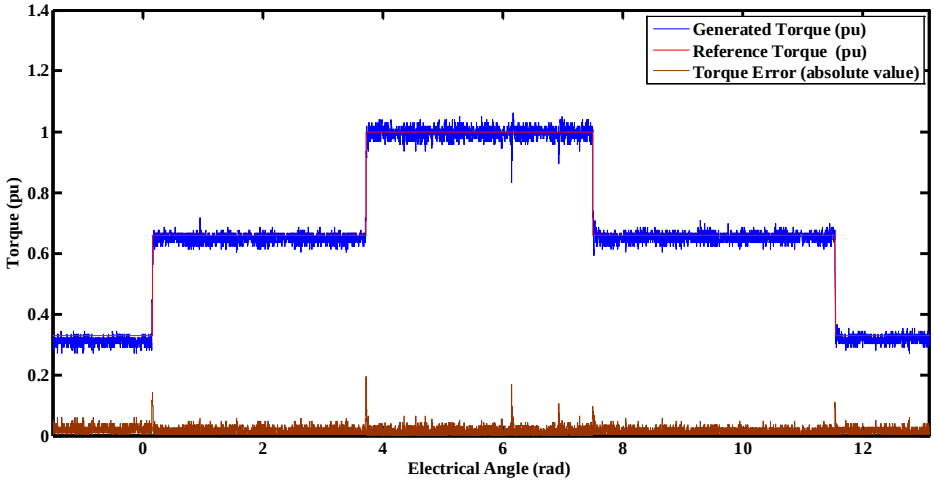

(b)

Figure 3-7-2 Dynamic behaviour of proposed controlling method while changing reference torque from 0.33 pu → 0.66 pu → 1.0 pu → 0.66 pu → 0.33 pu, (a) (first measurement) - stator phase currents, (b) (second measurement) - reference and real values of torque

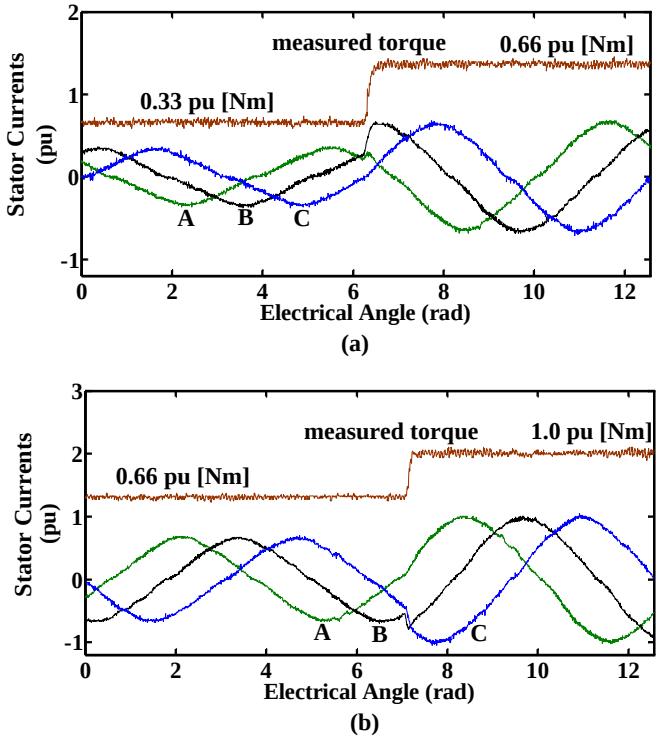

Figure 3-7-3 Measured value of generated torque during transient states, (a) changing reference torque from 0.33 pu → 0.66 pu , (b) changing reference torque from 0.66 pu → 1.0 pu

Proposed current controlling method does not include any integrator, and as a result there is almost no overshoot in measured values of stator phase currents and

generated torque.

3.7.2.1 Transient Analysis of Proposed EKF-PDC Method

Regarding the deadbeat nature of implemented control algorithm, torque rise time is expected to be as long as one modulation period (0.25 ms). However during transient states, measured value of torque rise-time is 0.53 ms which is almost 2 times its expected value.

The main reason of longer rise-time is limited value of dc-link voltage. Assuming that the main component of stator currents in each situation is i_{q1} and stator currents in the remaining directions are almost zero, the required voltage during transient states in different directions can be calculated from equation (3-4-4) and Table 3-6-2. Table 3-7-1 is a summary of required voltages in $d_1q_1d_3q_3$-directions during transient states, and their required peak-to-peak voltage in phase reference frame.

Table 3-7-1 The required voltage to complete the transient state in one controlling loop (0.25 ms)

Transient state	V_{d1}	V_{q1}	V_{d3}	V_{q3}	$V_{ABCDE\ (p-p)}$
0.33 pu → 0.66 pu	-3.5096 V	58.6317 V	0 V	0.6873 V	58 V
0.66 pu → 1.0 pu	-7.0191 V	59.5184 V	0 V	0.6873 V	59 V

As it can be seen, the required peak-to-peak value of applied voltage during each transient is more than dc-link value (48 V), which extends the rise-time to two consecutive controlling loops. It is important to note that the controlling algorithm is being executed with a frequency of 4 kHz while modulator frequency is 10 kHz. Higher frequency of modulator is the main reason of existing ripples during transient states (rise-time) of stator currents and electrical torque in Fig. 3-7-3.

Dynamic behaviour of generated torque is also considered. To have an analytical evaluation, the energy of torque error is integrated on four consecutive periods of stator phase currents. Both transient and steady state operation are considered in this evaluation. 20000 torque samples are measured, and in the case of transients, reference value of torque is changed in the middle of integration period. Integrated values of torque error are summarized in Table 3-7-2 for each operational condition.

Table 3-7-2 The energy of torque error during different operational conditions

	Torque Error Energy [Nm^2] (pu)	
Steady State	Rated Conditions	1.08e-005
Transient State	0.33 pu → 0.66 pu	1.83e-005
	0.66 pu → 1.0 pu	1.98e-005

As it can be seen, the minimum value of torque error energy is related to steady-state operation. Under this condition, dc-link voltage is used to cope with stator resistance voltage drop, and induced back-EMF. While working in transients, dc-link voltage should also be used to cope with inductance voltage drops in each direction. As it can be seen, the energy of torque error is higher in transient states. The main reason of higher torque error in transients is dc-link limitations during rise time periods.

3.7.2.2 Sensitivity Analysis of Proposed EKF-PDC

Sensitivity of proposed controlling method is experimentally evaluated respect to various system changes. Comparing to simulation section, experimental evaluation of sensitivity has some limitations. The first limitation is related to inverter block. As five-phase BLDC machine is always fed by an inverter, it is not possible to evaluate the ideal case (no voltage drop in semiconductors and zero value of dead time). In addition, magnetic flux of rotor magnets is a fixed value during all tests. Conducted tests to evaluate the sensitivity of proposed method are summarized in Table 3-7-3.

Table 3-7-3 The differences between controlling block assumptions and real situation

	difference between controlling unit assumption and real situation	
experiment	**controlling unit Assumption**	**real situation**
eperiment-1	Ideal inverter with no voltage drop and dead time	Real inverter
experiment-2	Ideal inverter and nominal value of dc-link voltage	Real inverter and 20% voltage drop in dc-link voltage
experiment-3	Ideal inverter and rated value of resistance	Real inverter and doubled values of stator resistance

In the first experiment (experiment-1), precise values of machine parameters are used in control algorithm. In addition, inverter block is considered ideal and nonlinear characteristics of its semiconductors are not considered in controlling algorithm.

In the next step (experiment-2), stator phase resistances are doubled by adding external resistances to machine terminals, and at the same time, rated values of stator resistances are used in controlling algorithm.

In the third step (experiment-3), the amplitude of dc-link voltage is reduced by 20%, and at the same time rated value of dc-link voltage is used in controlling algorithm.

Similar to simulation section, in each experiment the difference between real and reference values of stator phase currents are measured and its energy is integrated over one period of fundamental electrical frequency:

$$E = \int_{T} \sum_{j=d1,q1,d3,q3,o} \left[I_j^* - I_j(K+2) \right]^2$$

Eq.3-7-1

Figure 3-7-4 shows the energy of stator current errors for each experiment.

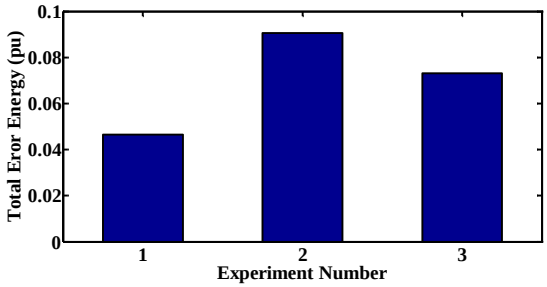

Fig. 3-7-4 The energy of current errors during each experiment

The minimum energy value of stator current errors is correspondent to experiment-1. The main sources of error during this experiment are nonlinear characteristics of inverter. The energy of current errors during experiment-1 is more than 50% its value during other experiments (51% its value during experiment-2 and 63% its value during experiment-3). As electrical machine is always fed by a real inverter, it is possible to write:

$$E_{nonlinear\ INV} > 0.5\ (E_{nonlinear\ INV} + E_{dc-link})$$

Eq.3-7-2

and

$$E_{nonlinear\ INV} > 0.5\ (E_{nonlinear\ INV} + E_{Rs})$$

Eq. 3-7-3

while $E_{nonlinear\ INV}$, $E_{dc\text{-}link}$, and E_{Rs} are respectively the energy of stator current errors due to “nonlinear inverter characteristics”, “inaccurate dc-link voltage” , and “stator resistance increment”. By considering (3-7-2) and (3-7-3) it is possible to conclude that the energy of stator current errors due to “inverter nonlinear characteristics” is higher than its value due to “inaccurate dc-link voltage” and “inaccurate stator resistance”. This result is in accordance with simulation results where the maximum value of stator current errors was due to inverter nonlinear characteristics.

In addition, the energy of stator current errors in experiment-3 is higher than its value in experiment-2. Regarding Table 3-7-3, it is possible to write:

$$(E_{nonlinear\ INV} + E_{dc-link}) > (E_{nonlinear\ INV} + E_{Rs})$$

Eq. 3-7-4

Regarding (3-7-4), it is possible to conclude that the energy of stator current errors due to "inaccurate dc-link voltage" is higher than its value due to "inaccurate stator resistance" which is again in accordance with simulation results.

3.8 Summary

In this chapter, electrical model of five-phase BLDC machine is derived. A new predictive deadbeat controlling method is developed to control the stator currents of a five-phase BLDC machine. Extended Kalman Filter is used in the estimation step of proposed method.

Simulations are developed to evaluate the sensitivity of proposed method respect to different system variations. In each case, the energy of stator current errors is measured by the end of estimation step and voltage application step. It is shown that inverter nonlinear characteristics and dc-link voltage drop result in more current error both in estimation step and voltage application step.

In addition, proposed controlling method is experimentally evaluated on five-phase BLDC machine. Although the objective of proposed EKF-PDC method is to eliminate the stator current errors in one modulation period, but limited values of dc-link voltage can reduce the speed of proposed controlling method. Proposed method is able to have a good utilization of dc-bus voltage with no overshoot and no need to anti-windup algorithm. Simulation results are also verified by experimental evaluations.

3.9 References

[1] A. Linder and R. Kennel, "Model predictive control for electrical drives," in Proc. IEEE Power Electron. Spec. Conf., Recife, Brazil, 2005, pp. 1793–1799.

[2] P. Cortés, M. P. Kazmierkowski, R. M. Kennel, D. E. Quevedo, and J. Rodríguez, "Predictive control in power electronics and drives," IEEE Trans. Ind. Electron., vol. 55, no. 12, pp. 4312–4324, Dec. 2008.

[3] M. R. Arahal, F. Barrero, S. Toral, M. J. Durán, and R. Gregor, "Multiphase current control using finite-state model-predictive control," Control Eng. Pract., vol. 17, no. 5, pp. 579–587, May 2009.

[4] F. Barrero,M. R. Arahal, R. Gregor, S. Toral, andM. J. Durán, "A proof of concept study of predictive current control for VSI-driven asymmetrical dual three-phase ac machines," IEEE Trans. Ind. Electron., vol. 56, no. 6, pp. 1937–1954, Jun. 2009.

[5] F. Barrero, M. R. Arahal, R. Gregor, S. Toral, and M. J. Durán, "Onestep modulation predictive current control method for the asymmetrical dual three-phase induction machine," IEEE Trans. Ind. Electron., vol. 56, no. 6, pp. 1974–1983, Jun. 2009.

[6] R. Gregor, F. Barrero, S. Toral, M. J. Durán, M. R. Arahal, J. Prieto, and J. L. Mora, "Predictive-SVPWM current control method for asymmetrical dual-three phase induction motor drives," IET Elect. Power Appl., vol. 4, no. 1, pp. 26–34, Jan. 2010.

[7] R. Gregor, F. Barrero, J. Prieto,M. R. Arahal, S. L. Toral, andM. J. Durán, "Enhanced predictive current control method for the asymmetrical dual three phase induction machine," in Proc. IEEE IEMDC,Miami, FL, 2009, pp. 265–272.

[8] M. J. Durán, M. R. Arahal, F. Barrero, S. L. Toral, and R. Gregor, "Restrained search predictive control of dual three-phase induction motor drives," in Proc. ICREPQ, Valencia, Spain, 2009.

[9] M. J. Durán, F. Barrero, S. L. Toral, M. R. Arahal, and J. Prieto, "Improved techniques of restrained search predictive control for multiphase drives," in Proc. EPE, Barcelona, Spain, 2009, pp. 1–9.

[10] M. J. Durán, F. Barrero, S. L. Toral, M. R. Arahal, and J. Prieto, "Improved techniques of restrained search predictive control for multiphase drives," in Proc. IEEE IEMDC, Miami, FL, 2009, pp. 239–244.

[11] M. J. Durán, J. Prieto, F. Barrero, and S. Toral, "Predictive current control of dual three-phase drives using restrained search techniques," IEEE Trans. Ind. Electron., DOI: 10.1109/TIE.2010.2087297.

[12] T. M. Jahns, "Improved reliability in solid state AC drives by means of multiple independent phase-drive units," IEEE Trans. Ind. App., vol. IA-16, no. 3, pp. 321-331, May 1980.

[13] Y. Fujimoto, T. Sekiguchi, "Fault-tolerant configuration of distributed discrete controllers," IEEE Trans. Ind. Elect., vol. 50, no. 1, pp. 86-93, Feb. 2003.

[14] A. Linder and R. Kennel, "Model predictive control for electrical drives," in Proc. IEEE Power Electron. Spec. Conf., Recife, Brazil, Jun. 2005, pp. 1793–1799.

[15] S. Mariethoz, A. Domahidi, and M. Morari, "Sensorless explicit model predictive control of permanent magnet synchronous motors," in Proc. IEEE Int. Elect. Mach. Drives Conf.,Miami, FL,May 2009, pp. 1250–1257.

[16] Errouissi, Rachid ; Ouhrouche, M. ; Wen-Hua Chen ; Trzynadlowski, A.M."Robust Cascaded Nonlinear Predictive Control of a Permanent Magnet Synchronous Motor With Antiwindup Compensator", IEEE Trans. Ind. Electron, Vol. 59 , num.: 8, pp. 1896-1908

[17] R. Dhaouadi, N. Mohan, and L. Norum, "Design and implementation of an extended Kalman filter for the state estimation of a permanent magnet synchronous motor," IEEE Trans. Power Electron., vol. 6, pp. 491–497, July 1991.

[18] B. J. Brunsbach and G. Henneberger, "Field-oriented control of synchronous and asynchronous drives without mechanical sensors using a Kalman filter," in Proc. EPE'91, vol. 3, Florence, Italy, 1991, pp. 3.664–3.671.

[19] H. Brunsbach, G. Henneberger, and T. Klepsch, "Position controlled permanent excited synchronous motor without mechanical sensors," in Proc. EPE'93, Brighton, U.K., 1993, pp. 38–43.

[20] G. Hock Beng Foo, Xinan Zhang, D. M. Vilathgamuwa, "Interior Permanent-Magnet Synchronous Motor Drives Based on an Extended Kalman Filter",
IEEE Trans. on Ind. Elec., Vol. 60, No. 8, Aug. 2013, 3485

[21] Rached Dhaouadi, Ned Mohan, Member, Lars Norum, “Design and Implementation of an Extended Kalman Filter for the State Estimation of a Permanent Magnet Synchronous Motor”, IEEE Trans. on Power Elec., Vol. 6, No. 3, July 1991 49 I

[22] Ede, J., Atallah, K., Wang, J., Howe, D. :'Effect of Optimal Torque Control on Rotor Loss of Fault-Tolerant Permanent-Magnet Brushless Machines’, IEEE Trans. Mag., 2002, 38, (5), pp. 3291–3293

[23] Parsa, L., Toliyat, H. :'Five-Phase Permanent-Magnet Motor Drives’, IEEE Trans. Ind. Appl., 2005, 41, (1), pp. 30-37

[24] Bianchi, N., Bolognani, S., Pré, M., Fornasiero, E. :'Post-fault operations of five-phase motor using a full-bridge inverter’, Power Electron. Specialists Conf., 2008, IEEE, pp. 2528–2534

[25] Villani, M., Tursini, M., Fabri, G., Castellini, L. :'Multi-phase permanent magnet motor drives for fault-tolerant applications’, Electric Machines & Drives Conf., IEMDC 2011, IEEE 2011, pp. 1351-1356

[26] Ayyar, K., Ramesh, K., Gurusamy, G., Kaewwiset, W., Thamaphat, K., Kaewkhao, Ja., Limsuwan, P. :'Design of Speed Controller for Permanent Magnet Synchronous Motor Drive Using Genetic Algorithm Based Lower Order System Modelling’, Journal of Computer Science, 2012, pp 1700-1710

[27] Soleimani, M., Asghar Gholamian, S. :'Optimum Design of a Three-Phase Permanent Magnet Synchronous Motor for industrial applications’, International Journal of Applied Operational Research, 2013, 2, (4), pp. 67-86

[28] Ryu, H., Kim, J., Sul, S. :'Analysis of Multi-phase Space Vector Pulse Width Modulation Based on Multiple d-q Spaces Concept’, IEEE Trans. Power Electron., 2005, 20, (6), pp. 1364-1371

[29] Prieto, J., Jones, M., Barrero, F., Levi, E., Toral, S. :'Comparative Analysis of Discontinuous and Continuous PWM Techniques in VSI-Fed Five-Phase Induction Motor’, IEEE Trans. on Ind. Electron., 2011, 58, (12), pp. 5324-5335

[30] Alonge, F. ; D'Ippolito, F. ; Sferlazza, A., “Sensorless Control of Induction-Motor Drive Based on Robust Kalman Filter and Adaptive Speed Estimation”, Industrial Electronics, IEEE Transactions on Vol. 61 , No. 3, 2014 , p-p. 1444 - 1453

[31] C´ardenas, R., Juri, C., Pe˜na, R., Wheeler, P., Clare J., "The Application of Resonant Controllers to Four-Leg Matrix Converters Feeding Unbalanced or Nonlinear Loads”, IEEE Trans. On Power Electron., 2012, 27, (3), pp. 1120 – 1129

4.

Chapter 4 Reference Current Optimization of Fault Tolerant Five-Phase BLDC Drive

This chapter is dedicated to improve the output power of five-phase brushless direct current (BLDC) motors under different faulty conditions. Different machine connections are considered while having open circuit fault in one and two stator phases, and both fundamental and third harmonic component of stator currents are controlled to improve the amplitude and quality of generated torque under faulty conditions. Rated RMS value of stator phase currents is considered as the main limiting factor of generated electrical torque. Genetic algorithm (GA) is used in the optimization procedure of stator reference currents to avoid additional simplifying constraints and gain more output power under the fault. Theoretical developments are verified by experimental tests on five-phase BLDC motor.

CONTENTS

4.7 References

4.1. Introduction

Higher reliability of multi-phase machines makes them good candidates for high safety applications [1]. Five-phase PM machines are able to continue their operation in the case of missing one or even two stator phases [2] [3]. Being capable to operate under faulty conditions is very interesting for applications such as automotive industries where sudden operational interrupts are not acceptable [4] [5].

Appropriate reference values of stator currents are calculated in [2] and [6] for a five-phase BLDC motor to generate a smooth torque under different faulty conditions. Both first and third current harmonics are used to suppress the second and fourth harmonic components of torque ripples. The same idea is used in [1] for a poly-phase PM motor where each phase is wounded around one stator tooth to reduce the mutual inductances of stator windings.

To improve the generated torque under faulty conditions, both amplitude and phase angle of fundamental and third current harmonics should be optimized in the remaining healthy phases. That is 16 unknown variables while missing one faulty phase, and 12 unknown variables in the case of missing two phases. Due to high number of unknown variables, long-step for-loops are used in the optimization procedure of [7] for a five-phase BLDC machine under faulty condition. In [8] third harmonic component of stator current is ignored to simplify the optimization procedure. However this simplification results in high electrical torque ripples under faulty conditions. Moreover, in both [7] and [8] rated value of total stator copper loss is considered as the main limitation of phase currents which leads to phase winding over-load and high operational temperature under faulty conditions.

In [2] and [9] reference values of stator currents are calculated while not having access to machine´s neutral point. To simplify the optimization procedure, amplitude of stator current fundamental component is considered the same for the remaining healthy phases, and the total sum of stator phase currents is limited to zero. This limitation is removed in [3] by using a full-bridge configuration for feeding each motor phase. In addition, to simplify the calculations it is assumed that: 1) the amplitudes of first and third current harmonics do not change from phase to phase, 2) electrical phase angle of first and third current harmonics are the same in each healthy phase, 3) six^{th} harmonic component of generated torque is negligible. In [9] a good comparison is carried out on different configurations of stator winding including star, pentagon and pentacle topologies, and it is shown that while there is no access to neutral point, penta-type winding configuration results in higher amount of ripple-free torque.

In this chapter, previous simplifications are removed from optimization procedure of stator current references by means of genetic algorithm (GA). This is an effective optimization tool which can be used in the case of multi-objective problems with high number of unknown variables and nonlinear relations. This method has been recently implemented for improving both the control and the design of a PM motor. In [10] GA is used to improve the speed controller of three-phase PM motor and its dynamic behavior. In [11],

this algorithm is implemented in a multi-objective PMSM design to improve motor efficiency and power density. In addition, GA is used in [12] to reduce the material cost of axial flux PM motors.

In this chapter, first and third harmonic component of stator currents are considered in the case of having both one and two faulty phases. Amplitude and phase angle of stator current harmonics are separately optimized in the remaining healthy phases. To consider all conditions, the limiting constraint of having zero sum of stator currents is removed by connecting machine´s neutral point to the inverter through an extra half-bridge leg. Rated RMS value of stator phase currents is considered as the main limiting factor of generated electrical torque, and it is shown that the derived current reference values result in higher amplitude of electrical torque. In addition, having access to neutral point improves fault tolerant capability of the machine. Theoretical developments are first simulated and later verified experimentally on a five-phase outer-rotor type of an in-wheel BLDC hub motor.

4.2. Optimization Objectives

In general, the main objective of optimization procedure is to increase the amplitude of generated ripple-free torque, and at the same time, to limit the RMS value of stator phase currents under 1 pu. In a five-phase BLDC machine, stator winding flux produced by rotor magnets can be estimated by its fundamental and third harmonic component:

$$\Lambda_m = \lambda_{m1}\begin{bmatrix} \sin(\theta) \\ \sin(\theta-\frac{2\pi}{5}) \\ \sin(\theta-\frac{4\pi}{5}) \\ \sin(\theta-\frac{6\pi}{5}) \\ \sin(\theta-\frac{8\pi}{5}) \end{bmatrix} + \lambda_{m3}\begin{bmatrix} \sin(3\theta) \\ \sin 3(\theta-\frac{2\pi}{5}) \\ \sin 3(\theta-\frac{4\pi}{5}) \\ \sin 3(\theta-\frac{6\pi}{5}) \\ \sin 3(\theta-\frac{8\pi}{5}) \end{bmatrix}$$

Eq. 4-2-1

where θ is rotor electrical angle and λ_{m1} and λ_{m3} are first and third harmonic components of rotor magnet flux linkage. As a result, the induced back-EMF waveform of such machines will be the derivative of (4-2-1) with respect to time:

$$E = E_1\begin{bmatrix} \cos(\theta) \\ \cos(\theta-\frac{2\pi}{5}) \\ \cos(\theta-\frac{4\pi}{5}) \\ \cos(\theta-\frac{6\pi}{5}) \\ \cos(\theta-\frac{8\pi}{5}) \end{bmatrix} + E_3\begin{bmatrix} \cos(3\theta) \\ \cos 3(\theta-\frac{2\pi}{5}) \\ \cos 3(\theta-\frac{4\pi}{5}) \\ \cos 3(\theta-\frac{6\pi}{5}) \\ \cos 3(\theta-\frac{8\pi}{5}) \end{bmatrix}$$

Eq. 4-2-2

while

$$E_1 = \lambda_{m1}\frac{d}{dt}\theta$$

$$E_3 = 3\lambda_{m3}\frac{d}{dt}\theta$$

Eq. 4-2-3

Taking into account the fundamental and third harmonic component of both stator current and back-EMF, the instantaneous power of each phase can be calculated as:

$$i(t) = I_1\cos(wt-\theta_{i1}) + I_3\cos(3wt-\theta_{i3})$$

$$e(t) = E_1\cos(wt-\theta_{e1}) + E_3\cos(3wt-\theta_{e3})$$

$$p(t) = e(t).i(t) \ = P_0 + P_2 + P_4 + P_6$$

Eq. 4-2-4

where

$$P_0 = 0.5I_1E_1\cos(\theta_{i1}-\theta_{e1}) + 0.5I_3E_3\cos(\theta_{i3}-\theta_{e3})$$

$$P_2 = 0.5I_1E_1\cos(2wt-\theta_{i1}-\theta_{e1}) +$$

$$+0.5I_1E_3\cos(2wt+\theta_{i1}-\theta_{e3}) +$$

$$+0.5I_3E_1\cos(2wt-\theta_{i3}+\theta_{e1})$$

$$P_4 = 0.5I_1E_3\cos(4wt-\theta_{i1}-\theta_{e3}) +$$

$$+0.5I_3E_1\cos(4wt-\theta_{i3}-\theta_{e1})$$

$$P_6 = 0.5I_3E_3\cos(6wt-\theta_{i3}-\theta_{e3})$$

Eq. 4-2-5

P_0 is the constant (non-oscillating) part of output power. On the other hand P_2, P_4, and P_6 are oscillating components of output power and responsible for electrical torque ripples. Operational temperature of motor windings is the main limiting factor of stator currents and consequently P_0. To avoid local stator thermal stress (hot spots), it is important to limit the maximum RMS value of stator phase currents [2]. BLDC motor of this study contains 11% of third harmonic component in its back-EMF waveform. Per unit (pu) values are considered in the calculations, and it is assumed that under normal conditions, the effective (RMS) value of stator phase currents is 1 pu.

Regarding machine symmetry, any of the stator phases can be considered as faulty phase. Assuming an open circuit fault in phase A, for example, stator phase currents can be considered as:

$$I_A = 0$$

$$I_B = I_{B1}\cos(\theta-\theta_{B1}) + I_{B3}\cos 3(\theta-\theta_{B3})$$

$$I_C = I_{C1}\cos(\theta - \theta_{C1}) + I_{C3}\cos 3(\theta - \theta_{C3})$$
$$I_D = I_{D1}\cos(\theta - \theta_{D1}) + I_{D3}\cos 3(\theta - \theta_{D3})$$
$$I_E = I_{E1}\cos(\theta - \theta_{E1}) + I_{E3}\cos 3(\theta - \theta_{E3})$$

Eq. 4-2-6

In addition, in the case of missing two adjacent phases (e.g., phase A and B), stator currents can be assumed as:

$$I_A = 0$$
$$I_B = 0$$
$$I_C = I_{C1}\cos(\theta - \theta_{C1}) + I_{C3}\cos 3(\theta - \theta_{C3})$$
$$I_D = I_{D1}\cos(\theta - \theta_{D1}) + I_{D3}\cos 3(\theta - \theta_{D3})$$
$$I_E = I_{E1}\cos(\theta - \theta_{E1}) + I_{E3}\cos 3(\theta - \theta_{E3})$$

Eq. 4-2-7

Stator phase currents of a five-phase BLDC machine with two nonadjacent faulty phases (e.g., phase A and C) would be:

$$I_A = 0$$
$$I_B = I_{B1}\cos(\theta - \theta_{B1}) + I_{B3}\cos 3(\theta - \theta_{B3})$$
$$I_C = 0$$
$$I_D = I_{D1}\cos(\theta - \theta_{D1}) + I_{D3}\cos 3(\theta - \theta_{D3})$$
$$I_E = I_{E1}\cos(\theta - \theta_{E1}) + I_{E3}\cos 3(\theta - \theta_{E3})$$

Eq. 4-2-8

In each set of equations (4-2-4) to (4-2-8), amplitude and phase angle of first and third current harmonics should be optimized to improve the quality and amplitude of generated torque. Several assumptions are considered in the literature to reduce the number of unknown variables and conduct an analytical optimization [2] [3]. However, none of these approaches consider a global current optimization. In the next section, all these variables will be optimized without additional simplifications to improve generated output torque of the machine under each faulty condition.

4.3. Optimization Method

The optimization procedure is realized by means of genetic algorithms. This is a searching technique which is based on natural evolution of individuals in a specific population. Three main GA operations are reproduction, crossover and mutation. During reproduction process, each individual string will be regenerated according to its fitness. Similar to natural selection, the chance of being copied is directly

proportional to the fitness of each individual. While having a crossover, new individuals are generated by selecting two individual strings and exchanging specific parts of their structures. Mutation is a local operation with low likelihood. During mutation a random bit of an individual string will be simply changed from 1 to 0 or vice versa [13].

In this chapter, GA is used to optimize the amplitude and electrical angle of each current harmonic component and improve the delivered mechanical power. Each individual is defined as an array of double-type variables. Depending on the fault type, the members of each individual represent the amplitude and phase angle of stator reference currents in the remaining healthy phases. The number of individuals is set to 4000 with a uniform stochastic distribution. As shown in Fig. 4-2-1, at the first step, the population is generated randomly and checked if the individuals satisfy the following constraints:

1) P_0 has been increased,
2) P_2, P_4, and P_6 values are negligible (less than 0.01 pu),
3) Maximum RMS value of stator currents in the remaining healthy phases is not more than 1 pu,
4) In the case of having an isolated neutral point, the total sum of stator currents is equal to zero (this constraint is ignored in the case of having access to motor neutral point):

$$i_A(t) + i_B(t) + i_C(t) + i_D(t) + i_E(t) = 0$$

Eq. 4-2-1

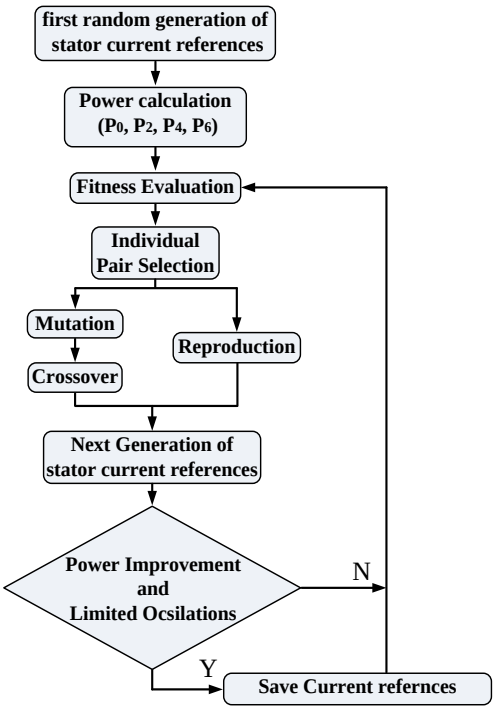

Figure 4-2-1 General block diagram of applied GA optimization

The next generation of population will be obtained by applying GA operators to the current population, and this procedure is repeated for each generation [11]. Maximum value of iterations is set to 100, and a maximum of 0.01 is considered as the upper limit of oscillating part of output power.

4.4. Optimized Reference Values

Optimized reference currents in the case of different faulty conditions are summarized in Fig.4-4-1 and Table 4-4-1 and Table 4-4-2. It is worth noting that although symmetry is not considered as a constraint in GA optimization, but as it can be seen, the results are symmetric respect to the faulty phases.

Table 4-4-1 Optimized phase currents - isolated neutral point

Currents	A	B	C	D	E
one faulty phase					
I_1 (pu)	0	0.99	0.99	1	0.98
θ_1°	-	51	137	232	-41
I_3 (pu)	0	0.17	0.08	0.09	0.19
θ_3°	-	23	52	186	-19
two adjacent faulty phases					
I_1 (pu)	0	0	0.59	0.95	0.67
θ_1°	-	-	82	218	1
I_3 (pu)	0	0	0.12	0.29	0.16
θ_3°	-	-	44	102	41
two nonadjacent faulty phases					
I_1 (pu)	0	0.99	0	0.98	0.99
θ_1°	-	77	-	197	-42
I_3 (pu)	0	0.16	0	0.19	0.17
θ_3°	-	15	-	55	-21

Table 4-4-2: Optimized phase currents - available Neutral

Currents	A	B	C	D	E
one faulty phase					
I_1 (pu)	0	0.98	0.99	1	0.98
θ_1°	-	68	150	-150	-68
I_3 (pu)	0	0.19	0.11	0.11	0.19
θ_3°	-	21	66	-66	-21
two adjacent faulty phases					
I_1 (pu)	0	0	0.98	0.98	0.99
θ_1°	-	-	153	216	281
I_3 (pu)	0	0	0.13	0.13	0.11
θ_3°	-	-	88	98	106
two nonadjacent faulty phases					
I_1 (pu)	0	0.96	0	0.99	0.98
θ_1°	-	64.2	-	194	309
I_3 (pu)	0	0.3	0	0.12	0.24
θ_3°	-	2.5	-	36	93

Once the optimization is completed, reference current amplitudes can be adjusted proportionally with the required torque demand. As it is shown in Fig. 4-4-2, by measuring rotor position, it is possible to calculate the optimized reference currents which result in 1-pu amount of electrical torque. By multiplying these current references by pu values of torque reference, it is possible to compute appropriate reference currents during each modulation period.

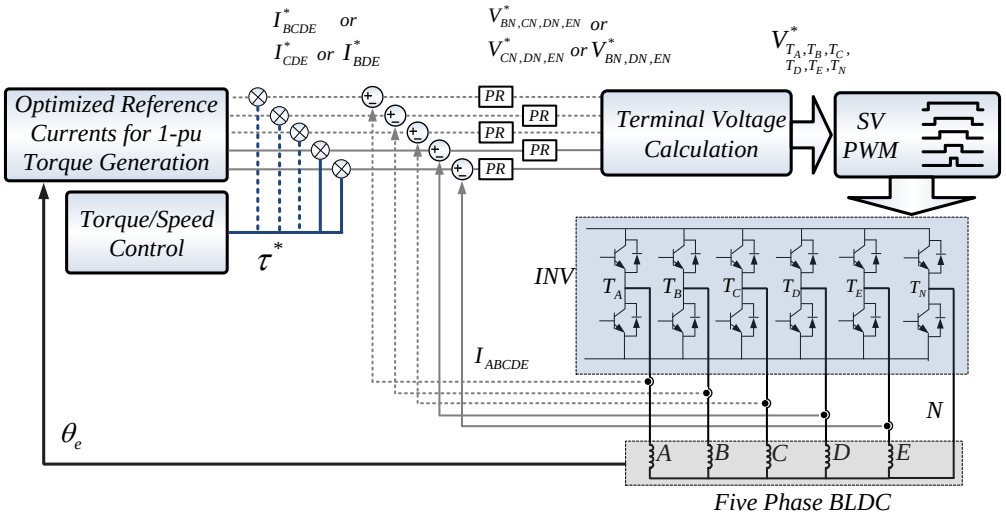

Figure 4-4-2 Implemented current control topology under different faulty conditions

Table 4-4-3 Computed output power of five-phase BLDC under different conditions

		Output Power (% rated value)		
Motor condition	$\sum_{k=A,B,C,D,E} i_k$	Genetic Algorithm	Analytical Calculation (Independent phase current control [3])	Analytical Calculation (Star connection with isolated neutral [2][9])
Healthy motor	0	100	100	100
One faulty phase	0	74.5	74	74.3 - 74.6
	no limitation	79.0	75	-
Two adjacent faulty phases	0	27.4	17	19
	no limitation	58.7	55	-
Two nonadjacent faulty phases	0	55.7	61	56.4 - 57
	no limitation	56.1	53	-

Table 4-4-3 presents a comparison between GA optimization results and previous studies. In all conditions, having access to neutral point removes the constraint of zero stator current sum, and this additional freedom factor results in more output power. Comparing with previous investigations, global optimization results in more output power in the case of having one faulty phase and two adjacent faulty phases which are the most common type of faults in five-phase BLDC motors. This increment is more remarkable in the case of having two adjacent faulty phases with an isolated neutral point. In the case of having two nonadjacent faulty phases, the results are close to previous published studies.

It is important to mention that, in the case of having two nonadjacent faulty phases and zero value of homopolar current, GA optimization results in less output power. In this case, the main reason of lower output power is torque ripple restrictions of GA optimization. During GA optimization, each component of oscillating power is limited to 0.01 pu, and maximum amplitude of total oscillating power is less than 0.0128 pu. This amplitude is higher in other studies and changes from 1.5% to 6% rated power.

4.5. Simulation and Experimental Results

To obtain the distribution of stator magnetic flux under each faulty condition, simulations are conducted in MATLAB environment. In addition, motor operation with optimized values of stator reference currents is evaluated by experimental tests.

Fundamental component of stator magnetic flux F_1 and its third harmonic F_3 are shown in Fig.4-5-1 for different faulty conditions. In all cases, F_3 rotates three times faster than F_1. To achieve constant torque with limited ripples, (multiplication of λ_{m1} by F_1-projection on q_1-axis) plus (multiplication of $3\lambda_{m3}$ by F_3-projection on q_3-axis) should be maintained constant in all rotor positions.

In the case of having one faulty phase, or two nonadjacent faulty phases, the main part of electrical torque is generated by F_1. Under these conditions, F_3 is mainly used to reduce the generated torque ripples and to satisfy (4-2-1). Considering only F_1 and no access to neutral point, generated peak-to-peak value of torque ripples are 19% of nominal torque in the case of one faulty phase and its 18% in the case of two nonadjacent faulty phases. Having access to neutral point, condition (4-2-1) can be neglected which results in a different path for F_3 in both cases. Moreover, this additional degree of freedom reduces F_1 ripples to 16% in the case of one faulty phase and 14% in the case of two nonadjacent faulty phases.

While having two adjacent faulty phases and no access to neutral point, generated torque ripples of F_1 reach up to 52% rated value. As a result high amplitude of F_3 is required to reduce the ripples and satisfy (4-2-1). However, as it is shown in Fig. 4-5-1, having access to neutral point reduces the generated ripples of F_1 to 6%. Lower amplitude of generated ripples reduces the required amount of F_3 and releases more capacity for fundamental current injection which itself results in noticeable torque increment of 30.5% rated torque.

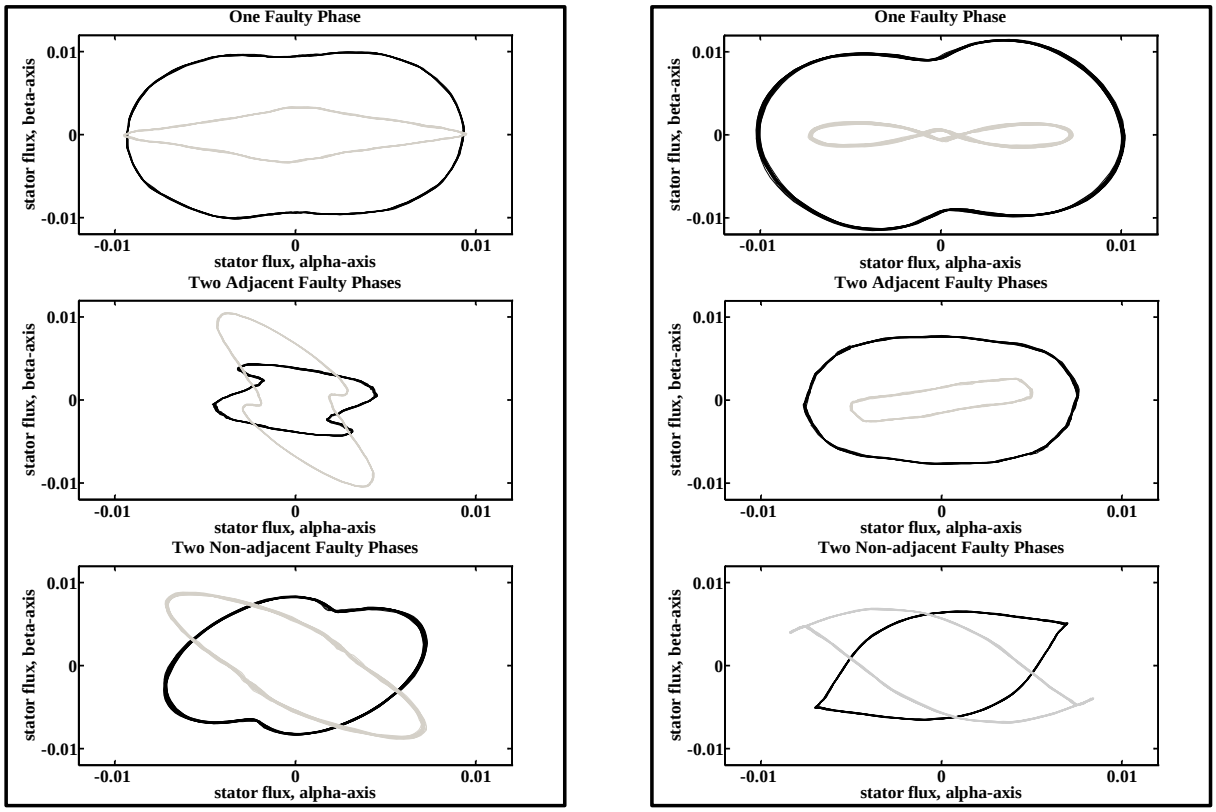

(a) (b)

Figure 4-5-1 Optimized flux path of first (black) and third (gray) stator current harmonics, (a) Isolated neutral point, (b) Connected neutral point

Optimized results are also evaluated by the existing experimental test bench in Laboratory. Fast Fourier transform of the measured back-EMF waveform results in 11% of third harmonic and 5% of seventh harmonic.

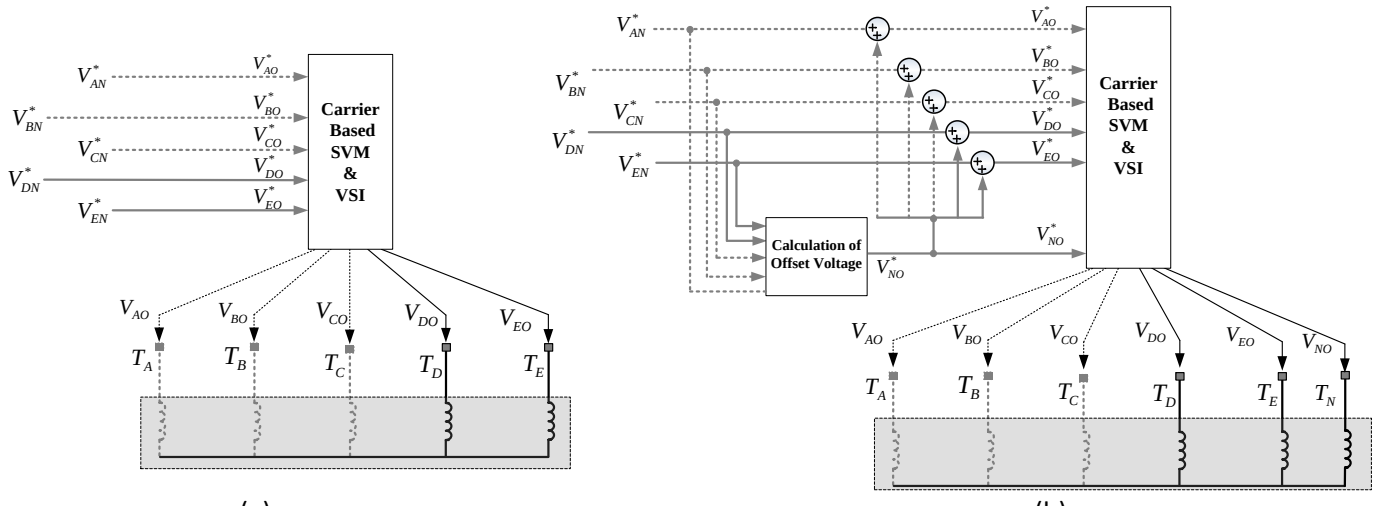

(a) (b)

Figure 4-5-2 (a) Implemented Carrier-Based SVM under faulty conditions and while neutral point is isolated, (b) implemented carrier-based SVM while neutral point is accessible

An IGBT-based six-leg two-level voltage source inverter (VSC) is connected to motor five terminals and its neutral point. The speed is fixed. Under each condition, real values of stator currents are compared to their reference values, and the resultant current errors are entered to proportional-resonant (PR) controllers to calculate the reference voltages of each stator phase [14].

Produced voltages at the controller outputs are applied to the pulse width modulation (PWM) block, and generated signals of PWM block are applied to voltage source inverter (VSI).

It is important to mention that in the case of having an isolated neutral point, appropriate voltage differences should be produced between the remaining terminals of electrical motor. That is {V_{AB}*, V_{BC}*, V_{CD}*, V_{DE}*}, {V_{BC}*, V_{CD}*, V_{DE}*}, {V_{CD}*, V_{DE}*} and {V_{BD}*, V_{DE}*} respectively while the motor is healthy, with one missing phase (phase A), with two adjacent missing phases (phases A and B), and with two non-adjacent missing phases (phases A and C). As shown in Fig. 4-5-2(a), while the neutral point of the machine is isolated calculated phase-to-neutral voltages of PR controllers are directly generated by their corresponding inverter legs, and each inverter leg is connected to its corresponding motor terminal.

In order to utilize the maximum capacity of available dc-link voltage, the presented modulation strategy of [15] is developed for the case of five-phase inverter when machine´s neutral is accessible. It should be noted that the developed carrier based modulation strategy is equivalent to the space vector modulation. This method is briefly explained in the following.

Computed reference values of phase-to-neutral voltages can be written as {V^*_{BN}, V^*_{CN}, V^*_{DN}, V^*_{EN}}, {V^*_{CN}, V^*_{DN}, V^*_{EN}}, {V^*_{BN}, V^*_{DN}, V^*_{EN}} respectively in the case of missing one phase (phase A), two adjacent phases (phases A and B), and two nonadjacent phases (phases A and C).

If the midpoint voltage of inverter dc-bus is V_O, then while having access to machine´s neutral point the required reference voltages can be written as {V^*_{BO}, V^*_{CO}, V^*_{DO}, V^*_{EO}, V^*_{NO}}, {V^*_{CO}, V^*_{DO}, V^*_{EO}, V^*_{NO}} and {V^*_{BO}, V^*_{DO}, V^*_{EO}, V^*_{NO}} respectively in the case of missing one phase (phase A), two adjacent phases (phases A and B), and two nonadjacent phases (phases A and C).

These reference voltages should be imposed to the remaining terminals of the machine and its neutral point. In the case of having access to machine's neutral point, appropriate value of V^*_{NO} for the neutral point of the machine are calculated as [15]:

$$V_{NO}^{*}=\begin{cases}-\dfrac{V_{\max}}{2}, & V_{\min}>0\\ -\dfrac{V_{\min}}{2}, & V_{\max}<0\\ -\dfrac{V_{\max}+V_{\min}}{2}, & Otherwise\end{cases}$$

Eq. 4-5-1

Where V_{min} is the minimum value of phase reference voltages, and V_{max} stands for the maximum value of phase reference voltages. Implemented PWM algorithm is shown in Fig.4-5-2(b). In this figure, dashed lines stand for the phases which can be with fault and disconnected.

During experimental tests, mechanical speed is fixed on 200 rpm by the load system. A DS1005 dSpace board is used to implement the control algorithms of five-phase stator currents. In addition, inverter controlling pulses are generated in dSpace block. Stator current feedbacks are realized by Hall Effect sensors, and a 9000-pulse/revolution incremental encoder is used to measure the mechanical position of the motor shaft. Motor speed is fixed by load system which is an independent AC SIEMENS drive (known as SINAMICS-S120) with a commercial three-phase PMSM motor. As a result, control schemes are equivalent to torque control. A real-time National Instruments controller (known as cRio) prepares the required interference between the host PC and three-phase drive. In order to evaluate dynamic behavior of control system, real values of stator currents are compared in Fig. 4-5-3. In each case, reference torque is changing from 0.5-pu to 1-pu which is measured and shown in Fig. 4-5-4 for all different conditions.

As it can be seen, even in the case of healthy machine and normal operation, there are some ripples in the measured torque. As non-salient structure of rotor does not introduce high amplitude of torque ripples, the main reasons of generated ripples can be mentioned as manufacturing problems and seventh harmonic of back-EMF waveform. These factors are ignored in the procedure of reference current calculation.

In many applications such as automotive industries, high current ripples are preferred to high switching frequency. This is because higher switching frequency leads to more losses in the inverter unit, and increases the generated electromagnetic interference. Moreover, high-frequency components of electrical torque can be effectively filtered by vehicle´s mechanical inertia. In addition, in many drive applications, the control algorithm is executed once in each modulation period which results in higher computational load in the case of higher switching frequencies. As a result (and due to limited computational power of implemented controller), the modulation (switching) frequency is selected as 5 kHz. In all cases, average values of measured torque are in accordance with the results of Table 4-4-3. In all faulty conditions, having access to neutral point results in more output power.

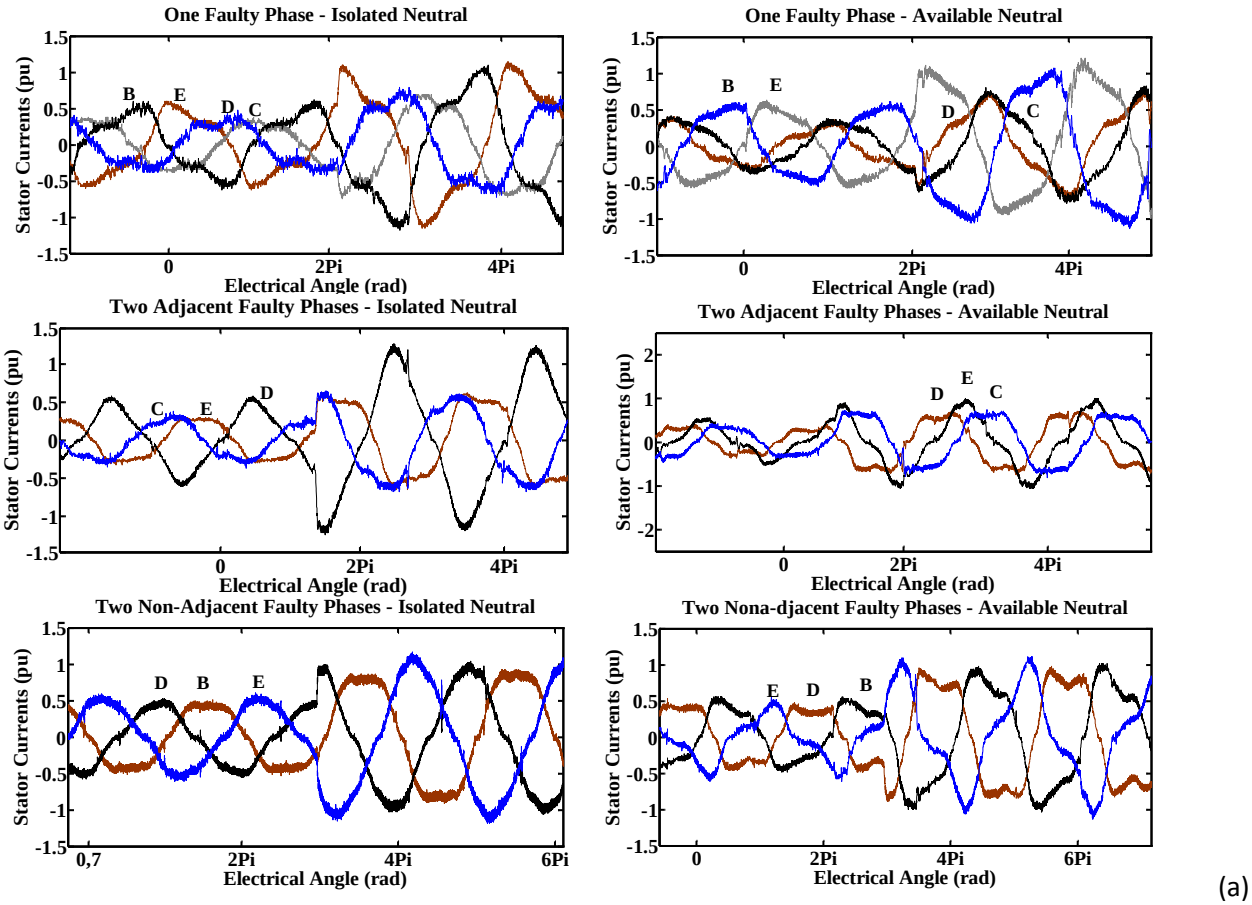

(a)

(b)

Fig.4-5-3: Real values of stator currents while changing reference torque from 0.5 to 1 rated torque, (a) isolated neutral point, (b) connected neutral point

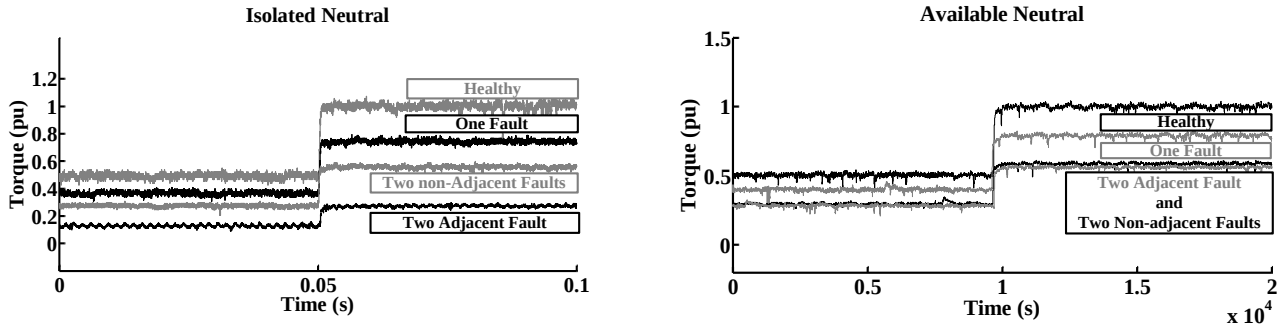

(a) (b)

Figure 4-5-4 Generated electrical torque under various conditions, (a) isolated neutral point, (b) connected neutral point

In the case of having one missing phase and no access to neutral point, RMS value of all currents are fixed to 1 pu. In this case, the maximum peak value of stator currents in the remaining healthy phases are $I_{B\text{-}peak}$=1.09 pu, $I_{C\text{-}peak}$=1.00 pu, $I_{D\text{-}peak}$=0.96 pu, and $I_{E\text{-}peak}$=1.13 pu. As stator neutral point is disconnected, there is no homopolar current in the stator phases. Simulated values of oscilating power components are respectively P_2=1.22%, P_4=1.35%, P_6= 0.21% of the output power (e. g. 74.5 pu). By connecting the neutral

point, the limiting constraint of zero current sum is removed, and electrical phase angle of current in the remaining healthy phases can be optimized to increase the average of output torque. RMS value of stator current in the remaining healthy phases are fixed to 1 pu. The peak value of stator currents in these phases are $I_{B\text{-}peak}$ = 0.96 pu, $I_{C\text{-}peak}$ = 1.01 pu, $I_{D\text{-}peak}$ = 1.00 pu, and $I_{E\text{-}peak}$ = 0.97 pu. RMS current value of stator neutral point is 0.72 pu and its peak value is 1.06 pu. Simulated values of generated torque oscillating terms are P_2=1.16%, P_4=1.13% and P_6=0.16% of the output power (e. g. 0.79 pu).

In the case of having two adjacent faulty phases and no access to neutral point, it is not possible to use the maximum current capacity of the three remaining healthy phases to generate ripple-free torque. RMS values of stator phase currents are I_C=0.58 pu, I_D=1.0 pu, and I_E=0.71 pu. The peak current values of these phases are $I_{C\text{-}peak}$ =0.62 pu, $I_{D\text{-}peak}$ = 1.24 pu, and $I_{E\text{-}peak}$ = 0.74 pu. As it can be seen, the peak value of phase B is more than 1 pu which in very low frequencies can lead to thermal stress both in the machine and in the inverter. Moreover, simulated values of ocsilating power components are P_2= 3.15%, P_4=3.12%, and P_6=3.10% of the generated output power (e. g. 0.274 pu). By connecting machine´s neutral point to the inverter, it is possible to use the maximum current capacity of the remaining healthy phases. Again the RMS current value in the remaining healthy phases is 1 pu. This time the peak current values in the remaining healthy phases are $I_{C\text{-}peak}$ = 0.89 pu, $I_{D\text{-}peak}$ = 1.13 pu, and $I_{E\text{-}peak}$ =0.90 pu, which results in better current balancing and also in more uniform temperature distribution among the stator windings. It is important to mention that in this case the RMS value of neutral point current is 1.34 pu which should be considered in the design procedure of corresponding power converter. Simulated values of oscillating power components are P_2=1.70%, P_4=1.68%, and P_6=0.13% of the output power.

While having open-circuit fault in two nonadjacent stator phases, the RMS current value in the remaining healthy phases are equal to 1 pu. Current peak values in these phases are fixed to $I_{B\text{-}peak}$ = 0.88 pu, $I_{D\text{-}peak}$ = 1.13 pu, and $I_{E\text{-}peak}$=1.12 pu. Simulated values of ocsilating power components under this condition are P_2=1.05%, P_4=0.76%, and P_6=0.80% output power. By connecting the neutral point, the electrical angle of current harmonics can be changed to increase the amplitude of ripple-free torque. Again, the RMS current values of remaining healthy phases is 1 pu. Peak current values of remaining healthy phases are $I_{B\text{-}peak}$=0.89 pu, $I_{D\text{-}peak}$=1 pu and $I_{E\text{-}peak}$=1.15 pu. RMS value of neutral current is 0.24 pu which is relatively low. This low value of neutral current is due to more appropriate physical position of the remaining healthy phases.

4.6. Summary

In this chapter, generated output power of five-phase BLDC motors is improved under faulty conditions. Open-circuit fault is considered for one, two adjacent, and two nonadjacent stator phases. To avoid overheating of the machine under faulty conditions, RMS value of stator phase currents are limited to their rated values (1pu). Genetic Algorithm is used to avoid additional simplifying constraints in the optimization procedure of stator current references. These references are optimized to maximize the generated

electrical torque with limited ripples. In half of the conditions, the limiting constraint of zero stator current sum is removed from GA optimization procedure by connecting machine´s neutral point through an additional half-bridge inverter leg. Having access to machine´s neutral point results in more output power in all faulty condition. This power increment is more notable (31.3% pu) in the case of having two adjacent faulty phases. It is shown that by running a global optimization on stator reference currents, it is possible to improve the machine´s output power in the case of having one faulty phase and two adjacent faulty phases. Theoretical developments are evaluated by simulations and verified experimentally on a five-phase outer-rotor BLDC hub motor.

4.7. References

[1] Xiang-Jun, Z., Yongbing, Y., Hongtao, Z., Ying, L., Luguang, F., Xu, Y. :'Modelling and control of a multi-phase permanent magnet synchronous generator and efficient hybrid 3L-converters for large direct-drive wind turbines', IET journal on Electric Power Appl., 2012, 6, (6), pp. 322-331

[2] Dwari, S., Parsa, L. :'Fault-Tolerant Control of Five-Phase Permanent-Magnet Motors with Trapezoidal Back EMF', IEEE Trans. Ind. Electron., 2011, 58, (2), pp. 476–485

[3] Bianchi, N., Bolognani, S., Pré, M., Fornasiero, E. :'Post-fault operations of five-phase motor using a full-bridge inverter', Power Electron. Specialists Conf., 2008, IEEE, pp. 2528–2534

[4] Wang, Y., Cheng, M., Chen, M., Du, Y., Chau, K.T. :'Design of high-torque-density double-stator permanent magnet brushless motors', IET journal on Electric Power Appl., 2011, 5, (3), pp. 317-323

[5] Campos-Delgado, D.U. ; Espinoza-Trejo, D.R. ; Palacios, E. :'Fault-tolerant control in variable speed drives: a survey', IET journal on Electric Power Appl., 2008, 2, (2), pp. 121-134

[6] Bianchi, N., Bolognani, S., Dai Pré, M. :'Strategies for the Fault-Tolerant Current Control of a Five-Phase Permanent-Magnet Motor', IEEE Trans. Ind. Appl., 2007, 43, (4), pp. 960-970

[7] Salehi Arashloo, R., Salehifar, M., Romeral Martinez, L., Sala, V. :'Ripple Free Fault Tolerant Control of Five Phase Permanent Magnet Machines', Accepted in Power Electron. and App. Conf., 2013, IEEE

[8] Salehi Arashloo, R., Salehifar, M., Romeral Martinez, L. :'On the Effect of Accessible Neutral Point in Fault Tolerant Five Phase PMSM Drives", Ind. Electron. Society Conf. IEEE, 2012, pp. 1934-1039

[9] Mohammadpour, A., Parsa L. :'A Unified Fault-Tolerant Current Control Approach for Five-Phase PM Motors with Trapezoidal Back EMF Under Different Stator Winding Connections', IEEE Trans. Power Electron., 2013, 28, (7), pp. 3517–3527

[10] Ayyar, K., Ramesh, K., Gurusamy, G., Kaewwiset, W., Thamaphat, K., Kaewkhao, Ja., Limsuwan, P. :'Design of Speed Controller for Permanent Magnet Synchronous Motor Drive Using Genetic Algorithm Based Lower Order System Modelling', Journal of Computer Science, 2012, pp 1700-1710

[11] Soleimani, M., Asghar Gholamian, S. :'Optimum Design of a Three-Phase Permanent Magnet Synchronous Motor for industrial applications', International Journal of Applied Operational Research, 2013, 2, (4), pp. 67-86

[12] Rostami, N., Feyzi, M., Pyrhonen, J., Parviainen, A., Behjat, V. :'Genetic Algorithm Approach for Improved Design of a Variable Speed Axial-Flux Permanent-Magnet Synchronous Generator', IEEE Trans. Mag., 2012, 48. (12), pp. 4860-4865

[13] Goldberg, D. :'Genetic Algorithms in Search, Optimization, and Machine Learning', Reading, MA: Addison-Wesley, 1989

[14] C´ardenas, R., Juri, C., Pe˜na, R., Wheeler, P., Clare J., "The Application of Resonant Controllers to Four-Leg Matrix Converters Feeding Unbalanced or Nonlinear Loads", IEEE Trans. On Power Electron., 2012, 27, (3), pp. 1120 – 1129

[15] Kim, J., Sul, S., "A Carrier-Based PWM Method for Three-Phase Four-Leg Voltage Source Converters", IEEE Trans. On Power Electron., 2004, 19, (3), pp. 66-75

5.

Chapter 5 Fault Tolerant Model Predictive Current Control of Five-Phase BLDC Drives

Fault tolerant control of five-phase BLDC machines is gaining more importance in high-safety applications such as automotive industries and offshore wind generators. In many applications, traditional controllers (such as PI controllers) are used to control the stator currents under faulty conditions. These controllers have good performance with dc signals. However, in the case of missing one or two of the phases, appropriate reference currents of these machines for improved ripple-free torque generation have oscillatory dynamics both in phase- and synchronous-reference frames. Non-constant nature of these reference values requires the implication of fast current controllers. In this chapter, model predictive deadbeat controllers are proposed to control the stator currents of five-phase BLDC machines under normal and faulty conditions. Open circuit fault is considered for both one and two stator phases, and the behaviour of proposed controlling method is evaluated. This evaluation is generally focused on first, sensitivity of proposed controlling method and second, its ability in following reference current values with fast speed. Proposed method is simulated and is verified experimentally on a five-phase BLDC drive.

CONTENTS

5.1. Introduction

Under faulty conditions, appropriate reference currents of a five-phase BLDC machine have oscillating dynamics both in phase- and rotating-reference frames [1]. As a result, high bandwidth controllers are required to control the stator currents under faulty conditions.

Comparing to traditional control structures (such as PI controllers), model predictive control (MPC) is able to provide fast and stable performance [2]. Regarding its high computational load, the first applications of MPC were usually related to slow dynamic systems such as chemical procedures and petroleum refineries. However, by appearance of powerful microcomputers, it is now possible to use MPC in applications with fast dynamics. In the case of electric drives, MPC is used to eliminate stator current errors in the shortest possible time [3]. Motion control applications of MPC are generally divided into three categories.

In the first category, future evolution of stator currents is estimated for all possible configurations of inverter legs. After that, a cost function is used to select the best switching state for the next modulation period. As inverter switching states are finite in each calculation step, this method is also termed Finite Control Set Model Predictive Control (FCS-MPC) [4-6].

In the second category, a combination of one zero vector and one active vector is used in the inverter to minimize the difference between stator current references and their real values. This method has been applied to control induction machines [7], doubly-fed induction machines [8], and synchronous-reluctance machines [9].

In the case of multi-phase electrical drives, high number of possible switching states results in high computational load in mentioned categories of MPC [10-12]. To reduce the computational burden, many studies have considered a limited set of active vectors in their controlling algorithm. As an example, to control the stator currents of an asymmetrical six-phase machine, reference [13] has only considered the switching states which correspond to large voltage vectors and zero vectors. A pre-defined criterion is used in [14] to avoid consecutive commutations in all inverter legs and only one commutation per modulation period. As a result, in each modulation period only 6, 11 or 16 vectors are considered in MPC algorithm which significantly reduces the computational load of controlling unit.

Model predictive control is also considered in the case of five-phase electrical motors [15-17]. In [16], FCS-MPC is used to control a five-phase induction motor drive. Although the proposed method has improved the transient behaviour of the whole drive, but as it is shown, steady state behaviour is always better in the case of using PI controllers. FCS-MPC of five-phase inverters is also used in [18] to control a two-motor six-phase drive with common inverter leg topology.

Finally, the last (third) category of MPC uses machine´s model to calculate the required voltages which lead to the desired reference currents during one modulation period. In other words, inverse model of the

system (machine) is used to calculate appropriate inputs (voltages) which are required to achieve the desired outputs (stator currents) [19-21]. As the main objective of this category is to eliminate the error in one modulation period, this method is also famous as predictive deadbeat control (PDC).

Comparing to previous categories of predictive controllers, PDC has several advantages. In this method, machine´s equations are used for only one time, and as a result, its computational load is lower than FCS-MPC methods. In addition, the modulation block is not dependent on controlling method, and as a result, the entire control block is more flexible. Moreover, nonlinear constraints of five-phase BLDC machines can be easily implemented in this method. Regarding the mentioned advantages of PDC method, the main objective of this chapter is to implement and evaluate a Fault Tolerant Predictive Deadbeat Controller (FT-PDC) for five-phase BLDC motor drives.

Open circuit fault is considered for one, two adjacent and two nonadjacent stator phases. In addition, two main aspects of proposed controlling method are evaluated in this chapter. These two aspects are firstly, the ability of proposed controllers in following the reference currents, and secondly, the sensitivity of proposed FT-PDC method.

5.2. Fault Tolerant Predictive Deadbeat Current Controllers

While missing one (or two) of the phases, it is required to add one (or two) additional equation to electrical model of a normal (healthy) five-phase BLDC machine. These additional equations increase the computational load of FT-PDC algorithms. As a result, EKF is not implemented in proposed FT-PDC methods.

In this section, fault tolerant predictive deadbeat control will be first developed for healthy (normal) conditions of five-phase BLDC machine, and after that, this controller will be applied to faulty conditions of this machine.

5.2.1 Decoupled Electrical Model of Five-Phase BLDC Machine-Normal Operation

Electrical model of five-phase BLDC machines is well studied in chapter 3. Equations of machine´s stator in two rotating refer

ence frames and homopolar axis can be summarized as:

$$v_{d1} = r_s i_{d1} + L_{d1}\frac{d}{dt}i_{d1} - \omega L_{q1} i_{q1}$$

Eq. 5-2-1

$$v_{q1} = r_s i_{q1} + L_{q1}\frac{d}{dt}i_{q1} + \omega(\psi_{pm1} + L_{d1} i_{d1})$$

Eq. 5-2-2

$$v_{d3} = r_s i_{d3} + L_{d3}\frac{d}{dt}i_{d3} - 3\omega L_{q3} i_{q3}$$

Eq. 5-2-3

$$v_{q3} = r_s i_{q3} + L_{q3}\frac{d}{dt}i_{q3} + 3\omega(\psi_{pm3} + L_{d3}i_{d3})$$

Eq. 5-2-4

$$v_o = r_s i_o + L_o\frac{d}{dt}i_o$$

Eq. 5-2-5

where v and i represent stator voltage and current in each direction, r_s is the stator phase resistance, L_{d1}, L_{q1}, L_{d3}, L_{q3} and L_o are stator inductance values in their corresponding directions, and ω is the electrical rotational velocity. In addition, ψ_{pm1} and ψ_{pm3} are first and third components of magnetic field which is generated by rotor magnets.

In the case of having an isolated neutral point, i_o is automatically forced to be zero, and there will be no need to control this homopolar component of stator currents. As a result, developed electrical model of five-phase BLDC machine can be represented by four independent state variables of i_{d1}, i_{q1}, i_{d3}, i_{q3}.:

$$\begin{bmatrix} \frac{d}{dt}i_{d1} \\ \frac{d}{dt}i_{q1} \\ \frac{d}{dt}i_{d3} \\ \frac{d}{dt}i_{q3} \end{bmatrix} = \begin{bmatrix} -\frac{r_s}{L_{d1}} & 0 & 0 & 0 \\ 0 & -\frac{r_s}{L_{q1}} & 0 & 0 \\ 0 & 0 & -\frac{r_s}{L_{d3}} & 0 \\ 0 & 0 & 0 & -\frac{r_s}{L_{q3}} \end{bmatrix} \begin{bmatrix} i_{d1} \\ i_{q1} \\ i_{d3} \\ i_{q3} \end{bmatrix} + \begin{bmatrix} \frac{v_{d1}}{L_{d1}} \\ \frac{v_{q1}}{L_{q1}} \\ \frac{v_{d3}}{L_{d3}} \\ \frac{v_{q3}}{L_{q3}} \end{bmatrix} + \begin{bmatrix} \frac{\omega}{L_{d1}}L_{q1}i_{q1} \\ -\frac{\omega}{L_{q1}}(\psi_{pm1} + L_{d1}i_{d1}) \\ \frac{3\omega}{L_{d3}}L_{q3}i_{q1} \\ -\frac{3\omega}{L_{q3}}(\psi_{pm3} + L_{d3}i_{d3}) \end{bmatrix}$$

Eq. 5-2-6

The last term of equation (5-2-6) is related to cross coupling terms of machine´s equations and the terms which are related to induced back EMF in q_1 and q_3 directions.

Similar to three-phase PM motor drives, it is possible to use feed forward compensation to remove these terms. In this case, implemented decoupling terms would be:

$$\begin{bmatrix} v_{dec-d1} \\ v_{dec-q1} \\ v_{dec-d3} \\ v_{dec-q3} \end{bmatrix} = -\begin{bmatrix} \frac{\omega}{L_{d1}}L_{q1}i_{q1} \\ -\frac{\omega}{L_{q1}}(\psi_{pm1} + L_{d1}i_{d1}) \\ \frac{3\omega}{L_{d3}}L_{q3}i_{q1} \\ -\frac{3\omega}{L_{q3}}(\psi_{pm3} + L_{d3}i_{d3}) \end{bmatrix}$$

Eq. 5-2-7

By implementing the decoupling terms in machine´s equation (5-2-6), the new representation of PM machine in rotating reference frames can be summarized as:

$$\begin{bmatrix} \frac{d}{dt}i_{d1} \\ \frac{d}{dt}i_{q1} \\ \frac{d}{dt}i_{d3} \\ \frac{d}{dt}i_{q3} \end{bmatrix} = \begin{bmatrix} -\frac{r_s}{L_{d1}} & 0 & 0 & 0 \\ 0 & -\frac{r_s}{L_{q1}} & 0 & 0 \\ 0 & 0 & -\frac{r_s}{L_{d3}} & 0 \\ 0 & 0 & 0 & -\frac{r_s}{L_{q3}} \end{bmatrix} \begin{bmatrix} i_{d1} \\ i_{q1} \\ i_{d3} \\ i_{q3} \end{bmatrix} + \begin{bmatrix} \frac{1}{L_{d1}} & 0 & 0 & 0 \\ 0 & \frac{1}{L_{q1}} & 0 & 0 \\ 0 & 0 & \frac{1}{L_{d3}} & 0 \\ 0 & 0 & 0 & \frac{1}{L_{q3}} \end{bmatrix} \begin{bmatrix} v_{d1} \\ v_{q1} \\ v_{d3} \\ v_{q3} \end{bmatrix}$$

Eq. 5-2-8

5.2.2 Proposed FT-PDC Method -Normal Operation

The main objective of the proposed deadbeat controlling method is to eliminate stator current errors in the smallest possible number of modulation periods. Center aligned space vector modulation (SVM) is used in many industrial drives. To reduce the introduced current measurement noise in such applications, current sampling is usually taken place exactly in the middle of zero-vector duty times. Moreover, implemented voltages of inverter are getting updated by the beginning of each modulation period. General sequence of stator current control is illustrated in Fig. 5-2-1:

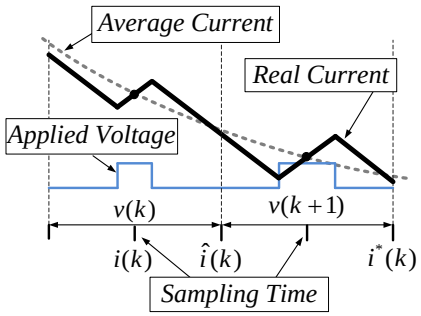

Figure 5-2-1 General sequence of stator current drive with center aligned SVM

As it is shown in Fig.5-2-1, stator phase currents are measured in the middle of k^{th} modulation period. From this moment until the end of current modulation period, implemented reference voltages of the inverter ($V^*_{d1q1d3q3}$) will be constant. As a result, it is possible to estimate stator phase currents by the end of current modulation period:

$$\begin{bmatrix} \hat{i}_{d1}(k) \\ \hat{i}_{q1}(k) \\ \hat{i}_{d3}(k) \\ \hat{i}_{q3}(k) \end{bmatrix} = \begin{bmatrix} i_{d1}(k) \\ i_{q1}(k) \\ i_{d3}(k) \\ i_{q3}(k) \end{bmatrix} + \frac{T_m}{2}\frac{d}{dt}\begin{bmatrix} i_{d1}(k) \\ i_{q1}(k) \\ i_{d3}(k) \\ i_{q3}(k) \end{bmatrix}$$

Eq. 5-2-9

where T_m is the modulation period length. Following the main concept of deadbeat controlling algorithm, stator phase currents should be forced to reach their reference values at the end of next modulation period:

$$\begin{bmatrix} i_{d1}^*(k) \\ i_{q1}^*(k) \\ i_{d3}^*(k) \\ i_{q3}^*(k) \end{bmatrix} = \begin{bmatrix} \hat{i}_{d1}(k) \\ \hat{i}_{q1}(k) \\ \hat{i}_{d3}(k) \\ \hat{i}_{q3}(k) \end{bmatrix} + T_m \frac{d}{dt} \begin{bmatrix} \hat{i}_{d1}(k) \\ \hat{i}_{q1}(k) \\ \hat{i}_{d3}(k) \\ \hat{i}_{q3}(k) \end{bmatrix}$$

Eq. 5-2-10

By implementing (5-2-9) and (5-2-10) in (5-2-8) it is possible to calculate the appropriate reference voltages for the next $(k+1)^{th}$ modulation period:

$$v_j^*(k+1) = \frac{L_j}{2T_m}(i_j^*(k) - i_j(k)) - \frac{1}{4}v_j(k) + \frac{r_s}{4}(i_j(k) + 2\hat{i}_j(k))$$

Eq. 5-2-11

where j can be replaced by d_1, q_1, d_3 and q_3.

Figure 5-2-2 illustrates the general structure of five-phase PM motor drive and its controlling unit under normal (healthy) operation. By having the measured values of stator phase currents, decoupling terms of equations (5-2-7) can be calculated and added to the computed reference voltages of deadbeat controller.

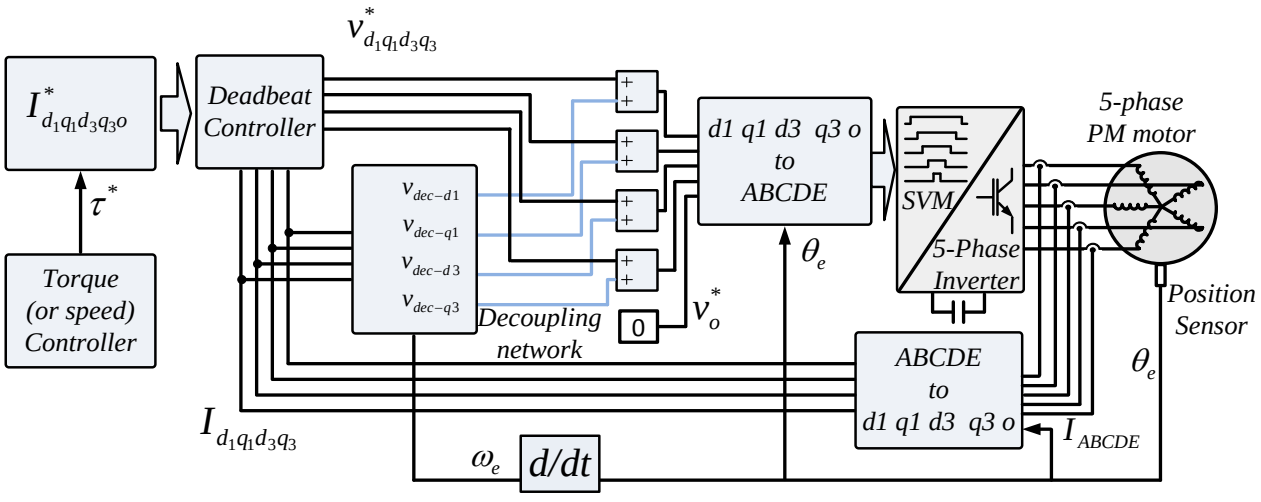

Figure 5-2-2 Deadbeat controlling structure of five-phase BLDC motor

5.2.3 Five-Phase BLDC Drive FT-PDC under Faulty Conditions

5.2.3.1 Motor Model and Reference Current Adaptation under Faulty Conditions

The problem of appropriate reference currents in the case of missing one or two stator phases is studied in several papers [22][23]. Table 5-2-1 shows the pu values of stator current references for a five-phase BLDC machine [1]. Multiplication of these current references by pu value of torque demand, results in appropriate pu values of reference currents for each modulation period.

Table 5-2-1: Appropriate reference current values of five-phase BLDC machines for producing 1-pu torque under different faulty conditions [1]

Phase	A	B	C	D	E
One missing phase					
I_1	-	0,39	0,39	0,39	0,39
θ_1	-	45,45	134,54	-134,54	-45,45
I_3	-	0,071	0,027	0,027	0,071
θ_3	-	288	216	-216	-288
Two non-adjacent missing phases					
I_1	-	0,39	-	0,39	0,39
θ_1	-	0	-	120	-120
I_3	-	-0,07	-	0,075	0,075
θ_3	-	0	-	-62,8	62,8
Two adjacent missing phases					
I_1	-	-	0,23	0,39	0,23
θ_1	-	-	147	0	-147
I_3	-	-	0,053	0,1	0,053
θ_3	-	-	159	0	-159

In the case of having an open circuit fault in one of the stator phases, an additional equation should be imposed to machine´s model to consider the zero current of opened phase. Assuming phase *A* as faulty phase, this additional equation in rotating reference frames can be derived from reverse transformation of equation (3-2-4):

$$T^{-1}\begin{bmatrix} i_{d1} \\ i_{q1} \\ i_{d3} \\ i_{q3} \\ i_o \end{bmatrix} = \begin{bmatrix} 0 \\ i_b \\ i_c \\ i_d \\ i_e \end{bmatrix} \quad ; i_a = 0$$

Eq. 5-2-12

or

$$i_{d1}\cos(\theta) - i_{q1}\sin(\theta) + i_{d3}\cos(3\theta) - i_{q3}\sin(3\theta) = 0 \qquad ; i_a = 0$$

Eq. 5-2-13

where $\theta = \omega t$ is the electrical angle.

To extract the machine´s model in the case of having one faulty phase, equation (5-2-13) should be implemented in machine´s state equations (5-2-8). Implementation of (5-2-13) reduces the number of independent state variables by one. As state variables of (5-2-8) are decoupled from each other, machine´s model in the case of missing one phase can be simply derived by ignoring one of the state variables (one raw) in (5-2-8) and directly computing it by (5-2-13)

A secondary equation should be imposed to machine´s model in the case of missing two stator phases. This additional equation while having two adjacent faulty phases (e.g. phase *A* and phase *B*) will be:

$$T^{-1}\begin{bmatrix} i_{d1} \\ i_{q1} \\ i_{d3} \\ i_{q3} \\ i_o \end{bmatrix} = \begin{bmatrix} 0 \\ 0 \\ i_c \\ i_d \\ i_e \end{bmatrix} \qquad ; i_b = 0$$

Eq. 5-2-14

or

$$\begin{cases} i_{d1}\cos(\theta) - i_{q1}\sin(\theta) + i_{d3}\cos(3\theta) - i_{q3}\sin(3\theta) = 0 \\ i_{d1}\cos(\theta-\alpha) - i_{q1}\sin(\theta-\alpha) + i_{d3}\cos 3(\theta-\alpha) - i_{q3}\sin 3(\theta-\alpha) = 0 \end{cases} \quad ; \text{Two adjacent faulty phases}$$

Eq. 5-2-15

Following the same procedure, the secondary imposed equation in the case of missing a non-adjacent stator phase (e.g. phase *A* and phase *C*) can be calculated as:

$$T^{-1}\begin{bmatrix} i_{d1} \\ i_{q1} \\ i_{d3} \\ i_{q3} \\ i_o \end{bmatrix} = \begin{bmatrix} 0 \\ i_b \\ 0 \\ i_d \\ i_e \end{bmatrix} \qquad ; i_c = 0$$

Eq. 5-2-16

or

$$\begin{cases} i_{d1}\cos(\theta) - i_{q1}\sin(\theta) + i_{d3}\cos(3\theta) - i_{q3}\sin(3\theta) = 0 \\ i_{d1}\cos(\theta-2\alpha) - i_{q1}\sin(\theta-2\alpha) + i_{d3}\cos 3(\theta-2\alpha) - i_{q3}\sin 3(\theta-2\alpha) = 0 \end{cases} \quad ; \text{Two non-adjacent faulty phases}$$

Eq. 5-2-17

Depending on the fault type, the model of five-phase BLDC machine under faulty conditions can be directly derived by removing one or two independent state variables from (5-2-8), and calculating the removed state variables by (5-2-13), (5-2-15) or (5-2-17).

5.2.3.2 Proposed FT-PDC Method under Faulty Conditions

Under faulty conditions, the main objective is to control the stator currents in the remaining independent directions. Similar to the case of normal operation, in the first step of the deadbeat control independent state variables of machine´s model are estimated for the end of current modulation period. By knowing the estimated values of independent state variables, their appropriate reference voltages for the next modulation period can be computed by equation (5-2-11).

It is important to mention that under faulty conditions, stator currents of five-phase BLDC machine are not balanced, and the voltage of machine´s neutral point is not equal to the voltage of inverter´s dc-bus midpoint. Under these conditions, the important point is to generate appropriate voltage differences between the remaining terminals of the machine. That is {V_{BC}*, V_{CD}*, V_{DE}*}, {V_{CD}*, V_{DE}*} and {V_{BD}*, V_{DE}*} respectively in the case of missing one phase (phase A), two adjacent phases (phases A and B), and two non-adjacent phases (phases A and C).

As shown in Fig.5-2-3-(a) calculated phase-to-neutral reference voltages are computed by controller block, and will be generated by their corresponding inverter legs. These generated phase-to-neutral voltages will be imposed to the remaining phases of electrical motor. As motor terminals of missing phases are isolated, their phase-to-neutral voltages are equal to the induced back-EMF in these phases. Figure 5-2-3-(b) is a summary of deadbeat control algorithm and voltage application method under faulty conditions.

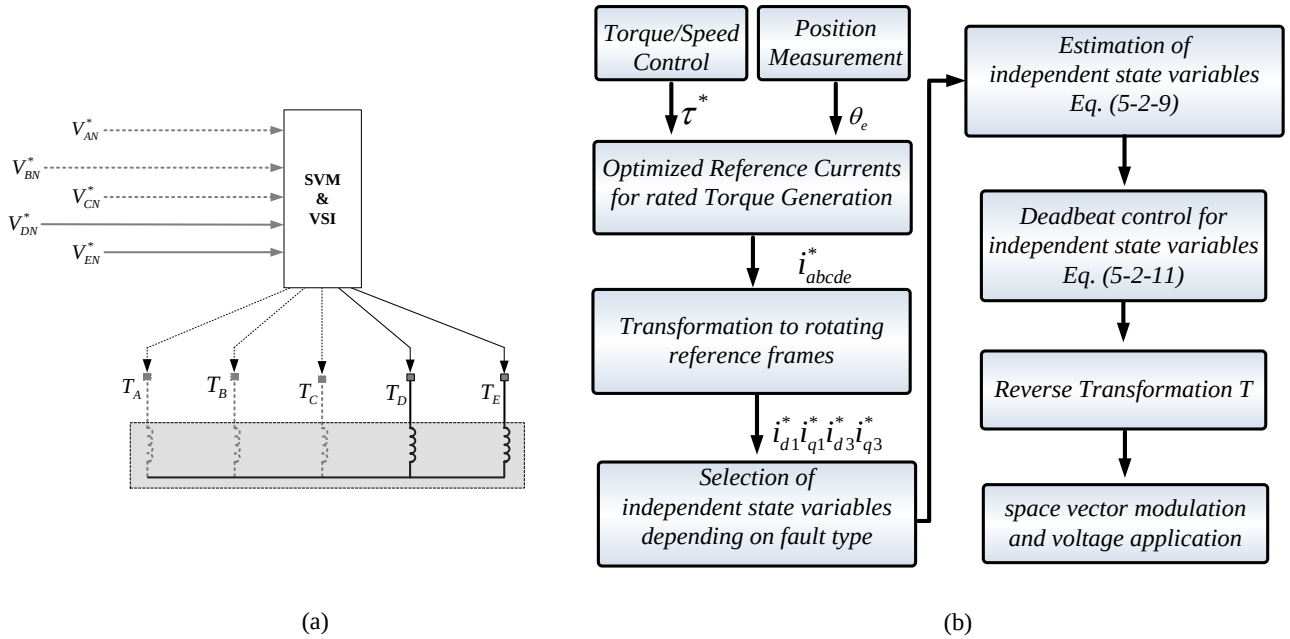

Figure 5-2-3 (a) Voltage application scheme under faulty conditions, dashed lines are correspondent to phases which can be disconnected, (b) deadbeat control algorithm of five-phase BLDC machine under faulty conditions

5.2.4 Sensitivity Analysis of Proposed FT-PDC Method by Simulations

5.2.4.1 Simulation Steps of Sensitivity Analysis for Proposed FT-PDC Method

Simulations are conducted in MATLAB environment to evaluate the sensitivity of developed FT-PDC algorithm. Simulation parameters are summarized in table 3-6-1 which are also correspondent to their real values in experimental test bench. In each case, the parameters of controlling block are remained constant, and at the same time, the characteristics of other simulation blocks (motor or inverter) are changed. During each test, stator current errors are evaluated in one period of fundamental frequency.

Simulations are completed in 6 steps. In each step a special type of disturbance is imposed to the control structure. Table 5-2-2 is a summary of considered disturbances during sensitivity analysis of proposed FT-PDC method.

Table 5-2-2 Considered disturbances during sensitivity analysis of proposed controlling method

Test	Disturbance Type	Parameter Values
Test 1	None (ideal case)	deadtime=0us, V_{diode}=0, V_{IGBT}=0
Test 2	Nonlinear Inverter Characteristics	deadtime=3us, V_{diode}=2.17, V_{IGBT}=1.85
Test 3	Inaccurate Stator Resistance	R_s=1.0 Ω R_s=2.0 Ω
Test 4 & 5	Inaccurate Magnetic Flux	0.8 rated value 1.2 rated value
Test 6	Inaccurate dc-bus Voltage	0.8 rated value

In the first step (test 1), inverter block is considered ideal, and machine parameters are equal to their corresponding values in the controlling block.

During the next step (test 2), inverter block is simulated while considering 3*us* of dead-time and real parameters of IGBTs (voltage drop and forward resistance) which are used in the experimental test.

The next simulation step (test 3) is conducted to evaluate the impact of inaccurate stator resistance on the controlling system behaviour. In this test, inverter block is ideal, and rated values of PM machine are used in computations of controlling block. Nominal value of stator resistance in the simulated machine is 0.1Ω. During test 3, this value is increased up to 0.2Ω to consider the effect of high operational temperatures.

The effect of flux amplitude variation is evaluated in the next two simulation steps. Again, inverter block is considered ideal, and controlling unit parameters are considered equal to motor rated values. At the same time and in the motor block, rotor magnetic flux is lowered down to 0.8 its rated value (test 4), and in the next step (test 5) it is increased up to 1.2 its rated value.

The effect of dc-bus voltage drop is evaluated in test 6. Nominal voltage of inverter dc-bus is used in controlling block computations. At the same time, dc-bus voltage is set to 0.8 rated value in inverter block.

5.2.4.2 Simulation Results and Discussion

As it was mentioned before, the final objective of proposed predictive deadbeat controllers is to have a precise control over stator phase currents. As a result, the energy of stator phase currents can be considered as an index to evaluate the precision of proposed controlling method under each condition. In each test, the energy of phase current errors is computed and integrated over one period of fundamental current frequency in (5-2-18):

$$E_{error} = \int_T (\Delta i_{d1}^2 + \Delta i_{q1}^2 + \Delta i_{d3}^2 + \Delta i_{q3}^2) dt$$

Eq.5-2-18

Figure 5-2-4 shows the pu values of error energy for different tests and under each operational condition.

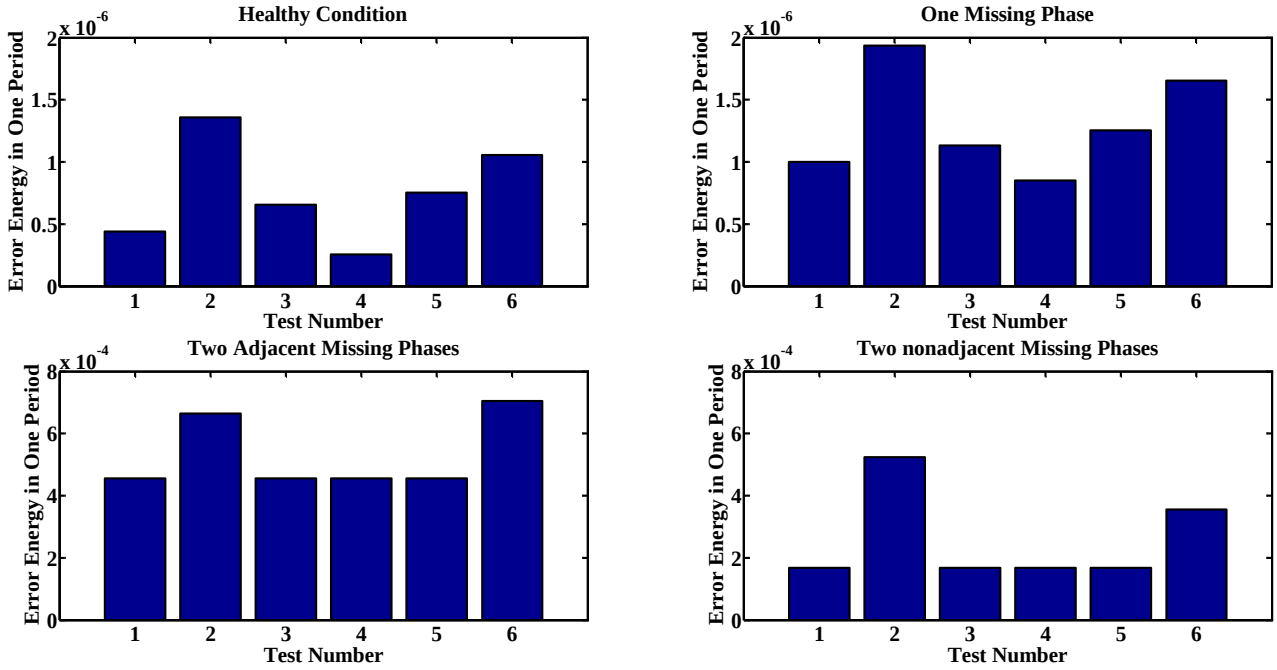

Figure 5-2-4 pu energy values of phase current error in one period of fundamental frequency

As it is shown in Fig. 5-2-4, under normal conditions the pu values of error energy in one period of fundamental frequency are less than 1.5 [uA^2 pu]. The main reason of current error in ideal simulations (test 1) can be referred to nonlinear behaviour of PM machine which introduces error in "current estimation step" and "voltage computation step". During "current estimation step", the derivative of stator currents in each direction will be calculated by using the measured values of currents in the middle of modulation step:

$$\frac{d}{dt}i_j = \frac{1}{L_j}(v_j - r_s i_j)$$

Eq. 5-2-19

where *j* can be d_1, q_1, d_3 *and* q_3, and i_j represents the sampled value of stator currents in each direction. Calculated values of current derivatives are assumed to be constant until the end of current modulation period. In addition, during "voltage calculation step" of control algorithm, the derivative of estimated currents is considered as a fixed value during the next modulation period. Variation of stator currents introduces error in both "estimation step" and "voltage computation step" of control algorithm.

As it can be seen from Fig. 5-2-4, nonlinear characteristics of the inverter (test 2) and dc-bus voltage errors (test 6) are correspondent to the highest values of stator current errors. In fact, nonlinear characteristics of the inverter (including deadbeat implementation and voltage drops along the IGBTs and diodes) can also be considered as a voltage drop of machine´s power supply unit.

To have an analytical evaluation on how dc-bus voltage drop can increase the stator current errors, let us assume that there is a difference between assumed values of applied voltage (in controlling unit) and their real values:

$$v_j(k) = v_{real}(k) + \Delta v_j(k)$$

Eq. 5-2-20

where $v_j(k)$ and $v_{real}(k)$ are respectively assumed and real values of applied voltage in direction *j*. The existing error in the assumed value of applied voltage ($\Delta v_j(k)$) results in an additional error in the estimated value of stator currents by the end of current modulation period:

$$i_{es} = i_k + \frac{T_m}{2}\frac{1}{L_j}(v_{real}(k) + \Delta v(k) - r_s i_k) = \left[i_k + \frac{T_m}{2}\frac{1}{L_j}(v_{real}(k) - r_s i_k) \right] + \left[\frac{T_m}{2}\frac{1}{L_j}\Delta v(k) \right] = i_{es(normal)} + \Delta i_{es}$$

Eq. 5-2-21

where $i_{es(normal)}$ is the estimated value of stator current in direction *j* under normal conditions, and Δi_{es} is the additional term which is generated due to dc-bus voltage error. In the next step, estimated value of stator current i_{es} will be used to calculate the appropriate reference voltage during the next modulation period:

$$v^*(k+1) = (i^* - (i_{es(norm)} + \Delta i_{es}))\frac{L}{T_m} + r(i_{es(norm)} + \Delta i_{es})$$

$$v^*(k+1)=\left[(i^*-i_{es(norm)})\frac{L}{T_m}+r(i_{es(norm)})\right]+\left[\frac{\Delta v(k)}{2}(\frac{r_s}{L}T_m-1)\right]=v^*(k+1)_{(norm)}+\Delta v^*(k+1)$$

Eq. 5-2-22

where $v^*(k+1)_{norm}$ is the calculated reference voltage under normal conditions, and $\Delta v^*(k+1)$ will be imposed to direction *j* due to dc-bus voltage error. Considering simulation parameters of table 5-2-2 and a switching frequency between 5-20 kHz, it can be concluded that:

$$\Delta v^*(k+1)\approx-\frac{\Delta v(k)}{2}$$

Eq. 5-2-23

In other words, in the case of having $k\%$ of error in dc-bus voltage, applied voltage amplitudes in $d_1q_1d_3q_3$-directions will be multiplied by $(100-\frac{k}{2})\%$ which results in higher amplitude of error energy. In the case of missing one stator phase, the same pattern of error energy can be observed from Fig. 5-2-4 However, comparing to healthy mode operations, the energy of phase current errors is relatively higher. One of the reasons of higher error energy in the case of missing one-phase is higher dynamics of current reference values under faulty conditions. Figure 5-2-5 illustrates the derivative of stator currents in $d_1q_1d_3q_3$-directions under faulty conditions. As it was explained, while FT-PDC algorithm is being executed, stator current derivatives are assumed to be fixed in "current estimation" and "voltage computation" steps, and variation of current derivatives will increase the energy of stator current errors.

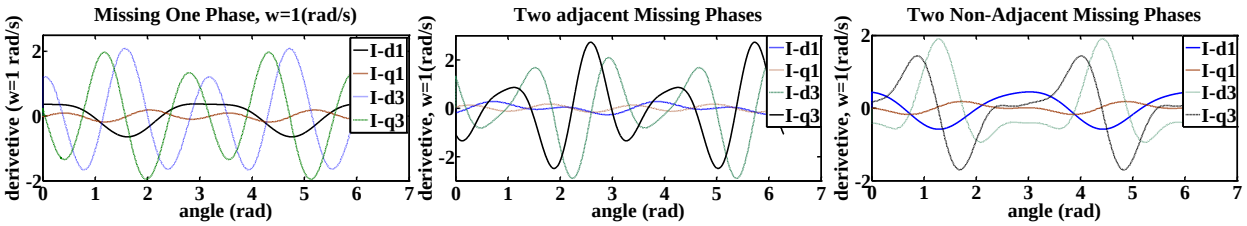

Figure 5-2-5 Derivative of reference currents in the case of missing one stator phase (e. g. phase A), two adjacent faulty phases (e. g. phase A and B), and two non-adjacent faulty phases (e. g. phase A and C)

Following the same pattern, the energy of stator current error increases in the case of missing two stator phases. Again nonlinear inverter characteristics (test 2) and lower amplitude of dc-bus voltage (test 6) are correspondent to the highest amplitude of current errors. While missing two phases, stator currents should be estimated in two (independent) directions. To compute the stator currents in the remaining directions, estimated values of independent state variables should be used in (5-2-15) or (5-2-17) to calculate the stator currents of the remaining (dependent) directions. Again, dynamic behaviour of phase current derivatives in different directions leads to current error in both estimation and computation steps of the controlling algorithm.

5.3. Experimental Evaluation

Experimental tests are completed to evaluate the behaviour of proposed deadbeat control in five-phase PM motor drives.

The implemented five-phase BLDC machine is including a double-layer fractional-slot winding configuration. Regarding its outer rotor structure and high power density, it is possible to directly mount the motor inside the vehicle´s wheel. Moreover, due to high number of machine pole pairs, rotor magnets are directly mounted on the inner surface of rotor. Measured back-EMF waveform of stator winding phase includes 11% of 3^{rd} harmonic component and 5% of 7^{th} harmonic component (machine parameters are explained in appendix A).

Stator five terminals are connected to an IGBT-based two-level inverter. DS1005 dSpace board is used to 1) execute predictive deadbeat control algorithm, 2) realize five-phase center-aligned SVM, and 3) generate the required controlling pulses for the inverter. In the case of missing one or two phases the correspondent motor terminals will be disconnected from the inverter.

The dc-bus voltage is set to 48 Volts. Moreover, due to limited computational power of the dSpace, the switching frequency is fixed on 5 kHz. Hall Effect sensors are used to establish stator current feedbacks, and position feedback loop is realized by means of a 9000-pulse/revolution incremental encoder. It is worth noting that in these tests, controlling algorithms of five-phase PM machine are correspondent to torque control because rotational velocity is fixed on 50 rpm by the load system.

Under each operational condition, the value of reference torque is changed from 0.5 to 1.0 of its maximum achievable value. The maximum achievable torque depends on machine´s operational condition. In other words, under each condition, stator phase currents are optimized (chapter 4) to maximize the generated ripple-free torque and at the same time, having an RMS value bellow 1-pu. Maximum achievable torque of each operational condition is brought in table 5-3-1.

Table 5-3-1 Maximum achievable value of reference torque under different operational conditions

Motor condition	Maximum Achievable Torque (%pu)
Healthy motor	100
One faulty phase	74.5
Two adjacent faulty phases	27.4
Two nonadjacent faulty phases	55.7

A four-channel digital oscilloscope is used to record the generated torque and current in three stator phases. As a result, under normal condition only three stator phases (phases B, C and D) are shown in Fig.5-3-1. Due to machine´s isolated neutral point, total sum of stator phase currents is always zero. Therefore, in

the case of having one faulty phase, stator current of phase B, C and D are directly measured and stator current of phase E is calculated.

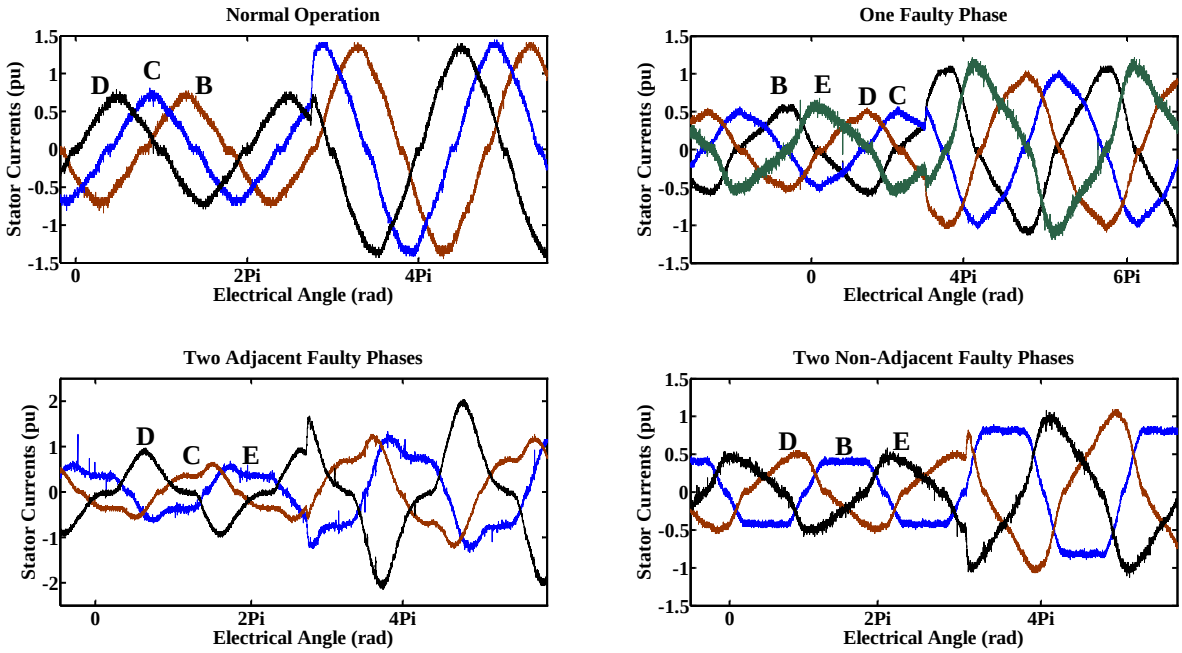

Fig. 5-3-1: Stator phase currents under healthy and different faulty conditions

In the following, the behaviour of proposed controlling method will be evaluated under steady states, and after that, under transient states.

5.3.1 Evaluation of Proposed FT-PDC in Steady States

Under steady states, the behaviour of proposed FT-PDC is evaluated. As it was explained in simulation section, the energy of stator phase currents can be considered as an index to evaluate the precision of proposed controlling method under each condition. In each test, the energy of phase current errors is computed and integrated over one period of fundamental current frequency:

$$E_{error} = \int_T (\Delta i_{d1}^2 + \Delta i_{q1}^2 + \Delta i_{d3}^2 + \Delta i_{q3}^2) dt$$

Eq. 5-3-1

Conducted experiments are preferred to be similar to simulations. As a result, it is tried to evaluate the sensitivity of proposed FT-PDC respect to different parameter changes.

However, because of some limitations, experimental test conditions cannot be exactly equal to simulation conditions. The first limitation is related to inverter nonlinear characteristics. As electrical motor is always fed by a five-phase inverter it is not possible to experimentally evaluate the ideal case which was considered in simulations (ideal inverter with no dead time and no voltage drop in semiconductors). In addition, rotor magnets (and their corresponding magnetic flux) are constant during all experimental tests. A summary of conducted experiments is brought in Table 5-3-2.

During the first evaluation (experiment-1), precise values of machine parameters are used in calculations of controlling unit. In the next step (experiment-2), stator resistances are changed from 0.1Ω to 0.2Ω by adding additional resistances in series with stator phase terminals. At the same time, their correspondent value in controlling algorithm is not changed. For the next evaluations (experiment-3), dc-link voltage of the inverter is reduced to 0.8 its rated value while in controlling unit, rated value of dc-link voltage is used for reference voltage calculations.

Table 5-3-2 Conducted experiments to evaluate the sensitivity of proposed controlling method

experiment	Existing disturbance	Controlling unit assumption
experiment-1	nonlinear inverter characteristics	Ideal inverter
experiment-2	nonlinear inverter characteristics and doubled value of stator resistance	Ideal inverter, and rated value of stator resistance
experiment-3	nonlinear inverter characteristics and dc-link reduction in the inverter	Ideal inverter and rated value of dc-link in inverter

Similar to simulations, the energy of stator current errors is integrated over one period of fundamental frequency under steady-state operation from Eq. (5-3-1). Figure 5-3-2 presents the pu values of this energy in one period of fundamental frequency and for different operational conditions of the motor.

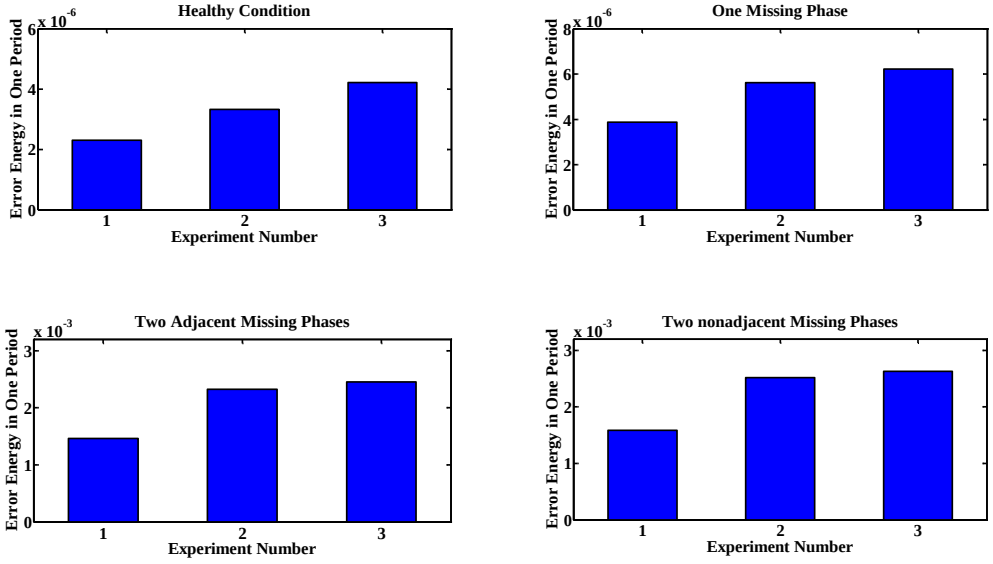

Figure 5-3-2 pu energy values of phase current error in one period of fundamental frequency

As it can be seen, the minimum value of measured error is related to experiment-1 where nonlinear characteristics of the inverter are the only source of disturbance. Under all operational condition, the

energy of error in “experiment-1” is higher than 50% of its value in “experiment-2” and “experiment-3”. By considering table 5-3-2 and Fig. 5-3-2, it is possible to write:

$$E_{nonlinear\ INV} > 0.5\ (E_{nonlinear\ INV} + E_{Rs})$$

Eq.5-3-2

which results in

$$E_{nonlinear\ INV} > E_{RS}$$

Eq.5-3-3

where $E_{nonlinear\ INV}$, E_{Rs} are respectively the energy of stator current errors due to “nonlinear inverter characteristics” and “stator resistance increment”.

In addition, from Fig. 5-3-2, it is obvious that under all conditions

$$E_{nonlinear\ INV} > 0.5\ (E_{nonlinear\ INV} + E_{dc-link})$$

Eq.5-3-4

which results in

$$E_{nonlinear\ INV} > E_{dc-link}$$

Eq.5-3-5

where $E_{dc\text{-}link}$ is the energy of stator current errors because of “inaccurate dc-link voltage”. Equations (5-3-3) and (5-3-5) are in accordance with simulation results where under all conditions, the highest value of stator current errors were because of nonlinear inverter characteristics.

Moreover, as it can be seen from Fig. 5-3-2, under all operational conditions the energy of current errors in “experiment-3” is higher than its value in “experiment-2” which means:

$$(E_{nonlinear\ INV} + E_{dc-link}) > (E_{nonlinear\ INV} + E_{Rs})$$

Eq. 5-3-6

or

$$E_{dc-link} > E_{RS}$$

Eq. 5-3-7

Equation (5-3-7) is also in accordance with simulations results where under all conditions, the introduced error due to wrong dc-link voltage is higher than introduced error due to wrong stator resistance error. In many industrial applications, the amplitude of dc-bus voltage is measured because of protection measurements. This measured value can be used in the control structure to reduce its correspondent error.

Moreover, similar to simulation results, the energy of stator current error increases by increasing the number of faulty phases. As it was discussed before, this increment is because of higher variations (dynamics) of stator reference currents under faulty conditions.

Although proposed FT-PDC is robust to parameter variation, but because the controller outputs are only dependent on the current values of system states (and not system past history), both system parameter variations and disturbance injection can lead to non-zero values of steady-state torque error.

This problem can be resolved by adding an integrator in the controlling loop of generated torque. That is to consider all disturbances as one additional signal on machine´s generated torque, and estimating this signal by integrating the difference of generated torque (τ_{real}) and its reference value [26]. In other words, instead of using reference torque (τ_{ref}), the following value ($\overline{\tau}_{ref}$) is used to compute stator current references:

$$\overline{\tau}_{ref} = \tau_{ref} + K_{\text{int}} \int (\tau_{ref} - \tau_{real})\ dt$$

Eq. 5-3-8

where K_{int} should be adjusted to eliminate the steady state error of generated torque. In this study, this value is set to 5 which let us to eliminate the steady state error without noticeable influence on machine´s dynamic behaviour. Moreover, to avoid the problem of *integrator-windup*, the integration of torque error will not be executed if absolute value of ($\overline{\tau}_{ref}$) becomes more than 1.5 pu.

5.3.2 Evaluation of Proposed FT-PDC in Transient States

In the next step, dynamic behaviour of proposed deadbeat control is evaluated. To have a better evaluation, the same test is also conducted in transient states by using proportional-resonant (PR) controllers.

Similar to the case of using FT-PDC method, in the case of using PR controllers the reference value of electrical torque is changed from 0.5 to 1.0 of its “maximum achievable values”. These maximum values are mentioned in table 5-3-1. Figure 5-3-3 presents the generated (measured) electrical torque in two different cases.

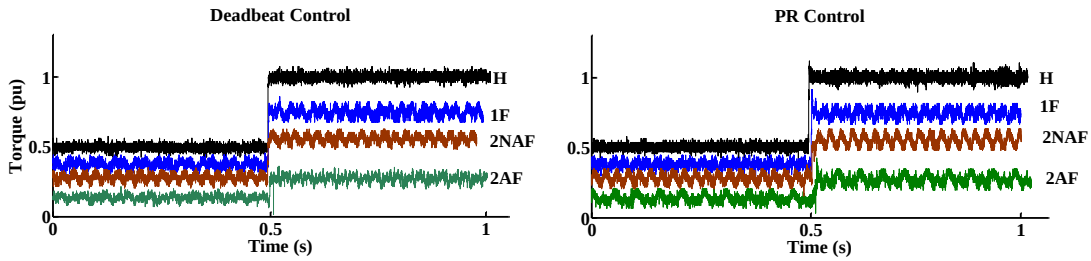

Fig. 5-3-3: Measured values of generated torque under healthy (H) condition and while missing one phase (1F), two adjacent phases (2AF), and two non-adjacent phases (2NAF)

As it can be seen from Fig. 5-3-3, proposed FT-PDC results in almost no overshoot. In addition, generated torque ripples have higher amplitudes in the case of PR controllers.

Generated electrical torque is directly dependent on stator phase currents. As a result, the energy of torque error can be considered as an index to evaluate current controllers. This value is computed under each operational condition. The switching frequency is set on 5 kHz, and the sampling rate of oscilloscope is set on 50 kHz. To evaluate the behaviour of both PD and PR controllers under transient operation, 4000 samples (equal to 400 modulation periods) are measured symmetrically with respect to the change of torque command. In the next step, the energy of torque error is integrated over all of these modulation periods:

$$E = \sum_{4000} (T_{measured} - T_{reference})^2$$

Eq. 5-3-9

Calculated values of torque error energy are summarized in Table 5-3-3.

Table 5-3-3: Calculated values of torque error energy under different operational conditions and in transient state

Error Energy	H	1F	2AF	2NAF
	Transient			
deadbeat control	2.83	3.39	4.01	3.83
PID control	5.8	7.15	7.48	7.20

Comparing to PR current controllers, deadbeat controllers result in less energy of torque error for each operational condition. Moreover, in each raw of table 5-3-3, the energy of torque error rises by increasing the number of faulty phases. This fact is in accordance with the increasing rate of current errors while missing more stator phases which was explained in simulation discussions (section 5-2-4-2). In addition, comparing to the case of missing two adjacent stator phases, missing two non-adjacent stator phases

results in less torque (and current) error which is due to more symmetric position of the remaining healthy phases.

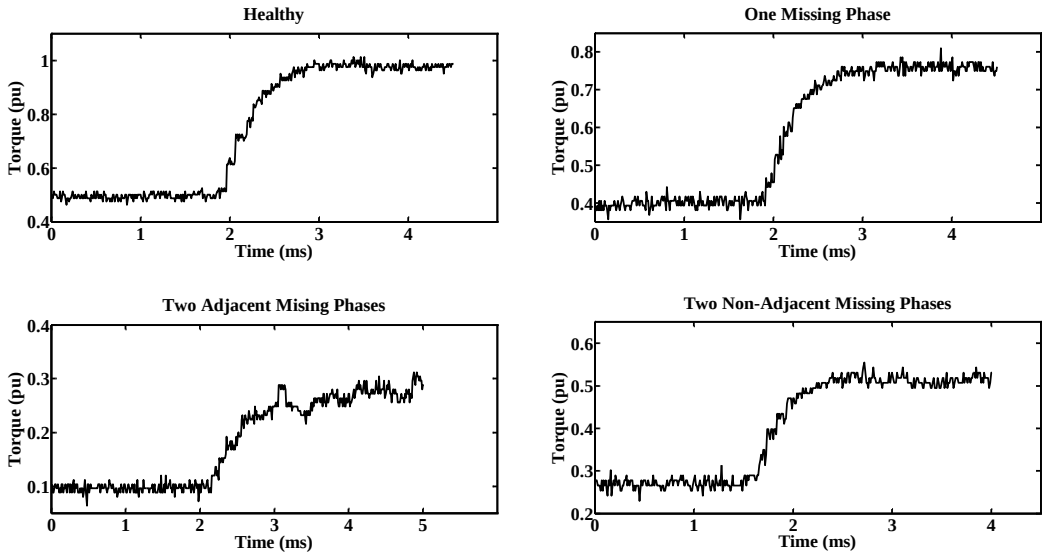

Fig. 5-3-4 Transient state of measured torque while using FT-PDC and under all operational conditions

In Fig. 5-3-4, transient state of measured torque is focused. As it is shown in this figure, under all operational conditions, the measured value of torque rise-time is 0.6 ms which is equal to 3 consecutive modulation period. However, the theoretical value of rise-time should be equal to one modulation period (0.2 ms). The main reason of longer rise-time period is limited value of inverter dc-link voltage. In other words, the required voltage for removing the stator current errors during only one modulation period is higher than available dc-link voltage which extends the rise-time to three consecutive modulation periods.

5.4. Summary

In this chapter, model predictive deadbeat control is developed for the case of five-phase BLDC motor drives under healthy and faulty conditions. Open circuit fault is considered in the case of missing one, two adjacent, and two nonadjacent stator phases. Proposed controlling method is designed to estimate the stator currents for the end of current modulation period, and eliminate the stator current errors during the next modulation period. To improve the quality of generated torque under faulty conditions, optimized reference values of chapter 4 are used in controlling block. Limited values of dc-link voltage can lead to slower dynamics of proposed method during transient states. Sensitivity of proposed controlling method is evaluated, and it is shown that nonlinear characteristics of inverter switches and inaccurate dc-bus voltage have the most noticeable impact on the error of stator phase currents. Therefore, these two parameters should be taken into account in practical predictive control applications of five-phase BLDC drives. Both simulations and experimental evaluations show that the proposed method is robust and able to provide

fast current response with no overshoot under healthy and open-circuit faulty conditions of five-phase BLDC machines.

5.5. References

[1] Dwari, S., Parsa, L. :'Fault-Tolerant Control of Five-Phase Permanent-Magnet Motors With Trapezoidal Back EMF', IEEE Trans. Ind. Electron., 2011 , 58 , (2), pp 476 – 485

[2] Chai, S., Wang, L., Rogers, E. :'A Cascade MPC Control Structure for a PMSM With Speed Ripple Minimization', IEEE Trans. Ind. Electorn., 2013, 60, (8), pp. 2978 – 2987

[3] Gregor, R., Barrero, F., Toral, S.L., Duran, M.J., Arahal, M.R., Prieto, J., Mora, J.L., :'Predictive-space Vector PWM Current Control Method for Asymmetrical Dual Three-phase Induction Motor Drives', IET journal on Electric Power Appl., 2010, 4, (1), PP. 26 - 34

[4] Phan, V.-T., Lee, H., :'Improved Predictive Current Control for Unbalanced Stand-alone Doubly-fed Induction Generator-Based Wind Power Systems', IET journal on Electric Power Appl., 2011, 5, (3), PP. 275-287

[5] Cortes, P., Kazmierkowski, M., Kennel, R., Quevedo, D., Rodriguez, J., :'Predictive Control in Power Electronics and Drives', IEEE Trans. Ind. Electron., 2008, 55, (12), pp. 4312–4324

[6] Arahal, M.R., Barrero, F., Toral, S., Duran, M., Gregor, R., :'Multi-phasecurrentcontrolusingfinite-statemodel-predictivecontrol', Elsevier Journal on Control Eng. Practice, 2009, 17, (5), pp 579-587

[7] Ambrozic, V., Buja, S., Menis R. :'Band-Constrained Technique for Direct Torque Control of Induction Motor', IEEE Trans. Ind. Electron., 2004, 51, (4), pp. 776–784

[8] Sarasola, I., Poza, J., Rodríguez, M., Abad, G. :'Predictive Direct Torque Control for Brushless Doubly Fed Machine with Reduced Torque Ripple at Constant Switching Frequency', Proc. IEEE ISIE, 2007, pp. 1074–1079

[9] Caporal, R., Pacas, M. :'A Predictive Torque Control for the Synchronous Reluctance Machine Taking into Account the Magnetic Cross Saturation', IEEE Trans. Ind. Electron., 2007, 54, (2), pp. 1161–1167

[10] Levi, E., Bojoi, R., Profumo, F., Toliyat, H., Williamson, S. :' Multiphase Induction Motor Drives - a Technology Status Review', IET journal on Electric Power Appl., 2007, 1, (4), pp. 489-516

[11] Jones, M., Vukosavic, S., Dujic, D., Levi, E., Wright, P. :' Five-leg Inverter PWM Technique for Reduced Switch Count Two-motor Constant Power Applications', IET journal on Electric Power Appl., 2008, 2, (5), pp. 275 – 287

[12] Barrero, F., Arahal, M. R., Gregor, R., Toral, S., J. Durán, M., :'A Proof of Concept Study of Predictive Current Control for VSI-Driven Asymmetrical Dual Three-Phase AC Machines', IEEE Trans. Ind. Electron., 2009, 56, (6), pp 1937-1954

[13] Barrero, F., Arahal, R., Gregor, R., Toral, S., Duran, J. :'One Step Modulation Predictive Current Control Method for the Asymmetrical Dual Three-phase Induction Machine', IEEE Trans. Ind. Electron., 2009, 56, (6), pp. 1974–1983

[14] Duran, J., Prieto, J., Barrero, F., Toral, S. :'Predictive Current Control of Dual Three-Phase Drives Using Restrained Search Techniques', IEEE Trans. Ind. Electron. 2011, 58, (8), pp. 3253–3263

[15] Riveros, J. A., Barrero, F., Levi E., Durán, M, J., Toral, S., Jones, M., :'Variable-Speed Five-Phase Induction Motor Drive Based on Predictive Torque Control', IEEE Trans. Ind. Electron., 2013, 60, (8), pp 2957 – 2968

[16] Lim, C., Levi, E., Jones, M., Rahim, Abd., Hew, P. :'FCS-MPC-Based Current Control of a Five-Phase Induction Motor and its Comparison with PI-PWM Control', IEEE Trans. Ind. Electron., 2014, 61, (1), pp. 149 - 163

[17] Tani, A., Mengoni, M., Zarri, L., Serra, G., Casadei, D., “Control of Multiphase Induction Motors With an Odd Number of Phases Under Open-Circuit Phase Faults”, IEEE Trans. Power Electron., 2011, 27, (2), pp 565 - 577

[18] Lim, S., Rahim, A., Hew, P., Levi, E. :'Model Predictive Control of a Two-Motor Drive with Five-leg Inverter Supply', IEEE Trans. Ind. Electron., 2013, 60, (1), pp. 54–65

[19] Morel, F., Lin-Shi, X., Rétif, J., Allard, B., Buttay, C. :' A Comparative Study of Predictive Current Control Schemes for a Permanent-Magnet Synchronous Machine Drive', IEEE Trans. Ind. Electron., 2009, 56, (7), pp 2715 – 2728

[20] Lee, J., Kim, C., Youn, M. :'A Dead-beat Type Digital Controller for the Direct Torque Control of an Induction Machine', IEEE Trans. Power Electron., 2002, 17, (5), pp. 739–746

[21] Kenny, H., Lorenz, D. :'Stator- and Rotor-flux-based Deadbeat Direct Torque Control on Induction Machines', IEEE Trans. Ind. Appl., 2003, 39, (4), pp. 1093–1100

[22] Dwari, S., Parsa, L. :'Fault-Tolerant Control of Five-Phase Permanent-Magnet Motors with Trapezoidal Back EMF’, IEEE Trans. Ind. Electron., 2011, 58, (2), pp. 476–485

[23] Bianchi, N., Bolognani, S., Pré, M., Fornasiero, E. :'Post-fault operations of five-phase motor using a full-bridge inverter’, Power Electron. Specialists Conf., 2008, IEEE, pp. 2528–2534

[24] S. Bolognani, L. Peretti, and M. Zigliotto, “Design and implementation of model predictive control for electrical motor drives,” IEEE Trans. Ind. Electron., vol. 56, no. 6, pp. 1925–1936, Jun. 2009.

[25] C´ardenas, R., Juri, C., Pe˜na, R., Wheeler, P., Clare J., "The Application of Resonant Controllers to Four-Leg Matrix Converters Feeding Unbalanced or Nonlinear Loads”, IEEE Trans. On Power Electron., 2012, 27, (3), pp. 1120 – 1129

[26] Bolognani, S., Peretti, L., Zigliotto, M., “Design and Implementation of Model Predictive Control for Electrical Motor Drives”, IEEE Trans. Ind. Electron., Vol. 56, No. 6, PP. 1925–1936, 2009

6.

Chapter 6 Efficiency Evaluation of Five-Phase BLDC Drives under Faulty Conditions

Among different configurations of fault tolerant motor drives, five-phase BLDC drives are gaining more importance which is because of their compactness and high efficiency. Due to replacement of field windings by permanent magnets in their rotor structure, the main sources of power losses in these drives are iron (core) losses, copper (winding) losses, and inverter unit (semiconductor) losses. Although low amplitude of power losses in five-phase BLDC drives is an important aspect for many applications, but their efficiency under faulty conditions is not considered in previous studies. In this chapter, the efficiency of an outer-rotor five phase BLDC drive is evaluated under normal and different faulty conditions. Open-circuit fault is considered for one, two adjacent and two non-adjacent faulty phases. Iron core losses are calculated via FEM simulations in Flux-Cedrat® software, and moreover, inverter losses and winding copper losses are simulated in MATLAB® environment. Experimental evaluations are conducted to evaluate the efficiency of the entire BLDC drive which verifies the theoretical developments.

CONTENTS

6.1 Introduction

Regarding their high efficiency and compactness, permanent magnet (PM) motors are gaining more interest in the field of electrical and hybrid electrical vehicles. Absence of field windings and rotor currents in PM motors not only reduces the required maintenance, but also increases the motor efficiency and its robustness [1] [2].

The efficiency of an electric drive directly depends on the generated losses of its inverter block and electric motor. In the inverter block, the main sources of power loss are related to inverter snubbers and semiconductors. However, in many IGBT based topologies, it is not necessary to implement snubbers, and as a result, power losses can be categorized as IGBT and diode conduction losses, IGBT and diode off-state losses and IGBT switching losses. Among these categories, switching losses are the most important type of losses in the inverter block.

Switching algorithm has also an important impact on the final losses of inverter block. Different modulation strategies are proposed in literature to improve the quality of converter outputs. These modulation methods can be categorized in two main groups including space vector modulation (SVM), and carrier based (CB) pulse width modulation (PWM) [3] [4]. SVM methods let us to have a better utilization of dc bus. On the other hand, CB methods (equivalent to SVM algorithms) are easier to implement.

The second important source of drive losses is the electrical motor. During the last two decades, many controlling algorithms have been proposed in literature to minimize the motor losses by adapting machine flux to the load. These algorithms can be generally divided in three categories.

In the first category motor power factor [5] or rotor slip frequency [6] is controlled. Control of motor power factor is a practical choice for industrial drives as there is no need to speed or load information, and moreover, its adaptation is relatively fast (1 s). On the other hand, to control the rotor slip, it is required to know both speed and load information.

In the second category, the output power of the drive is kept constant and motor flux is adapted to reduce the input power of the machine [7]. However these methods are usually accompanied by several disadvantages. For example, precise load information is always required in their algorithms, and the adaptation period of these methods is quite long (7 s) [8]. In addition, a continuous disturbance can be observed in generated electrical torque. As a result, this category of efficiency improvement methods is not very popular in industrial applications.

In the third category, efficiency optimization methods are directly based on the loss model of electrical motor. These methods can be easily combined by field oriented controlling (FOC) algorithms which are already based on machine´s knowledge [9]. Although efficiency optimization algorithms provide fast and smooth control of stator flux, but they usually require machine parameters and their computational loads is relatively high.

In addition to control algorithm, machine design has also an important effect on the final efficiency of electrical drive. Efficiency maps are usually used to describe the generated losses of an electrical motor with respect to a particular speed/torque. In permanent magnet machines, power losses can be divided into winding (copper) losses and core (iron) losses [10][11].

Comparing to induction machines, core losses in PM motors stand for a larger portion of the total losses. A three-term core-loss model is used in [12-13] to calculate the generated core losses of a PM machine. In [12] [14] the flux density waveforms are estimated in stator tooth and yoke, and some analytical expressions are derived to calculate hysteresis loss and eddy-current loss. However, these approaches are usually used in the design procedure of PM machines where iron losses should be calculated many times while executing the design algorithms.

Finite-element methods (FEM) are used in [13] and [15] to precisely calculate tangential and radial flux densities within the stator core and to calculate hysteresis and eddy current loss of each element. The ratio between winding and core losses is a key factor in determining the maximum efficiency point of an electrical motor. While having a constant-speed application, this point can be considered in the design procedure of electrical motor.

Fault tolerant concept is an important issue in applications where the process cannot be stopped due to additional cost penalties or safety reasons [16]. PM drive faults can be generally categorized as actuator faults, airgap irregularities, rotor magnet faults, and stator winding faults [17]. Among these categories, stator winding open-circuit fault and semiconductor failures are the most common ones [18]. Fault tolerant inverter topologies are considered in many papers. In many studies, an additional leg is implemented in inverter configuration to be replaced with the faulty inverter leg, or to feed the machine´s neutral point [19].

Compared with standard three-phase systems, five-phase motor drives present better fault tolerant capabilities. These systems are able to maintain operational in the case of one or even two faulty phases [11] [16] [20-21]. Fault tolerant capability can be achieved by means of modifying stator reference currents and inverter topology.

In [18] [22-23] stator reference currents are optimized to improve the generated output torque of five-phase PM machines and at the same time to limit the stator ohmic losses of each winding to its 1 pu. Although the calculation methods of these studies are quite different, but the resultant values of reference currents are in common.

In this chapter, the efficiency of a fault-tolerant five-phase BLDC drive is evaluated for healthy and different faulty conditions. Open-circuit fault is considered for one, two-adjacent and two-nonadjacent stator phases, and in each case, optimized reference current values of [18] [23] are used to drive the faulty machine. Copper loss and switching loss are calculated by analytical simulations in MATLAB, and stator core

losses are computed by FEM simulations in Flux. Different speed values are considered in the efficiency evaluation of five-phase drive. Automotive applications are kept in mind and experimental tests are conducted on the in-wheel five-phase BLDC machine.

6.2 Power Losses in a Five-Phase BLDC Drive

6.2.1 Stator Iron Losses

Iron losses can play an important role in generated thermal stresses of stator core. However, as stator core losses are a function of used material, winding configuration and machine design, it is not possible to generally optimize the reference values of stator phase currents for all types of five-phase BLDC machines under faulty conditions. In this section, optimized values of stator currents are used to evaluate both copper and iron losses of an outer-rotor five-phase BLDC machine.

Stator core losses W_t can be divided into three categories of hysteresis losses W_h, eddy current losses W_e, and anomalous (or excess) losses W_e [10][24]:

$$W_t = W_h + W_e + W_f$$

Eq. 6-2-1

Hysteresis losses of the stator core can be calculated as:

$$W_h = k_h B_{\max}^2 f$$

Eq. 6-2-2

where k_h is the experimental coefficient of magnetic losses due to hysteresis [WsT^2m^3], B_{max} is the peak value of magnetic flux density [T], and f represents the electrical frequency [Hz] [10] [25]. In addition, the losses related with induced eddy currents can be computed as:

$$W_e = \frac{\pi^2 \sigma d^2}{6} B_{\max}^2 f^2$$

Eq. 6-2-3

where σ is the electrical conductivity of implemented ferromagnetic material [S/m], and d is lamination thickness [m]. Moreover, anomalous power losses can be calculated as:

$$W_a = 8.67 k_e (B_{\max} f)^{1.5}$$

Eq. 6-2-4

where k_e is the experimental coefficient of anomalous (excess) losses [$W(Ts^{-1})^{-1.5}m^{-}$]. Assuming the stacking factor of K_f for steel laminations, equation (6-2-1) can be written as:

$$W_t = k_f \left[k_h B_{\max}^2 f + \frac{\pi^2 \sigma d^2}{6} B_{\max}^2 f^2 + 8.67 k_e (B_{\max} f)^{1.5} \right]$$

Eq. 6-2-5

In this equation σ, d and k_f are known values. Moreover, k_h and k_e can be provided by lamination´s

manufacturer. As a result, equation (6-2-5) can be used to compute stator iron losses [10][24].

6.2.2 Stator Copper Losses

Stator copper losses in the remaining healthy phases can be calculated as:

$$p(t) = v(t)i(t) = ri^2(t)$$

Eq. 6-2-6

6.2.3 Inverter Switching Losses

As it was mentioned previously, off-state losses are not considered in this study. To calculate the conduction losses, IGBT and diode models are considered as voltage sources with a resistor in series. The average value of conduction losses during the modulation period T can be computed as:

$$P_{cond} = \frac{1}{T}\int_0^T (V_{Fo} + R_{on}i_F)i_F dt$$

Eq. 6-2-7

while V_{Fo}, i_F and R_{on} are respectively threshold voltage, forward current and dynamic resistance of semiconductors. The main reason of switching losses is non-ideal characteristics of IGBTs during turn-on and turn-off moments (switching instants). As a result, switching losses are directly dependent on inverter switching frequency and modulation period. Average value of switching losses in one modulation period can be calculated as [24]:

$$P_{sw} = \frac{1}{T}\sum_{j=1}^{n}\left[E_{on}(i_F, v_{off}) + E_{off}(i_F, v_{off}) + E_{rec}(i_F, v_{off})\right]$$

Eq. 6-2-8

while n is the number of transitions in each switching period, E_{on}, E_{off} and E_{rec} are turn-on, turn-off and reverse recovery losses of IGBT switch, and T is the fundamental period of drive component. To simulate the inverter losses, it is required to formulate dynamic and static characteristics of implemented IGBTs and diodes. These characteristics include turn-on and turn-off energy and voltage drop of each semiconductor.

6.3 Power Losses Simulation

6.3.1 Iron Loss Simulation

To compute stator iron losses, FEM simulations are conducted in two dimensions by Flux-Cedrat® software. Simulation sampling frequency is set on 4.9 kHz, and the total numbers of simulated points are set to 2048. Stator winding configuration is similar to Fig. 6-3-1 with 26 pole-pairs. This figure shows the Stator winding configuration, core laminations, and applied 2D mesh plot of the simulations.

Non-oriented electrical steel M235-35A laminations are considered in the simulation. Specific losses of soft ferromagnetic materials include hysteresis losses, eddy losses and excess losses. Figure 6-3-2 shows the specific losses of M235-35A steel as a function of magnetic polarization. This information is provided by

manufacturer at f_e=100 Hz and f_e=200 Hz. By applying interpolation, specific losses of these laminations can be computed for the rated frequency of five-phase BLDC machine in the test bench (f_e = 173 Hz).

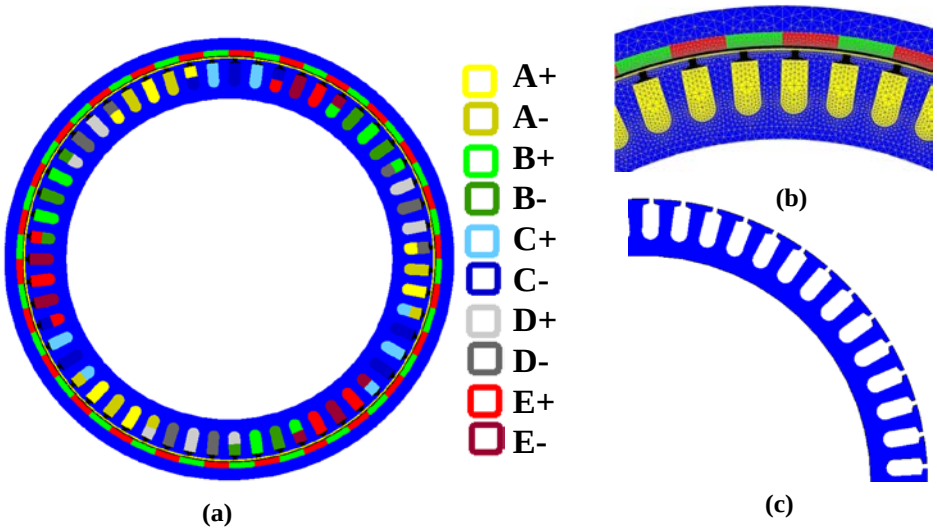

Figure 6-3-1. Five-phase BLDC machine stator, (a) winding configuration, (b) 2D mesh plot, (c) stator core lamination

Figure 6-3-2 presents the specific losses of M235-35A steel as a function of peak value of magnetic flux density. As a result, by extracting the information of two separate points in Fig. 6-3-2, it is possible to compute the experimental coefficients of k_h and k_e at rated frequency of 173 Hz. Physical properties of simulated laminations are summarized in table 6-3-1.

The derived coefficients are used in FEM simulations to calculate stator core losses while the machine is rotating at its rated speed. Table 6-3-2 presents the simulated values of stator core losses for five-phase BLDC machine under healthy and different faulty conditions. As it can be seen from table 6-3-2, in the case of missing one phase, $P_{loss\text{-}iron}$ is less than its value in normal conditions. In fact, if reference currents were not modified and stator windings were physically separated, then iron losses due to stator currents should be reduced to 80% its rated value. However, $P_{loss\text{-}iron}$ is reduced to 84% of its value under normal conditions.

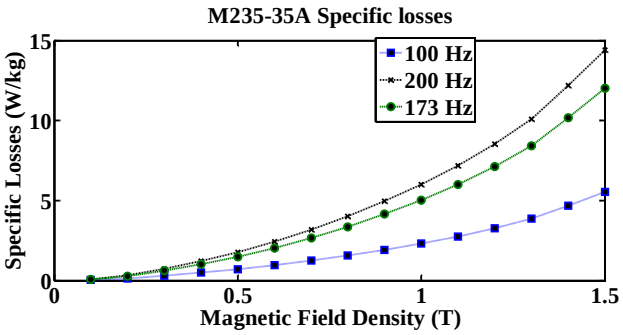

Figure 6-3-2. Specific losses of steel lamination as a function of magnetic field density

Table 6-3-1. Physical properties of steel laminations

Electrical Conductivity, σ	$1.695.10^{6}\,Sm^{-1}$
Density, ρ	$7850kgm^{-3}$
Thickness, d	$0.35.10^{-3}m$
Hysteresis coefficient, kh	$67.38100WsT^{-2}m^{-3}$
Excess losses coefficient, ke	$0.95211W(Ts^{-1})^{-1.5}m^{-3}$
Stacking factor, kf	0.96

Table 6-3-2. Stator iron losses of five-phase BLDC machine at its rated speed

Motor Condition	Stator core (iron) losses (pu)
Normal (Healthy)	0.06
One missing phase	0.0504
Two adjacent missing phases	0.0456
Two non-adjacent missing phases	0.0432

This higher value of losses is due to double-layer configuration of stator winding which leads to iron loss in all regions of stator core. Moreover, although the RMS value of stator phase currents is still 1 pu, but the peak value of optimized reference currents has increased by 10% in two of the remaining stator phases which increases the saturation level of implemented laminations. In addition, rotor magnetic field does not depend on stator winding currents and generates a constant value of iron losses in the stator.

In the case of missing two adjacent faulty phases, $P_{loss\text{-}iron}$ is 76% of its value under normal conditions. Again, in the case of separated windings and no modification in stator reference currents, the expected value of $P_{loss\text{-}iron}$ due to stator currents should be 60% its rated value.

However, to generate a ripple-free torque, the stator phase currents should be adapted. In fact, in this case the peak value of stator phase currents are $I_{C\text{-}peak}$ =0.68 pu, $I_{D\text{-}peak}$ = 1.24 pu, and $I_{E\text{-}peak}$ = 0.68 pu. High value of $I_{D\text{-}peak}$, double-layer configuration of stator windings, and constant value of rotor magnetic field are the main reasons of higher core losses in the case of missing two adjacent phases.

In the case of missing two non-adjacent phases, the physical situation of the remaining healthy phases are quite symmetric, and peak values of stator reference currents are $I_{B\text{-}peak} \approx$ 0.88 pu, $I_{D\text{-}peak} \approx$ 1.12 pu, and $I_{E\text{-}peak} \approx$ 1.12 pu. Under this operational condition, $P_{loss\text{-}iron}$ is 72% of its value while operating under normal conditions. Comparing to the case of having two adjacent missing phases, stator current peak values are more moderated. However, again peak values of stator reference currents are more than 1 pu in two of the remaining phases. As it can be seen in this case $P_{loss\text{-}iron}$ is 4% less than its value in the case of missing two

adjacent faulty phases which is firstly due to a reduction in maximum peak value of stator current in the remaining healthy phases, and secondly, more uniform distribution of remaining phase windings.

6.3.2 Copper Loss Simulation

Using the reference values of [22] and by knowing that $r_s = 0.1\ \Omega$, pu values of generated copper loss in stator windings are summarized in Fig. 6-3-3 for each condition.

RMS value of stator phase currents is the main limiting factor in the optimization procedure of stator reference currents while missing one or two stator phases. In the case of missing one stator phase, copper losses are 1 pu in the remaining healthy phases, and total amount of stator copper losses is 80% of its value under normal operation.

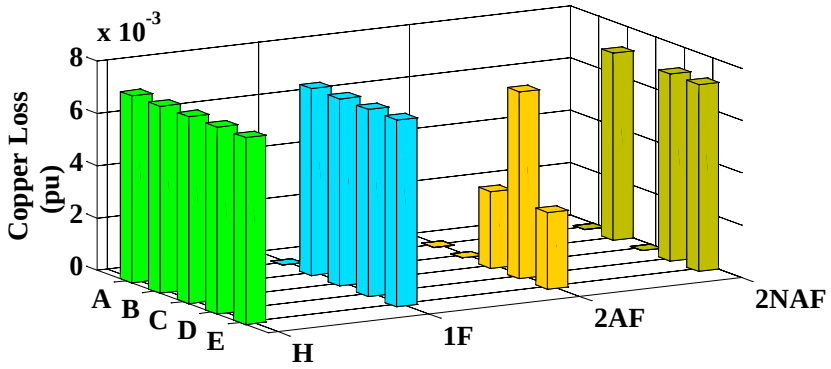

Figure 6-3-3. pu values of stator copper loss under healthy condition (H) and while missing one phase (1F), two adjacent phases (2AF) and two non-adjacent phases (2NAF)

While missing two adjacent stator phases, stator copper losses are less in the two non-adjacent remaining phases. The main reason of this fact is torque ripple constraints in the optimization procedure of stator reference currents. In other words, to generate a ripple-free torque in the case of missing two-adjacent phases, it is not possible to use the entire copper capacity of the remaining three healthy windings. The entire copper losses under this condition is 37% its value under normal operation.

6.3.3 Inverter Loss Simulation

Inverter characteristics are formulated by using datasheet information of inverter semiconductors and MATLAB Curve Fitting toolbox. Table 6-3-3 presents the derived polynomial functions of FP15R06W1E3 IGBT model and their reverse diodes.

Table 6-3-3 Estimated data for FP15R06W1E3

	Estimated characteristic
	Transistor
Voltage drop	$0.1056\times i^{0.4602} + 0.3161$
Turn on Energy: E_{on}(mJ)	$0.0001723\times i^2 - 0.02001\times i + 7.423$
Turn off Energy: E_{off}(mJ)	$0.0936\times i + 3.2687$

	Diode
Voltage drop	$0.6781\times i^{0.2387}-0.2912$
Turn off Energy: E_{off}(mJ)	$63\times\exp(-0.001732\times i)-58.3\times\exp(-0.0029\times i)$

Moreover, Fig. 6-3-4 illustrates the simulated losses of inverter block. Five-phase BLDC drive is simulated and inverter losses are computed (in watts) for steady states and under healthy and each faulty condition. In the case of healthy conditions, total amount of conduction and switching losses in each leg is 0.83% of the rated power. In this case, conduction losses and switching losses are equal for all inverter legs.

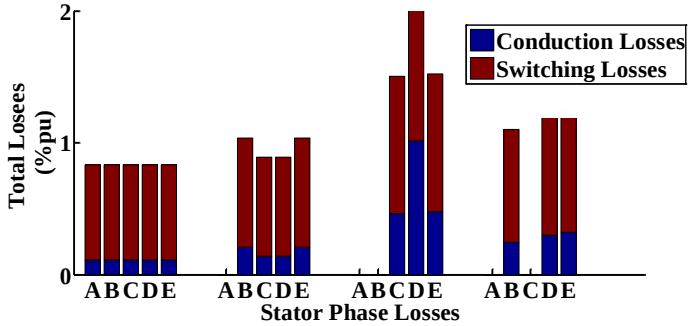

Figure 6-3-4. Simulated values of conduction and switching losses of five-phase inverter under healthy and different faulty conditions

While missing one stator phase, both switching and conduction losses increase in the remaining inverter legs. Under this condition, $I_{B\text{-}peak}$=1.12 pu, $I_{C\text{-}peak}$=1.00 pu, $I_{D\text{-}peak}$=1.00 pu, and $I_{E\text{-}peak}$=1.12 pu. As a result, it is expected that the losses increase more in phases B and E. comparing to the healthy case, conduction loss increment of phase B and E is 0.10% rated power. Moreover, switching loss increment is 0.10% rated power. The increment of both conduction and switching losses for the remaining two phases is 0.028 % rated power.

In the case of missing two adjacent phases, both conduction and switching losses increase in the remaining three phases. Comparing to normal (healthy) operation, the increment of conduction losses in phases C, D and E are respectively 0.35%, 0.90% and 0.36% of the rated power. The increment of switching losses for phases C, D and E are 0.32%, 0.72% and 0.32% rated power, respectively. As it can be seen from Fig. 6-3-4, inverter losses are higher in leg D of the inverter which is due to higher peak value of stator currents in its corresponding phase.

On the other hand, while missing two non-adjacent phases, stator phase currents are more symmetric. As a result, comparing to the case of missing two adjacent faulty phases, the switching losses are less in this case. Comparing to normal operation, the conduction loss in phases B, D and E have an increment of 0.13%, 0.19% and 0.21% of the rated power. Moreover, switching loss increment in each one of these cases is 0.14%, 0.17% and 0.19% of the rated power.

6.4 Experimental Evaluation

To evaluate the theoretical investigations, experimental tests are conducted in laboratory on the existing test bench. Motor phase terminals are fed by the existing five-phase inverter with a 48V dc-bus and 5 kHz of switching frequency. In addition, stator current controlling algorithm is realized by DS1005 dSpace board, and mechanical speed is controlled (fixed) by the load system. Under each operational condition, real and reference values of stator phase currents are compared, and the resultant current errors are used in controllers to calculate the required reference voltages of each phase. Under faulty conditions, stator phase currents are directly controlled in phase reference coordination. Proportional-resonant (PR) controllers are used to calculate the reference values of phase terminal voltages [27].

An incremental encoder and 5 Hall Effect sensors are used to close the position and current loops. Load system is a commercial three-phase PMSM which is driven independently by a three-phase AC drive (famous as SINAMICS S120). A real-time controller (known as cRio) is used as an interference between host computer and three-phase inverter. Stator currents under healthy and each faulty condition are summarized in Fig. 6-4-1.

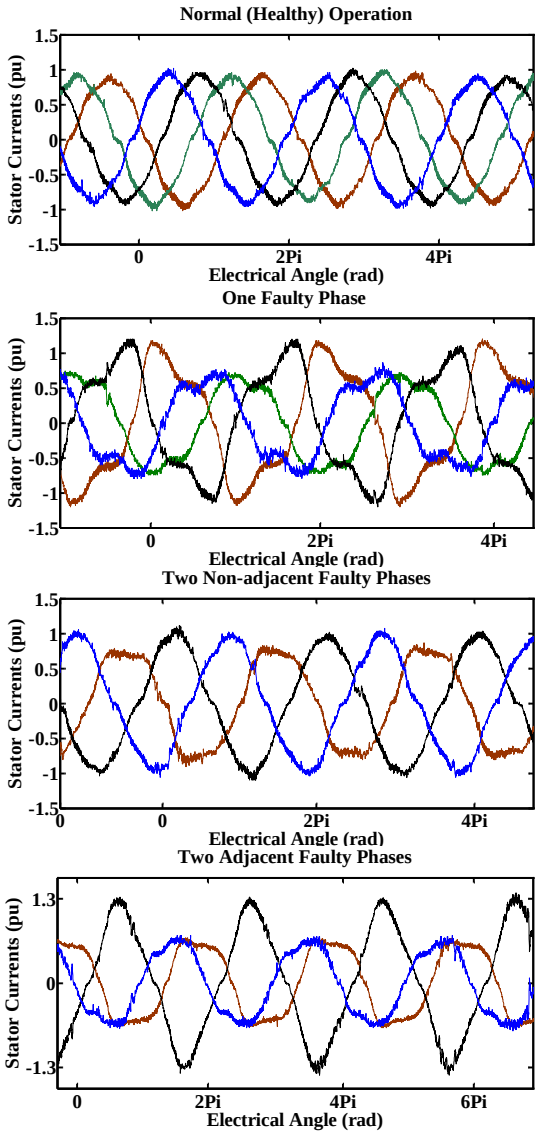

Figure 6-4-1. Stator phase currents under healthy and various faulty conditions

The computational power of implemented dSpace and its IO port speed are limited. As a result, 5 kHz is the maximum achievable switching frequency. It is worth noting that due to relatively low value of motor speed, air friction losses and ball bearing losses are negligible. As a result, these sources of losses are not considered in simulation evaluations.

In each case, input and output power of BLDC drive are measured under steady state to evaluate the efficiency of BLDC drive. Input power is directly calculated by measuring the output current of dc power supply and multiplying it by dc bus voltage. On the other hand, to compute the output power of five-phase BLDC drive, mechanical torque is measured in healthy and different faulty conditions. Table 6-4-1 summarizes the measured values of input and output power for each case. While operating under normal conditions, the measured efficiency value of the entire drive is 88.4% which is close to its simulated value (87.9%).

Table 6-4-1. Measured values of BLDC drive input and output powers and its efficiency

Condition	$P_{in\text{-}elec}$. (pu)	$P_{out\text{-}mech}$. (pu)	$P_{loss\text{-}tot}$. (pu)	Eff.
Normal (H)	1.13	1	0.13	0.88
1F	0.86	0.73	0.13	0.84
2AF	0.39	0.26	0.13	0.66
2NAF	0.66	0.55	0.11	0.83

Regarding simulation results, while working with a healthy machine the main part of BLDC drive losses are related to iron core (0.06 pu), and after that, inverter unit losses (0.04 pu) and stator windings copper losses (0.03 pu).

Comparing to normal operation, the measured value of drive efficiency is less in the case of missing one stator phase (84%). In this case, the maximum value of output power is reduced to 0.73 pu [23], and as the RMS value of stator currents in the remaining healthy phases is kept on 1 pu, stator copper losses are 80% their rated value. Stator current peak values are higher than 1 pu in two of the remaining phases which results in higher amplitudes of conduction and switching losses in their correspondent inverter legs. Regarding the simulations, in this case the main part of BLDC drive losses are again generated by stator iron core (0.05 pu), and after that, inverter unit losses (0.04 pu) and stator copper losses (0.028 pu) are the most important reasons of efficiency reduction in the drive.

In the case of missing two adjacent phases, measured drive efficiency decreases down to 66% which is highly noticeable comparing to its value under normal conditions (88%). The main reason of this efficiency reduction is related to optimized values of stator reference currents under this condition [22] [23]. In fact to limit the generated ripples in the case of missing two adjacent phases, fundamental component of stator currents should be less than 0.7 pu in two non-adjacent healthy phases, and high amplitudes of third harmonic components are required. Moreover, theoretical value of ripple-free output power is reduced to 0.27 pu. In this case, the main parts of BLDC drive losses are related to the inverter losses (0.0548 pu) which is due to high peak value of stator currents. After inverter losses, stator core losses (0.04 pu) is the biggest source of power losses in BLDC drive. In addition, as it is not possible to use the entire copper capacity of the remaining healthy phases, stator copper losses are reduced to 0.013 pu in this case.

In the case of missing two non-adjacent stator phases, the measured value of BLDC drive efficiency is 83% which is close to its simulated value (84.7%). Comparing to the case of two adjacent faulty phases, there is a noticeable increment in final value of drive efficiency. The main reason of higher efficiency is more symmetric situation of the remaining healthy phases which allows having a better utilization of stator copper capacity to generate more ripple-free output power. The maximum achievable output power in this case is limited to 0.55 pu which is due to keeping the RMS value of stator reference current under 1 pu. Regarding simulations, in this case, the main source of BLDC drive losses are related to stator core iron

(0.04 pu), and after that Inverter block losses (0.03 pu) and stator copper losses (0.02 pu) are the most important reasons of efficiency reduction.

6.5 Summary

In this chapter, the efficiency of a fault tolerant five-phase PM drive is evaluated for a five-phase outer-rotor BLDC motor with a double-layer winding configuration. Open-circuit fault is considered in one, two adjacent and two non-adjacent stator phases. In each case, RMS value of stator reference currents is the main limiting constraint of generated ripple-free torque. Stator core losses are calculated by means of simulations in Flux-Cedrat® environment. It is shown that iron losses are the most important part of BLDC drive losses under normal operation and while missing one phase and two non-adjacent phases. In addition, inverter unit losses and stator winding (copper) losses are simulated in MATLAB environment. In the case of having two adjacent faulty phases, inverter losses are the most important reason of BLDC drive losses. Regarding simulations, the final efficiency of BLDC drive is 87%, 86%, 70% and 84% respectively in the case of working with a healthy machine, a machine with one missing phase, a machine with two adjacent missing phases, and a machine with two non-adjacent missing phases. In addition, experimental tests are conducted to verify the simulation results. Measured value of BLDC drive efficiency is 89%, 84%, 66% and 83% respectively in the case of working with a healthy machine, and while missing one phase, two adjacent phases and two non-adjacent phases.

6.6 References

[1] D. Ha, C. Lim, D. Hyun, “Robust Optimal Nonlinear Control with Observer for Position Tracking of Permanent Magnet Synchronous Motors,” Journal of Power Electronics, vol. 13, no. 6, pp. 975-984, Nov. 2013

[2] J. Yu, H. Cho, J. Choi, S. Jang, S. Lee, “Optimum Design of Stator and Rotor Shape for Cogging Torque Reduction in Interior Permanent Magnet Synchronous Motors,“ Journal of Power Electronics, vol. 13, no. 4, pp. 546-551, Nov. 2013

[3] D. Nguyen, H. Lee, T. Chun, “A Carrier-Based Pulse Width Modulation Method for Indirect Matrix Converters,” Journal of Power Electronics, vol. 12, no. 3, pp. 448-457, Nov. 2012

[4] J. Abu Qahouq, V. Arikatla, T. Arunachalam, “Modified Digital Pulse Width Modulator for Power Converters with a Reduced Modulation Delay,” Journal of Power Electronics, vol. 12, no. 1, pp. 98-103, Jan. 2012

[5] T.W. Jian, N. L. Schmitz, D.W. Novotny, “Characteristic induction motor slip values for variable voltage part load performance optimization,” IEEE Trans. Power App. Syst., vol. PAS-102, no. 1., pp. 38–46, Jan. 1983.

[6] H. G. Kim, S. K. Sul, M. H. Park, “Optimal efficiency drive of a current source inverter fed induction motor by flux control,” IEEE Trans. Ind. Applicat., vol. IA-20, no. 6, pp. 1453–1459, Nov./Dec. 1984.

[7] A. Kusko, D. Galler, “Control means for minimization of losses in AC and DC motor drives,” IEEE Trans. Ind. App., vol. IA-19, no. 4, pp. 561–570, July/Aug. 1983.

[8] F. Abrahamsen, F. Blaabjerg, J. K. Pedersen, P. Grabowski, P. Thoegersen, “On the energy optimized control of standard and high-efficiency induction motor in CT and HVAC applications,” IEEE Trans. Ind. App., vol. 34, no. 4, pp. 822–831, July/Aug. 1998.

[9] K. S. Rasmussen, P. Thoegersen, “Model based energy optimizer for vector controlled induction motor drives,” in Proc. EPE’97, 1997, pp. 3.711–3.716.

[10] G. Bertotti, “General Properties of Power Losses in Soft Ferromagnetic Materials,” IEEE Trans. Magn., vol. 24, no. 1, pp. 621-630, Jan. 1988.

[11] L. Parsa, H. A. Toliyat, “Five-Phase Permanent-Magnet Motor Drives”, IEEE Trans. Ind. App., vol. 41, no. 1, January/February 2005

[12] G. R. Slemon, L. Xian, “Core losses in permanent magnet motors,” IEEE Trans. Magn., Vol. 26, No. 5, pp. 1653–1655, Sep. 1990.

[13] K. Yamazaki, H. Ishigami, “Rotor-shape optimization of interior-permanent-magnet motors to reduce harmonic iron losses,” IEEE Trans. Ind. Electron., vol. 57, no. 1, pp. 61–69, Jan. 2010.

[14] W. Jiabin, T. Ibrahim, D. Howe, “Prediction and measurement of iron loss in a short-stroke, single-phase, tubular permanent magnet machine,”IEEE Trans. Magn., vol. 46, no. 6, pp. 1315–1318, Jun. 2010.

[15] K. Atallah, Z. Q. Zhu, D. Howe, “An improved method for predicting iron losses in brushless permanent magnet DC drives,” IEEE Trans. Magn., vol. 28, no. 5, pp. 2997–2999, Sep. 1992.

[16] B. Park, R. Kim, D. Hyun, “Open Circuit Fault Diagnosis Using Stator Resistance Variation for Permanent Magnet Synchronous Motor Drives,” Journal of Power Electronics, vol. 13, no. 6, pp. 985-990, Nov. 2013

[17] L. Romeral, J. C. Urresty, J. R. R. Ruiz, A. G. Espinosa, “Modeling of Surface-Mounted Permanent Magnet Synchronous Motors With Stator Winding Interturn Faults,” IEEE Trans. Ind. Elect., vol. 58, no. 5, pp. 1576-1585, May 2011

[18] A. Mohammadpour, L. Parsa, “A Unified Fault-Tolerant Current Control Approach for Five-Phase PM Motors With Trapezoidal Back EMF Under Different Stator Winding Connections,” IEEE Trans. Power Elect., vol. 28, no. 7, pp. 3517-3527, July 2013

[19] R. Brian, A. Welchko, T. A. Lipo, T. M. Jahns, S. E. Schulz, “Fault Tolerant Three-Phase AC Motor Drive Topologies: A Comparison of Features, Cost, and Limitations,” IEEE Trans. on Power Electron., vol. 19, no. 4, pp. 1108-1116, July 2004

[20] B. Park, K. Lee, R. Kim, D. Hyun, “Low-Cost Fault Diagnosis Algorithm for Switch Open-Damage in BLDC Motor Drives,” Journal of Power Electronics, vol. 10, no. 6, pp. 702-708, Nov. 2010

[21] A. Jack, B. Mecrow, J. Haylock, “A Comparative Study of Permanent Magnet and Switched Reluctance Motors for High-performance Fault Tolerant Applications,” IEEE Trans. Ind. App., vol. 32, no. 4, Jul. 1996

[22] S. Dwari, L. Parsa,“Fault-Tolerant Control of Five-Phase Permanent-Magnet Motors With Trapezoidal Back EMF”, IEEE Trans. Industrial Electronics, vol. 58 , no. 2, pp- 476 – 485, Feb. 2011

[23] R. Salehi Arashloo, J. L. Romeral Martinez, M.Salehifar, M. Moreno-Eguilaz, “Genetic Algorithm Based Output Power Optimization of Fault Tolerant Five-Phase BLDC Drives Applicable for Electrical and Hybrid Electrical Vehicles”, submitted to IET Journal on Electric Power Applications, 2014

[24] H. Saavedra, J. Riba, L. Romeral, “Inter-turn fault detection in five-phase pmsms. Effects of the fault severity”, IEEE symposium on Diagnostics for Electric Machines, Power Electronics and Drives (SDEMPED), pp. 520-526, Aug. 2013

[25] J. Siahbalaee, S. Vaez-Zadeh, F. Tahami, “A Loss Minimization Control Strategy for Direct Torque Controlled Interior Permanent Magnet Synchronous Motors”, Journal of Power Electronics, vol. 9, no. 6, pp. 940-948, Nov. 2009

[26] R. C´ardenas, C. Juri, R. Pe˜na, P. Wheeler, J. Clare, "The Application of Resonant Controllers to Four-Leg Matrix Converters Feeding Unbalanced or Nonlinear Loads”, IEEE Trans. Power Electron., vol. 27, no. 3, pp. 1120 – 1129, March 2012

7.

Chapter 7 General conclusions and future work

The main contributions of this thesis research, as well as the conclusions and future work, are presented in this chapter.

CONTENTS:

7.1 General conclusions

Equipped with appropriate control strategies, permanent magnet (PM) machines are becoming one of the most flexible types of actuators for motion control applications. Among different types of PM machines, five-phase BLDC machines are becoming interesting in many industrial applications such as automotive industries and power generation. Consequently, torque improvement of five-phase BLDC machines is an important factor in such applications. The **main goal** of this thesis has been the improvement of generated electrical torque by implementing fast and robust current controllers in the controlling loops of stator currents of electrical drive.

The **first contribution** of this study is to propose a new current controller for improving the quality of generated torque under normal (healthy) conditions of five-phase BLDC machine. Proposed current controllers are based on the combination of predictive deadbeat control and Extended Kalman Filter estimation. The proposed controller is simulated and evaluated experimentally, and It is shown that the proposed method is robust and with high bandwidth. As a result, its implementation in five-phase BLDC drive leads to less torque ripples and faster torque response.

In the case of missing one or two stator phases (open-circuit fault), stator reference currents of first and third harmonics should be optimized to improve the amplitude and quality of generated torque. The **second contribution** of this paper is to conduct a global optimization on stator reference currents by means of genetic algorithm (GA). First and third harmonic component of stator currents are considered in the case of having both one and two faulty phases, and amplitude and phase angle of stator current harmonics are separately optimized in for each harmonic component. To consider all conditions, the limiting constraint of having zero sum of stator currents is removed by connecting machine´s neutral point to the inverter through an extra half-bridge leg. It is shown that the derived current reference values result in higher amplitude of electrical torque. In addition, having access to neutral point improves fault tolerant capability of the machine. Theoretical developments are both simulated and verified experimentally on a five-phase outer-rotor type of an in-wheel BLDC hub motor.

Under faulty conditions, appropriate reference currents of a five-phase BLDC machine have oscillating dynamics both in phase- and rotating-reference frames. As a result, high bandwidth controllers are required to control the stator currents under faulty conditions. The **third contribution** of this thesis is to implement and evaluate a Fault Tolerant Predictive Deadbeat Controller (FT-PDC) for faulty conditions of five-phase BLDC motor drives. Open circuit fault is considered for one, two adjacent and two nonadjacent stator phases. Proposed controlling method is designed to estimate the stator currents for the end of current modulation period, and eliminate the stator current errors during the next modulation period. To improve the quality of generated torque under faulty conditions, optimized reference values of chapter 4 are used in controlling block. Sensitivity of proposed controlling method is evaluated, and it is shown that

nonlinear characteristics of inverter switches and inaccurate dc-bus voltage have the most noticeable impact on the error of stator phase currents. Both simulations and experimental evaluations show that the proposed method is robust and able to provide fast current response with no overshoot under healthy and open-circuit faulty conditions of five-phase BLDC machines.

Although low amplitude of power losses in five-phase BLDC drives is an important aspect for many applications, but their efficiency under faulty conditions is not considered in previous studies. The **fourth contribution** of this study is to evaluate the efficiency of an outer-rotor five phase BLDC drive under normal and different faulty conditions. Open-circuit fault is considered for one, two adjacent and two non-adjacent faulty phases. It is shown that iron losses are the most important part of BLDC drive losses under normal operation and while missing one phase and two non-adjacent phases. In the case of having two adjacent faulty phases, inverter losses are the most important reason of BLDC drive losses. Regarding simulations, the final efficiency of BLDC drive is 87%, 86%, 70% and 84% respectively in the case of working with a healthy machine, a machine with one missing phase, a machine with two adjacent missing phases, and a machine with two non-adjacent missing phases.

As a summary, the final conclusions of this study can be written as:

- **EKF-based predictive deadbeat current control is a robust controlling method which can result in torque improvement of five-phase BLDC machines under healthy conditions.**
- **Comparing to previous studies, global GA optimization of stator reference currents results in higher power of five-phase BLDC machines under open-circuit faulty conditions.**
- **Predictive deadbeat current control results in torque quality improvement of five-phase BLDC machines under open-circuit faulty conditions.**
- **For the case of considered five-phase BLDC machine (in laboratory) Iron losses are the most important source of BLDC drive losses under normal operation and while missing one phase and two non-adjacent phases.**

7.2 Future work

Despite the progress made in this dissertation as well as in the earlier research work by others, fault tolerant operation is still a topic of ongoing investigation. Several aspects of fault tolerant PM machine drives can be recommended for future consideration:

7.2.1 Reliability Aspect

Due to its complexity, the reliability of a PM drive has always been investigated by simulations. It is possible to develop an analytical methodology to evaluate the reliability of multi-phase PM drives. This is quite a huge work because many variables can be considered for a special drive such as phase numbers,

converter topology, sensor configuration, implemented capacitors in dc-link and so on. Any of these parameters can affect the final performance of the remaining healthy components of the drive. Moreover, depending on the operational condition (healthy and faulty) the sensitivity of PM drives can be changed respect different parameter variations.

7.2.2 Fault detection and isolation aspect

Proposed controlling methods under faulty conditions have always had the assumption of isolated faulty phases. However, a fault tolerant drive should be able to detect the fault and isolate the faulty phase from the remaining parts of the drive. Different fault detection and fault isolation methods can be combined with proposed controlling methods to develop an industrial fault tolerant drive.

7.2.3 Design aspect

Regarding the design of fault-tolerant BLDC drives, there are several aspects that should be further investigated. A good thermal analysis allows us to determine the maximum available current in different modes of operations. This analysis can be used to increase the amplitude of generated electrical torque while operating under faulty conditions.

7.2.4 Control aspect

Accordingly, one of the possible topics for future research is the continuing effort to develop more advanced “predictive” strategies for various types of faults that can potentially occur in a five-phase BLDC drive. This includes faults in the rectifier bridges, capacitor links, inverter bridges, sensors, control boards, or even the input and output terminals of a drive.

8.

Chapter 8 Thesis results dissemination

The direct contributions resulting from this Thesis work, in international journals as wells as in specialized conferences, are collected in this Chapter. Additionally, the contributions in research projects related with the Thesis topic are also briefly exposed.

CONTENTS:

8.1 Publications

Publications directly related with the thesis contributions

Journals

R. Salehi Arashloo, J. L. Romeral Martinez, M. Salehifar, M. Moreno-Eguilaz, "Genetic Algorithm Based Output Power Optimization of Fault Tolerant Five-Phase BLDC Drives Applicable for Electrical and Hybrid Electrical Vehicles" ***accepted in*** *IET Electric Power Application Journal,* vol., no., pp., ***pending publication***, March 2014.

R. Salehi Arashloo, M. Salehifar, H. Saavedra, J. L. Romeral Martinez, "Efficiency Evaluation of Five-Phase Outer-Rotor Fault-Tolerant BLDC Drives under Healthy and Open-Circuit Faulty Conditions" AECE Advances in Electrical and Computer Engineering, vol. 14, no. 2, May 2014

R. Salehi Arashloo, J. L. Romeral Martinez, M. Salehifar, "Impact of Neutral Point Current Control on Copper Loss Distribution of Five Phase PM Generators Used in Wind Power Plants" AECE Advances in Electrical and Computer Engineering, vol. 14, no. 2, May 2014

R. Salehi Arashloo, M. Salehifar, J. L. Romeral Martinez, V. Sala "A Robust Predictive Deadbeat Current Control for Five-Phase BLDC Drives under Healthy and Open-Circuit Faulty Conditions" ***prepared and submitted to*** *International Journal of Electrical Power & Energy Systems*

Conferences

R. Salehi Arashloo, J. L. Romeral Martinez, M. Salehifar, J. M. Moreno, "Model predictive current control of five phase permanent magnet motor", European Conference on Power Electronics and Applications (EPE), PP. 1-6, 2013

R. Salehi Arashloo, M. Salehifar, J. L. Romeral, V. Sala, "Fault-tolerant model predictive control of five-phase permanent magnet motors", IEEE Conference on Industrial Electronics Society (IECON), pp. 2857-2862, 2013

R. Salehi Arashloo, J. L. Romeral Martinez, M. Salehifar, “A novel broken rotor bar fault detection method using park's transform and wavelet decomposition”, IEEE Conference on Diagnostics for Electric Machines, Power Electronics and Drives (SDEMPED), pp. 412-419, 2013

R. Salehi Arashloo, M. Salehifar, J. L. Romeral, V. Sala, “Ripple free fault tolerant control of five phase permanent magnet machines”, European Conference on Power Electronics and Applications (EPE), PP. 1-5, 2013

R. Salehi Arashlo, M. Salehifar, J. L. Romeral, “ On the effect of accessible neutral point in fault tolerant five phase PMSM drives”, IEEE Conference on Industrial Electronics Society (IECON), pp. 1934-1939, 2012

Publication resulting from additional collaborations related with the thesis work

Journals

M. Salehifar, **R. Salehi Arashloo**, J. M. Moreno-Equilaz, V. Sala, J. L. Romeral, “Fault Detection and Fault Tolerant Operation of a Five Phase PM Motor Drive Using Adaptive Model”, IEEE Journal of Emerging and Selected Topics in Power Electronics, Vol. 2 , Issue 2, pp. 212-223, 2014

M. Salehifar, J. M. Moreno, **R. Salehi Arashloo**, V. Sala, "FPGA Based Robust Open Transistor Fault Diagnosis and Fault Tolerant Sliding Mode Control of a Five-Phase PM Motor Drive", Submitted to Journal of Power Electronic (JPE) - South Korea

Conferences

M. Salehifar, **R. Salehi Arashloo**, M. Moreno-Eguilaz, V. Sala, J. L. Romeral, “Fault tolerant operation of a five phase converter for PMSM drives”, IEEE conference on Applied Power Electronics Conference and Exposition (APEC), pp. 1177-1184, 2013

V. Sala, **R. Salehi Arashloo**, M. Moreno Eguilaz, M. Salehifar, J. L. Romeral, “ Clamping diode caused distortion in multilevel NPC Full-Bridge audio power amplifiers”, IEEE Conference on Industrial Electronics Society (IECON), pp. 4941-4948, 2012

M. Salehifar, **R. Salehi Arashoo**, J. M. Moreno, V. Sala, L. Romeral, “A simple and robust method for open switch fault detection in power converters”, IEEE conference on Diagnostics for Electric Machines, Power Electronics and Drives (SDEMPED), pp. 461-468, 2013

M. Salehifar, **R. Salehi Arashloo**, J. M. Moreno, V. Sala, “Open circuit fault detection based on emerging FCS-MPC in power electronics systems”, IEEE Conference on Power Electronics and Applications (EPE), pp. 1-10, 2013

M. Salehifar, J. M. Moreno, V. Sala, **R. Salehi Arashloo**, “Fault detection in multi-phase two-level inverters using Cauchy distribution of normalized phase currents”, IEEE Conference on Industrial Electronics Society (IECON), p.p 761-766, 2013

M. Salehifar, J. M. Moreno, V. Sala, **R. Salehi Arashloo**, L. Romeral, “Improved open switch fault detection based on normalized current analysis in multiphase fault tolerant converters”, IEEE conference on Diagnostics for Electric Machines, Power Electronics and Drives (SDEMPED), pp. 512-519, 2013

8.2 Collaboration in technologic transfer projects

Pojects

Project Title: VERDE
Founding entity: MICINN-CDTI-CENIT **Partners:**

Partners: 16 companies (SEAT, SIEMENS, LEAR, INFRANOR, MaproTechnologies and others), and 14 Research centers (Fundació CTM Centre Tecnològic, Universitat Politècnica de Catalunya, ASCAMM and others)

Tasks description: Development of Field Oriented Control Method for 28 kw 800 Am_{pp}-p 8-pole PM motor in motoring mode, generating mode, and high-speed field weakening mode

Duration: **2009-2013**

Project Title: Pulsed Power Excimer

Founding entity: Private agreement

Partners: Fraunhofer-Institut IGB

Duration: 2013-2014

Tasks description: Development of controlling unit and protection system (software code) to control four current source inverters byexas Instrument DSP controllers